Lodin Ellingsen

An Investigation of the Thermodynamic and Dielectric Properties of Primitive and Non-Primitive Electrolyte Models in the Limit of Infinite Dilution Using a Simplest Possible First-Principle Approach

Master's thesis

NTNU
Norwegian University of Science and Technology
Faculty of Natural Sciences
Department of Chemistry

Master's thesis in Chemical Engineering and Biotechnology

Supervisor: Ida-Marie Høyvik

July 2020

NTNU
Norwegian University of
Science and Technology

Lodin Ellingsen

An Investigation of the Thermodynamic and Dielectric Properties of Primitive and Non-Primitive Electrolyte Models in the Limit of Infinite Dilution Using a Simplest Possible First-Principle Approach

Master's thesis in Chemical Engineering and Biotechnology
Supervisor: Ida-Marie Høyvik
July 2020

Norwegian University of Science and Technology
Faculty of Natural Sciences
Department of Chemistry

NTNU
Norwegian University of
Science and Technology

I will remember the spring of 2020 as a different semester. With a ravaging global pandemic and a challenging master's thesis topic, my final semester at NTNU has been a worthy final hurdle of my five-year master's degree journey. Nevertheless, a daunting obstacle becomes beatable with help along the way. In this regard, I wish to express my sincere appreciation to my supervisor Ida-Marie Høyvik and my co-supervisor Tore Haug-Warberg. The time and effort they have put into my project have helped ease this semester's stresses and made my master's thesis a more enjoyable and enriching experience.

— Lodin Ellingsen

Abstract

Electrolyte models can be classified as primitive or non-primitive. Primitive models do not represent the solvent as particles or molecules, but as a dielectric continuum characterized by a permittivity. Oppositely, non-primitive electrolyte models explicitly consider the solvent on a molecular level. This thesis focuses on how modeling the solvent using a primitive or non-primitive approach changes the behavior of dilute electrolyte solutions. Specifically, the solvent's role in electrolyte solutions is investigated by establishing a non-primitive electrolyte model and comparing its dielectric and thermodynamic properties to the primitive Debye–Hückel theory in the limit of infinite dilution.

The non-primitive electrolyte model used in this work consists of an anion, a cation, and a solvent species of the same size. The ions and solvent particles interact according to a soft-core potential with a point-charge or a point-dipole at their respective centers. Molecular dynamics simulations are used to estimate the thermodynamic and dielectric properties of the non-primitive electrolyte model. Post-processing the particle configurations from the molecular dynamics simulations demonstrate that the non-primitive electrolyte model's permittivity decreases with increasing ion concentration. This phenomenon is also observed in real electrolyte solutions and is known as dielectric decrement.

Debye–Hückel theory does not consider dielectric decrement as it models the solvent as a continuous dielectricum of constant permittivity. This work derives an expression for the mean ionic activity coefficient using a Debye–Hückel inspired theory that does not assume that the solution's permittivity is independent of the concentration of ions. The resulting series expansion demonstrates that introducing a permittivity that depends on ion concentration does not alter the Debye–Hückel limiting law. The unaltered limiting law suggests that dielectric decrement does not change the non-primitive model's thermodynamics in the limit of infinite dilution.

A regression method is used to investigate the non-primitive electrolyte model's asymptotic thermodynamic behavior. Since the Debye–Hückel theory correctly describes the thermodynamics of sufficiently dilute real electrolytes, the thermodynamics of a correct non-primitive electrolyte model should converge to that of the Debye–Hückel theory in the limit of infinite dilution. However, the limit of infinite dilution is unattainable using this work's molecular dynamics procedure. Instead, this thesis demonstrates that it is possible to recover the Debye–Hückel theory's asymptotic behavior in the limit of infinite dilution from the non-primitive electrolyte model's molecular dynamics results at high temperatures. Further work is required to determine if it is possible to recover the Debye–Hückel theory's asymptotic behavior by sufficiently reducing the magnitude of the ions' charge.

Sammendrag

Elektrolyttmodeller kan klassifiseres som primitiv eller ikke-primitiv. Primitive modeller representerer ikke løsningsmidlet som partikler eller molekyler, men som et dielektrisk kontinuum karakterisert av en permittivitet. Dette er i motsetning til ikke-primitive elektrolyttmodeller som representerer løsningsmidlet på et molekylært nivå. Denne oppgaven undersøker hvordan modellering av et løsningsmiddel ved bruk av en primitiv eller ikke-primitiv tilnærming forandrer oppførselen til fortynnede elektrolyttløsninger. Spesifikt så undersøker dette arbeidet løsningsmidlets rolle i elektrolyttløsninger ved å etablere en ikke-primitiv elektrolyttmodell og sammenligne dens dielektriske og termodynamiske egenskaper med den primitive Debye–Hückelteorien i grensen ved uendelig fortynning.

Den ikke-primitive elektrolyttmodellen som brukes i dette arbeidet består av anioner, kationer og løsningsmiddelpartikler av samme størrelse. Ionene og løsningsmiddelpartiklene interager gjennom et mykt-kjernepotensial med en punktladning eller en punkt-dipol. Molekylær dynamiske simuleringer brukes for å estimere de termodynamiske og dielektriske egenskapene til den ikke-primitive elektrolyttmodellen. En etterbehandlingsprosedyre av partikkelkonfigurasjonene fra simuleringene viser at permittiviteten til den ikke-primitive elektrolyttmodellen avtar med økende ionkonsentrasjon. Dette fenomenet blir også observert i ekte elektrolyttløsninger og er kjent som dielektrisk dekrement.

Debye–Hückelteorien tar ikke hensyn til dielektrisk dekrement da den modellerer løsningsmidlet som et kontinuerlig dielektrikum med konstant permittivitet. Dette arbeidet utleder et utrykk for den gjennomsnittlige ioniske aktivitetskoeffisienten ved bruk av en Debye–Hückel inspirert teori som ikke antar at løsningens permittivitet er uavhengig av ionkonsentrasjon. Det resulterende rekkeutviklingsutrykket viser at å introdusere en permittivitet som er avhengig av ionkonsentrasjon ikke forandrer grenselovene til Debye–Hückelteori. De uendrede grenselovene antyder at dielektrisk dekrement ikke endrer den ikke-primitive modellens termodynamikk i grensen ved uendelig fortynning.

En regresjonsmetode brukes til å undersøke den ikke-primitive elektrolyttmodellens asymptotiske termodynamiske oppførsel. Siden Debye–Hückelteorien korrekt beskriver termodynamikken til fortynnede elektrolyttløsninger, bør termodynamikken til en riktig ikke-primitiv elektrolyttmodell konvergere til lignende fysisk oppførsel som Debye–Hückelteorien ved uendelig fortynning. Grensen for uendelig fortynning er uoppnåelig ved bruk av dette arbeidets molekylær dynamikkprosedyre. I stedet demonstrerer denne avhandlingen at det er mulig å gjenvinne Debye–Hückelteoriens asymptotiske oppførsel fra den ikke-primitive elektrolyttmodellens molekylær dynamikkresultater ved høye temperaturer. Det kreves ytterligere arbeid for å avgjøre om det er mulig å gjenvinne Debye–Hückelteoriens asymptotiske oppførsel ved å redusere ionenes ladning.

Table of Contents

Symbols

a	Ionic-atmosphere radius
a_i	Ionic-atmosphere radius of species i
a_{NaCl}	Ionic-atmosphere radius of sodium chloride
b	Index
b_s	Regression coefficient used to model the permittivity of an electrolyte solution
c_i	Concentration of component i
c_s	Salt concentration
f	Arbitrary function
f_{ij}	Electrostatic force due to the interactions between point charges i and j
$g_{\pm}$	Radial distribution function between anions and cations
i	Index
j	Index
k	Index
k_{C}	Coulomb constant
k_{B}	Boltzmann constant
m	Mass of particle
m_i	Real-space integer coordinate in Cartesian i direction
n_i	Number density of species i in bulk solution
n_i'	Number density of species i
p	Pressure
q	Elementary charge
$q_{\pm}$	Magnitude of an ion or point-charge
$q_{\pm}^*$	Reduced magnitude of ion charge
r	Distance from origin or center of ion
r_{cut}	Distance where the pair-potential is truncated
r_{ij}	Distance between particle i and j
s	Number of ionic species in a solution
t	Time

t^*	Reduced time
t_b	Number of dumped time-steps in a simulation block
t_s	Number of time-steps
x	Arbitrary variable or a Cartesian coordinate
x_{bs}	Binary solvent mole fraction
$x_{bs}^{(i)}$	Binary solvent mole fraction for molecular dynamics simulation i
x_i	Mole fraction of species i
x_{ions}	Mole fraction of ions
x_{ip}	Mole fraction of ion-pairs
$x_{ip}^{(i)}$	Mole fraction of ion-pairs for molecular dynamics simulation i
x_{solv}	Mole fraction of solvent
u_i	Electrostatic potential energy experienced by an ion due to the ionic-atmosphere
u_{ij}^{cc}	Pairwise potential energy due to charge-charge interactions between particles i and j
u_{ij}^{cd}	Pairwise potential energy due to charge-dipole interactions between the point-charge of particle i and the point-dipole of particle j
u_{ij}^{dc}	Pairwise potential energy due to charge-dipole interactions between the point-dipole of particle i and the point-charge of particle j
u_{ij}^{dd}	Pairwise potential energy due to dipole-dipole interactions between particles i and j
u_{ij}^{LJ}	Pairwise potential energy due to Lennard-Jones interactions between particles i and j
u_{ij}^{WCA}	Pairwise potential energy due to WCA interactions between particles i and j
w_i	Work required to move a particle of species i through an electric field
y	Arbitrary variable or a Cartesian coordinate
z	Cartesian coordinate
z_i	Charge number of species i
A^{el}	Contribution to Helmholtz energy due to the presence of an ionic-atmosphere
B	Extensive property
$\overline{B}_i$	Partial molar derivative of B with respect to species i
C^{z_k}	Species of charge z_k
C_i	Constant i used in the derivation of Debye-Hückel theory
D^{z_k}	Species of charge z_k
F	Faraday's constant
I_s	Moment of inertia of a solvent particle
I_s^*	Reduced moment of inertia of a solvent particle

L	Length of simulation box
$M_{s,j}^{(k)*}$	Solvent particles' contribution to the dipole moment of an electrolyte solution at a time-step j in a direction k
N_{A}	Avogadro's constant
N_{an}	Number of anions
N_{block}	Number of blocks in a molecular dynamics simulation
N_{cat}	Number of cations
N_{ions}	Number of ions
N_{ip}	Number of ion pairs
$N_{ip}^{(i)}$	Number of ion pairs in molecular dynamics simulation i
N_{solv}	Number of solvent particles
$N_{solv}^{(i)}$	Number of solvent particles in molecular dynamics simulation i
N_{step}	Number of time-steps in a molecular dynamics simulation
N_{tot}	Total number of particles
Q	Total charge of a system
R	Ideal gas constant
S	Surface
S^{z_k}	Species of charge z_k
T	Temperature
T^*	Reduced temperature
U	Potential energy
U^{DH}	Debye-Hückel electrostatic energy
U^{DH*}	Reduced Debye-Hückel electrostatic energy
$U^{DH(i)}$	Debye-Hückel electrostatic energy for simulation i
$U^{DH*(i)}$	Reduced Debye-Hückel electrostatic energy for simulation i
U^{elec}	Total electrostatic energy of the electrolyte
$U^{elec(i)}$	Total electrostatic energy of a molecular dynamics electrolyte for simulation i
$U^{elec*(i)}$	Reduced total electrostatic energy of a molecular dynamics electrolyte solution for simulation i
$\overline{U}_{ip}$	Partial molar electrostatic energy with respect to ion pairs
$\overline{U}_{ip}^{\infty}$	Partial molar electrostatic energy with respect to ion pairs in the limit of infinite dilution
$\overline{U}_{ip}^{\infty *}$	Reduced partial molar electrostatic energy with respect to ion pairs in the limit of infinite dilution
$\overline{U}_{solv}$	Partial molar electrostatic energy with respect to solvent particles
$\overline{U}_{solv}^{\infty}$	Partial molar electrostatic energy with respect to solvent particles in the limit of infinite dilution

$\overline{U}_{solv}^{\infty *}$	Reduced partial molar electrostatic energy with respect to solvent particles in the limit of infinite dilution
V	Volume
V^*	Reduced volume
α	Damping parameter
δt	Molecular dynamics simulation time-step
δt^*	Reduced molecular dynamics simulation time-step
δ_s	Regression coefficient used to model the permittivity of an electrolyte
ϑ	Index value
$\gamma_{\pm}^{el}$	Mean-ionic activity coefficient
γ_i^{el}	Activity coefficient of species i due to the presence of an ionic-atmosphere
ϵ_{LJ}	Lennard-Jones well-depth maximum
ε	Permittivity
ε_0	Permittivity of vacuum
ε_r	Relative permittivity
$\varepsilon_{r,b}$	Relative permittivity calculated using the data from a block b
ε_s	Permittivity of the solvent
ε_s'	Partial derivative of the solvent permittivity with respect to the constant permittivity inverse-Debye length at infinite dilution
ε_s''	Partial double derivative of the solvent permittivity with respect to the constant permittivity inverse-Debye length at infinite dilution
ε_{sm}	Permittivity of surrounding medium
θ	Angular coordinate
$\theta_{\mathbf{ab}}$	Angle between the $\mathbf{a}$ and $\mathbf{b}$ vectors
κ	Inverse Debye length with changing permittivity
κ_0	Inverse Debye length at constant permittivity
λ	Fraction of the final charge the ions have at a particular stage of the partial integration process
μ	Magnitude of a dipole moment vector
μ_i	Chemical potential of species i
μ_i^{el}	Chemical potential contribution of species i due to the presence of an ionic-atmosphere
μ_i^o	Chemical potential reference state of species i
μ_s	Magnitude of the dipole moment of solvent particles
μ_s^*	Reduced magnitude of the dipole moment of solvent particles
$\mu_{s,i}^{(k)*}$	Reduced dipole moment of a particle i in the k direction
ν_i	Stoichiometric coefficient of a reaction of species i
ξ	Variable that is independent of a variable x

ρ	Number density
ρ^*	Reduced number density
ϱ	Electric charge density
σ	Collision diameter
χ_i	Auxiliary function for an ion species i
ψ	Electrostatic potential
ψ_i	Electrostatic potential at a distance r from an ion i
ψ_i^{el}	Electrostatic potential at a distance r from an ion i due to the ionic-atmosphere
$\psi_i^{el,ion}$	Electrostatic potential experienced by an ion i due the ionic-atmosphere
ψ_i^{self}	Electrostatic potential at a distance r due to the central point-charge of an ion i
φ	Angular coordinate
Ω_i	Angular coordinate of particle i
$\langle P \rangle$	Ensemble average of a property P
$\langle P \rangle_b$	Ensemble average of a property P for simulation block b
$\mathbf{k}$	Reciprocal-space integer coordinates
$\mathbf{k}_{cut}$	Upper limit of reciprocal-space integer coordinates
$\mathbf{n}$	Normal vector to a surface
$\mathbf{m}$	Real-space integer coordinates
$\mathbf{m}_{cut}$	Upper limit of real-space integer coordinates
$\mathbf{r_i}$	Position vector of a particle i
$\mathbf{r_{ij}}$	Position vector of a particle j subtracted from a position vector of a particle i
$\mathbf{E}$	Electric field vector
$\mathbf{M}_s$	Solvent particles' contribution to the total dipole moment of an electrolyte solution
$\mathbf{M}_s^*$	Reduced solvent particles' contribution to the total dipole moment of an electrolyte solution
$\mathbf{M}_{s,j}^*$	Reduced solvent particles' contribution to the total dipole moment of an electrolyte solution at a time-step j
$\boldsymbol{\mu}$	Dipole moment vector
$\boldsymbol{\mu}_i$	Dipole moment of particle i
$\boldsymbol{\mu}_{s,i}$	Dipole moment of solvent particle i

List of Tables

List of Figures

Acronyms

DH	=	Debye–Hückel
MD	=	Molecular Dynamics
LJ	=	Lennard-Jones
WCA	=	Weeks–Chandler–Andersen
MSA	=	Mean Spherical Approximation
AMSA	=	Associative Mean Spherical Approximation

Preface

At the beginning of my master's thesis, I decided to investigate electrolytes' behavior in the limit of infinite dilution using molecular dynamics. In hindsight, I was naive to the large number of particles molecular dynamics simulations require to observe the limiting behavior of electrolytes by reducing the ion concentration. For context, Frank and Thompson [5] estimate that the Debye-Hückel theory breaks down for binary monovalent aqueous electrolytes at approximately 36 ions per million water molecules at room temperature. This work's molecular dynamics procedure is incapable of modeling electrolytes at this concentration for even a single cation and anion pair. Accordingly, this thesis aims to recover the infinite dilution behavior of electrolytes by other means than decreasing the ion concentration.

Chapter 1

Introduction

Without electrolyte solutions, the cells in our body would swell, proteins would denature, and life as we know it would be impossible [6]. Despite electrolytes being essential to life and present in most natural and industrial processes, modeling electrolyte solutions remains a difficult challenge with many unanswered questions. In a 2010 paper investigating the thermodynamic needs of the oil and gas, chemical, and pharmaceutical industries, Hendriks et al. [7] resonate this reality by concluding that "there is a need to bring electrolyte thermodynamic models to a level comparable to other fields." Many of the difficulties in modeling electrolyte solutions arise from the ions' long-ranged nature.

The long-range electrostatic interactions of ions ensure that electrolyte models require a more extensive thermodynamic framework than non-electrolyte systems. Prausnitz et al. [8] excellently summarizes the difference between electrolytes and non-electrolytes through an example; "When two ions are five (molecule) diameters apart, there is a strong interaction between them. However, when two uncharged molecules are five diameters apart, one molecule hardly knows that the other one is there." This long-ranged nature of ions leads to electrolyte-specific phenomena, such as ionization and electroneutrality, that electrolyte models need to consider.

A contested topic in the thermodynamic modeling community is how to incorporate the solvent in thermodynamic models [9]. There are two rivaling methods for representing the solvent, namely the primitive and non-primitive approaches. In the primitive approach, the solvent is a dielectric continuum characterized by a macroscopic static permittivity. Supporters of this method state that its simplistic representation of the solvent is the most promising strategy for obtaining models with few parameters that are practical for engineering purposes. Others advocate for a non-primitive approach where the solvent consists of molecules, stating that a realistic microscopic description is necessary for improving current electrolyte models. The non-primitive approach's explicit description of solvent-solvent and solvent-ion interactions does, however, significantly increase the models' complexity. For a review of different non-primitive and primitive electrolyte models, see the work of

Kontogeorgis et al. [9]. The role of the solvent in electrolyte models and the difference between non-primitive and primitive models are essential themes of this thesis.

The quintessential primitive model for electrolytes that incorporates the long-range interactions of ions is the Debye–Hückel (DH) theory. Although first published by Peter Debye and Erich Hückel in 1923, the theory is still the foundation for many state-of-the-art electrolyte models [9]. Debye–Hückel theory describes a single ion as a point-charge surrounded by an oppositely charged and linear Poisson–Boltzmann distributed ionic-atmosphere. Other ions are not treated as individual particles, but rather as contributors to this ionic atmosphere. The solvent, on the other hand, is a dielectric continuum characterized by a constant permittivity. Although many of the assumptions in Debye–Hückel are unphysical, such as the solvent having no microscopic structure, experimental results confirm that the theory correctly describes the thermodynamics of very dilute electrolyte solutions [10]. All correct electrolyte models should, therefore, converge towards Debye–Hückel thermodynamics in the limit of infinite dilution.

Since the time of Debye and Hückel, the invention of the computer and subsequent improvements in processing power, hardware, and software have lead to new techniques for modeling electrolyte solutions. Molecular modeling methods, such as molecular dynamics and Monte-Carlo simulations, predict the thermodynamics of a substance by specifying intermolecular forces and sampling thermodynamic averages over a large number of possible particle configurations in a simulation box. Electrolyte solutions require particular consideration in molecular modeling as, unlike for short-range interactions, the long-ranged interactions of the ions remain significant at the length scale of large simulation boxes [11]. One way of dealing with the long-range interactions is to use periodic boundary conditions where particles interact with periodic images of themselves. In popular lattice sum methods, such as Ewald summation, the particles interact with all periodic mirror images by calculating some of the long-range interactions in reciprocal space. In this work, molecular dynamics and Ewald summation is used to estimate the dielectric and thermodynamic properties of a simple non-primitive electrolyte model.

This thesis's objective is to investigate the asymptotic thermodynamic properties of dilute electrolyte solutions using a simplest-possible first-principle approach, with a large emphasis on the effects of representing the solvent as a (primitive) dielectric continuum or as having a (non-primitive) microscopic structure. Specifically, this work compares the asymptotic thermodynamic properties of the Debye–Hückel theory and a simple non-primitive electrolyte model. The objectives of this thesis can be summarized as:

1. To develop a simple first-principle non-primitive electrolyte model and investigate its dielectric properties using molecular dynamics.

2. To investigate when the Debye–Hückel theory's assumption that the solvent is a dielectric continuum of constant permittivity is valid.

3. To examine whether it is possible to recover the Debye–Hückel theory's behavior in the limit of infinite dilution from the molecular dynamics results of the non-primitive model.

This work consists of a thorough derivation of the Debye–Hückel theory, a description of the non-primitive electrolyte model, an explanation of how molecular dynamics can be used to estimate the non-primitive model's thermodynamic and dielectric properties, a description of various analysis techniques, as well as a discussion of the aforementioned objectives.

Chapter 2

Debye–Hückel Theory and a Non-Primitive Electrolyte Model

This thesis's objective is to investigate how representing the solvent using a primitive or non-primitive approach changes the dielectric and thermodynamic behavior of dilute electrolyte solutions. The two electrolyte models this work uses for this investigation are the Debye–Hückel theory and the non-primitive model presented in sections 2.1 and 2.2.

2.1 Debye–Hückel Theory

This section describes and derives the Debye–Hückel theory in three separate stages. Subsection 2.1.1 explains fundamental electrostatics. Subsection 2.1.2 presents the Debye–Hückel electrolyte model, as well as Debye and Hückel's original derivation of the electrostatic energy of an electrolyte solution. Subsection 2.1.3 derives the mean ionic activity coefficient of an electrolyte solution using a partial charging process.

2.1.1 Electrostatics

This subsection derives the Poisson equation with spherical symmetry used in Debye–Hückel theory from Gauss' Law. Unless otherwise specified, this subsection follows the work of Dobbs [12].

Gauss' law states that the total electric flux out of a closed surface S equals the total charge Q enclosed by it divided by the absolute permittivity ε;

$$\oiint_S \mathbf{E} \cdot \mathbf{n} \mathrm{d}S = \frac{Q}{\varepsilon}. \tag{2.1}$$

$\mathbf{E}$ is the electric field and $\mathbf{n}$ is the normal vector to the closed surface. Introducing the total electric charge density ϱ and applying the divergence theorem, Gauss' law can be expressed

in terms of volume integrals as

$$\iiint_V \nabla \cdot \mathbf{E} \mathrm{d}V = \iiint_V \frac{\varrho}{\varepsilon} \mathrm{d}V. \tag{2.2}$$

Since equation (2.2) is valid for any volume element, Gauss's law can be written in differential form as

$$\nabla \cdot \mathbf{E} = \frac{\varrho}{\varepsilon}. \tag{2.3}$$

For a static system, the electric field is related to the electrostatic potential ψ according to

$$\mathbf{E} = -\nabla\psi. \tag{2.4}$$

Substitution equation (2.4) into equation (2.3) leads to the Poisson's equation

$$\nabla^2\psi = -\frac{\varrho}{\varepsilon}, \tag{2.5}$$

which relates the electrostatic potential to the charge distribution of a system. Introducing the spherical Laplace operator

$$\nabla^2 = \frac{1}{r^2}\frac{\partial}{\partial r}\left(r^2\frac{\partial}{\partial r}\right) + \frac{1}{r^2\sin\theta}\frac{\partial}{\partial\theta}\left(\sin\theta\frac{\partial}{\partial\theta}\right) + \frac{1}{r^2\sin\theta}\frac{\partial^2}{\partial\varphi^2} \tag{2.6}$$

to equation (2.5), and assuming spherical symmetry in the θ and φ angular coordinate directions, leads to the Poisson equation with spherical symmetry

$$\frac{1}{r^2}\frac{\partial}{\partial r}\left(r^2\frac{\partial\psi}{\partial r}\right) = -\frac{\varrho}{\varepsilon}. \tag{2.7}$$

In equations (2.6) and (2.7) r is the distance from the origin of a spherical coordinate system. Equation (2.7) is the differential equation that is solved in Debye–Hückel theory.

2.1.2 Debye–Hückel Model and Electrostatic Potential

The following subsection introduces the Debye–Hückel model of electrolyte solutions and derives the Debye–Hückel electrostatic energy for completely dissociated electrolytes. Unless otherwise specified, this section follows Debye and Hückel's original 1923 article as translated by Michael J. Braus [13].

For an electrolyte solution that consists of s different ionic species, Debye–Hückel theory models an ion of species i as a sphere of radius a_i with a point charge of size $z_i q$ at its center. Here, z_i is the charge number of the ion, and q is the elementary charge. The inside and outside of the sphere are labeled the ion-exclusion zone and the ionic-atmosphere, respectively. This work refers to a_i as the ionic-atmosphere radius of species i. The ionic-atmosphere radius does not represent the true radius of the ion, but rather a mean distance to which the surroundings (positive and negative ions) can approach it. The solvent is a continuous dielectricum of permittivity ε_s and is present in both the ionic-atmosphere and ion-exclusion zone. Figure 2.1 illustrates this electrolyte model.

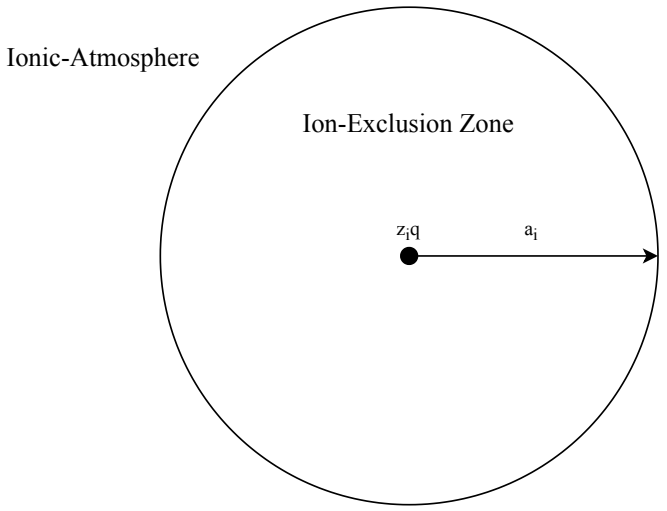

Figure 2.1: An illustration of the electrolyte model used in Debye–Hückel theory. The ion is modelled as a sphere of radius a_i where a_i indicates some mean distance to which the surroundings can approach the ion. At the center of the the ion-exclusion zone is a point charge of size $z_i q$. All other ions are represented by an oppositely charged surrounding ionic-atmosphere. The solvent is present in both the ion-exclusion zone and ionic-atmosphere. This figure does not attempt to represent the charge distribution in the ionic-atmosphere.

Assigning the center of an ion of species i as the origin, the spherically symmetric Poisson expression from equation (2.7) becomes

$$\frac{1}{r^2}\frac{\partial}{\partial r}\left(r^2\frac{\partial \psi_i}{\partial r}\right) = -\frac{\varrho}{\varepsilon_s}, \tag{2.8}$$

where ψ_i is the electrostatic potential at a distance r from the center of an ion i. Equation (2.8) assumes that the ionic species has spherical symmetry such that any variations of the electrostatic potential in the angular θ and φ directions are negligible.

The Debye–Hückel theory's derivation of an expression for the electrostatic energy of an electrolyte solution consists of solving equation (2.8) for the electrostatic potential in the ion-exclusion zone and ionic-atmosphere separately, before combining the resulting expressions.

Electrostatic Potential of the Ion-Exclusion Zone

The first stage in estimating the electrostatic energy of an electrolyte solution is to calculate the electrostatic potential in the ion-exclusion zone ($0 \leq r \leq a_i$) due to the ionic-atmosphere. Since there is no charge in the ion-exclusion zone except for the central point-charge which is not considered a part of the ionic-atmosphere, the right hand side of

equation (2.8) is equal to zero;

$$\frac{1}{r^2}\frac{\partial}{\partial r}\left(r^2\frac{\partial\psi_i}{\partial r}\right) = 0. \tag{2.9}$$

The solution to equation (2.9) is

$$\psi_i = \frac{C_1}{r} + C_2, \tag{2.10}$$

where C_1 and C_2 are constants. The next step is to divide the total electrostatic potential in the ionic-exclusion zone into contributions due to the central point charge ψ_i^{self} and due to the ionic-atmosphere ψ_i^{el};

$$\psi_i = \psi_i^{self} + \psi_i^{el}. \tag{2.11}$$

Whereas the point-charge contribution can be calculated from the definition of electrostatic potential and Coulomb's law as

$$\psi_i^{self} = \frac{z_i q}{4\pi\varepsilon_s}\frac{1}{r}, \tag{2.12}$$

the ionic-atmosphere contribution is set equal to the constant

$$\psi_i^{el} = C_2. \tag{2.13}$$

Debye and Hückel do not justify why the ionic-atmosphere contribution is a constant, but their choice can be rationalized by considering the ionic-atmosphere as a set of infinitesimal, concentric, symmetric, and charged shells. By introducing the well known result that the potential inside a hollow charged shell is constant [14], the superposition principle of electric potentials ensures that total potential due to the ionic-atmosphere is also a constant [15]. Combining equations (2.11), (2.12), (2.13), the electrostatic potential of the ion-exclusion zone is

$$\psi_i = \frac{z_i q}{4\pi\varepsilon_s}\frac{1}{r} + C_2. \tag{2.14}$$

Electrostatic Potential of the Ionic-Atmosphere

The second stage in estimating the electrostatic energy of an electrolyte solution is to calculate the electrostatic potential of the ionic-atmosphere ($r > a_i$). The electric charge density in the ionic-atmosphere is equal to

$$\varrho = \sum_{i=1}^{s} n_i'(r) z_i q, \tag{2.15}$$

where $n_i'(r)$ is the number density of ionic species i at a distance r from a particular ion. A fundamental assumption in Debye–Hückel theory is that ions in an electrolyte solution are distributed according to a Boltzmann distribution. $n_i'(r)$ is thus related to the bulk density

$n_i = N_i/V$, where N_i is the number of particles of ionic species i in a volume V, through the expression

$$n_i'(r) = n_i e^{-\frac{w_i(r)}{k_\mathrm{B}T}}. \tag{2.16}$$

In equation (2.16) T and k_B are the temperature and the Boltzmann constant. $w_i(r)$ is the work required to move an ion of type i from $r = \infty$ where the electrostatic potential is zero to a distance r of the central ion where the potential is ψ_i. The work required to move a charged particle through an electric field is equal to the product of the charge and electrostatic potential difference;

$$w_i(r) = qz_i\psi_i. \tag{2.17}$$

Substituting this result and equation (2.16) into equation (2.15), the electric charge density is

$$\varrho = \sum_{i=1}^{s} n_i z_i q e^{-\frac{z_i q \psi_i}{k_\mathrm{B}T}}. \tag{2.18}$$

Substituting equation (2.18) into equation (2.8) leads to the Poisson–Boltzmann equation for a potential with spherical symmetry

$$\frac{1}{r^2}\frac{\partial}{\partial r}\left(r^2\frac{\partial\psi_i}{\partial r}\right) = -\frac{1}{\varepsilon_s}\sum_{i=1}^{s} n_i z_i q e^{-\frac{z_i q \psi_i}{k_\mathrm{B}T}}. \tag{2.19}$$

For sufficiently low ion concentrations the exponential can be approximated using a first-order Maclaurin expansion of the form

$$\exp \xi x = 1 + \xi x + \mathcal{O}(\xi^2 x^2), \tag{2.20}$$

where ξ is a constant. Neglecting second and higher-order terms, equation (2.19) becomes

$$\frac{1}{r^2}\frac{\partial}{\partial r}\left(r^2\frac{\partial\psi_i}{\partial r}\right) = -\frac{1}{\varepsilon_s}\sum_{i=1}^{s} n_i z_i q\left[1 - \frac{z_i q \psi_i}{k_\mathrm{B}T}\right]. \tag{2.21}$$

Electroneutrality guarantees that

$$\sum_{i=1}^{s} n_i z_i = 0, \tag{2.22}$$

such that the zeroth-order term in the expansion can be set to zero. Defining the inverse Debye length κ_0 from the expression

$$\kappa_0^2 = \frac{q^2}{\varepsilon_s k_\mathrm{B}T}\sum_{i=1}^{s} n_i z_i^2 = \frac{q^2}{\varepsilon_s k_\mathrm{B}TV}\sum_{i=1}^{s} N_i z_i^2, \tag{2.23}$$

equation (2.21) becomes

$$\frac{1}{r^2}\frac{\partial}{\partial r}\left(r^2\frac{\partial\psi_i}{\partial r}\right) = \kappa_0^2\psi_i. \tag{2.24}$$

Equation (2.24) is the differential equation that describes the electrostatic potential's distribution in the ionic-atmosphere. The solution to equation (2.24) is

$$\psi_i = C_3 \frac{e^{-\kappa_0 r}}{r} + C_4 \frac{e^{\kappa_0 r}}{r}, \tag{2.25}$$

where C_3 and C_4 are constants. Since the potential vanishes for large r, C_4 is necessarily equal to zero. Accordingly, the electrostatic potential of the ionic-atmosphere is

$$\psi_i = C_3 \frac{e^{-\kappa_0 r}}{r}. \tag{2.26}$$

Equation (2.26) demonstrates that $1/\kappa_0$ dictates the rate at which the ionic-atmosphere's charge magnitude decreases in the radial direction. Consequently, $1/\kappa_0$ is a measure of the thickness of the ionic-atmosphere. This thickness can be considered a type of average distance from the central ion where other ions make significant contributions to the ionic-atmosphere.

Combing the Electrostatic Potentials and Calculating the Electrostatic Energy

The final stage in estimating the electrostatic energy of an electrolyte solution is to combine the electrostatic potential expressions for the ion-exclusion zone and ionic-atmosphere;

$$\psi_i = \begin{cases} \frac{z_i q}{4\pi\varepsilon_s}\frac{1}{r} + C_2 & 0 < r \leq a_i \\ C_3 \frac{e^{-\kappa_0 r}}{r} & r > a_i \end{cases} \tag{2.27}$$

Boundary conditions at $r = a_i$ are necessary to calculate explicit expressions for C_2 and C_3. Maxwell's laws of electromagnetism guarantee that the electric field and electrostatic potential are constant across an interface of constant spatial permittivity [16]. Consequently, equation (2.4) demonstrates that both ψ_i and $\frac{\partial \psi_i}{\partial r}$ are continuous at $r = a_i$. Using these interface conditions leads to the system of equations

$$0 = \frac{z_i q}{4\pi\varepsilon_s}\frac{1}{a_i} + C_2 - C_3 \frac{e^{-\kappa_0 r}}{r} \tag{2.28a}$$

$$0 = -\frac{z_i q}{4\pi\varepsilon_s}\frac{1}{a_i^2} + C_3 \left[\frac{\kappa_0}{a_i} e^{-\kappa_0 a_i} + \frac{1}{a_i^2} e^{-\kappa_0 a_i}\right], \tag{2.28b}$$

which can be solved for C_2 and C_3 as

$$C_2 = -\frac{z_i q \kappa_0}{4\pi\varepsilon_s}\frac{1}{1+\kappa_0 a_i}, \tag{2.29}$$

and

$$C_3 = \frac{z_i q}{4\pi\varepsilon_s}\frac{e^{\kappa_0 a_i}}{1+\kappa_0 a_i}, \tag{2.30}$$

respectively. Substituting equation (2.29) and (2.30) into equation (2.27) leads to a final expression for the electrostatic potential surrounding an ion;

$$\psi_i = \begin{cases} \frac{z_i q}{4\pi\varepsilon_s}\frac{1}{r} - \frac{z_i q}{4\pi\varepsilon_s}\frac{\kappa_0}{1+\kappa_0 a_i} & 0 < r \leq a_i \\ \frac{z_i q}{4\pi\varepsilon_s}\frac{e^{\kappa_0 a_i}}{1+\kappa_0 a_i}\frac{e^{-\kappa_0 r}}{r} & r > a_i \end{cases} \tag{2.31}$$

The C_2 coefficient (see equation (2.13)) corresponds to the electrostatic potential experienced by an ion due to the ionic-atmosphere. Correspondingly, the electrostatic potential energy of a single ion due to the presence of an ionic-atmosphere u_i is

$$u_i = -\frac{z_i^2 q^2}{4\pi\varepsilon_s}\frac{\kappa_0}{1+\kappa_0 a_i}. \tag{2.32}$$

Summing over all ions in an electrolyte solution, the corresponding electrostatic potential energy for an electrolyte solution is

$$U^{DH} = \sum_{i=1}^{s}\frac{N_i u_i}{2} = -\sum_{i=1}^{s}\frac{N_i}{2}\frac{z_i^2 q^2}{4\pi\varepsilon_s}\frac{\kappa_0}{1+\kappa_0 a_i}. \tag{2.33}$$

This report refers to U^{DH} as the Debye–Hückel electrostatic energy of an electrolyte solution.

2.1.3 Helmholtz Energy and Mean Ionic Activity Coefficient

This section derives expressions for the Helmholtz energy of the electrolyte solution and the mean ionic activity coefficient due to the ionic-atmosphere introduced in the previous section. Michelsen and Mollerup [17] have demonstrated several inconsistencies in the original derivations of the Helmholtz energy by Debye and Hückel. This section will instead follow the partial charging process derivation of the Helmholtz energy as described by Michelsen and Mollerup [17] and Fowler and Guggenheim [18].

Fowler and Guggenheim [18] show that the Helmholtz energy due to the presence of an ionic-atmosphere A^{el} is equal to the electrical work required to charge each ion to the electrostatic potential they experience due to the ionic-atmosphere $\psi_i^{el,ion}$ at a constant temperature, volume, and composition. In section 2.1.2 this potential was found to equal the constant C_2;

$$\psi_i^{el,ion}(\kappa_0) = C_2 = -\frac{z_i q}{4\pi\varepsilon_s}\frac{\kappa_0}{1+\kappa_0 a_i}. \tag{2.34}$$

Consequently, the Helmholtz energy term is

$$A^{el} = \sum_{i=1}^{s}\int_0^1 N_i\psi_i^{el,ion}(\lambda\kappa_0)z_i q d\lambda, \tag{2.35}$$

where $\lambda \in [0,1]$ is the fraction of the final charge the ions have at a particular stage of the partial-charging process. Substituting $\psi_i^{el,ion}(\lambda\kappa_0)$ from equation (2.34) into equation (2.35) leads to

$$\begin{aligned} A^{el} &= -\sum_{i=1}^{s} \int_0^1 N_i \frac{\lambda z_i^2 q^2}{4\pi\varepsilon_s} \frac{\lambda\kappa_0}{1+\lambda\kappa_0 a_i} d\lambda \\ &= -\frac{k_{\mathrm{B}}TV}{4\pi \sum\limits_{j=1}^{s} N_j z_j^2} \sum_{i=1}^{s} \frac{N_i z_i^2}{a_i^3} \left[\ln\left(1+\kappa_0 a_i\right) - \kappa_0 a_i + \frac{1}{2}\left(\kappa_0 a_i\right)^2 \right] \\ &= -\frac{k_{\mathrm{B}}TV}{4\pi \sum\limits_{j=1}^{s} N_j z_j^2} \sum_{i=1}^{s} N_i z_i^2 \chi_i, \end{aligned} \tag{2.36}$$

where χ_i is the auxiliary function

$$\chi_i = \frac{1}{a_i^3} \left[\ln\left(1+\kappa_0 a_i\right) - \kappa_0 a_i + \frac{1}{2}\left(\kappa_0 a_i\right)^2 \right]. \tag{2.37}$$

Equation (2.36) is the final expression for the Helmholtz energy contribution due to an ionic-atmosphere in Debye–Hückel theory. The next step consists of differentiating equation (2.36) to find the expressions for the chemical potential and mean ionic activity coefficients. The chemical potential contribution of a species k due to the presence of an ionic-atmosphere μ_k^{el} is the partial derivative of A^{el} with respect to the number of k molecules at a constant temperature, volume, and composition of non k species;

$$\mu_k^{el} = \left(\frac{\partial A^{el}}{\partial N_k} \right)_{T,V,N_{i\neq j}}. \tag{2.38}$$

By applying the chain and product rules of differentiation, equation (2.38) can be expressed as the sum

$$\mu_k^{el} = \left(\frac{\partial A^{el}}{\partial N_k} \right)_{T,V,\chi_i} + \sum_{i=1}^{s} \left(\frac{\partial A^{el}}{\partial \chi_i} \right)_{T,V,N_i} \left(\frac{\partial \chi_i}{\partial \kappa_0} \right)_{T,V,N_i} \left(\frac{\partial \kappa_0}{\partial N_k} \right)_{T,V,N_{i\neq k}}. \tag{2.39}$$

All of the partial derivative terms in equation (2.39) can be calculated by differentiating previously derived expressions. The first-term in equation (2.39) can be calculated by

differentiating equation (2.36) as

$$\begin{aligned}\left(\frac{\partial A^{el}}{\partial N_k}\right)_{T,V,\chi_i} =& -\left\{\left[4\pi\sum_{j=1}^{s}N_j z_j^2\right]\left(\frac{\partial k_\mathrm{B}T\sum\limits_{i=1}^{s}N_i z_i^2\chi_i}{\partial N_k}\right)_{T,V,\chi_i}\right.\\ &\left.-\left[k_\mathrm{B}T\sum_{i=1}^{s}N_i z_i^2\chi_i\right]\left(\frac{\partial 4\pi\sum\limits_{j=1}^{s}N_j z_j^2}{\partial N_k}\right)_{T,V,\chi_i}\right\}\\ &\times\frac{1}{\left(4\pi\sum\limits_{j=1}^{s}N_j z_j^2\right)^2}\\ =& -\frac{k_\mathrm{B}Tz_k^2\chi_k}{4\pi\sum\limits_{j=1}^{s}N_j z_j^2}+\frac{k_\mathrm{B}Tz_k^2\sum\limits_{i=1}^{s}N_i z_i^2\chi_i}{4\pi\left(\sum\limits_{j=1}^{s}N_j z_j^2\right)^2}.\end{aligned} \tag{2.40}$$

Similarly, the second term from equation (2.39) is

$$\left(\frac{\partial A^{el}}{\partial \chi_i}\right)_{T,V,N_i} = -\frac{k_\mathrm{B}TV}{4\pi\sum\limits_{j=1}^{s}N_j z_j^2}N_i z_i^2. \tag{2.41}$$

The third and fourth terms in equation (2.39) are calculated by differentiating the definition of χ_i from equation (2.37) and κ_0 from equation (2.23) as

$$\left(\frac{\partial \chi_i}{\partial \kappa_0}\right)_{T,V,N} = \frac{1}{a_i^2}\left[\frac{1}{1+\kappa_0 a_i}+\kappa_0 a_i - 1\right] = \frac{1}{a_i^2}\frac{(\kappa_0 a_i)^2}{1+\kappa_0 a_i}, \tag{2.42}$$

and

$$\left(\frac{\partial \kappa_0}{\partial N_k}\right)_{T,V,\varepsilon_s} = \frac{\kappa_0}{2}\frac{z_k^2}{\sum\limits_{j=1}^{s}N_j z_j^2}. \tag{2.43}$$

Substituting equations (2.40), (2.41), (2.42), and (2.43) into equation (2.39) leads to the the final expression for μ_k^{el};

$$\begin{aligned}\mu_k^{el} =& \frac{k_\mathrm{B}TVz_k^2\sum_{i=1}^{s}N_i z_i^2\chi_i}{4\pi\left(\sum\limits_{j=1}^{s}N_j z_j^2\right)^2}-\frac{k_\mathrm{B}TVz_k^2}{4\pi\sum\limits_{j=1}^{s}N_j z_j^2}\left(\chi_k\right.\\ &\left.+\frac{\kappa_0}{2\sum\limits_{j=1}^{s}N_j z_j^2}\sum_{i=1}^{s}N_i z_i^2\frac{1}{a_i^2}\frac{(\kappa_0 a_i)^2}{1+\kappa_0 a_i}\right).\end{aligned} \tag{2.44}$$

For a binary system, where the ionic species have the same ionic-atmosphere radius a, equation (2.44) simplifies to

$$\mu_k^{el} = -\frac{k_\mathrm{B}TVz_k^2}{4\pi(N_+z_+^2 + N_-z_-^2)}\left(\frac{\kappa_0}{2}\frac{1}{a^2}\frac{(\kappa_0 a)^2}{1+\kappa_0 a}\right). \tag{2.45}$$

The subscripts $k = \{+, -\}$ denote the cation and anion respectively. Expressing $(N_+z_+^2 + N_-z_-^2)$ in equation (2.45) in terms κ_0 using its definition from equation (2.23) leads to

$$\mu_k^{el} = -\frac{z_k^2 q^2}{8\pi\varepsilon_s}\frac{\kappa_0}{1+\kappa_0 a}. \tag{2.46}$$

Chemical potentials are often expressed in terms of reference chemical potentials. In the unsymmetrical reference case, the chemical potential of a solute species i is expressed in terms of the chemical potential of the solute in the solvent at infinite dilution μ_i^o [19]. For ideal solutions the chemical potential becomes;

$$\mu_i = \mu_i^o + k_\mathrm{B}T\ln(x_i). \tag{2.47}$$

For non-ideal solutions it is required to introduce an activity coefficient γ_i that accounts for non-ideal behavior such that

$$\mu_i = \mu_i^o + k_\mathrm{B}T\ln(\gamma_i x_i). \tag{2.48}$$

In equations (2.47) and (2.48) x_i is the mole fraction of species i in the solution. Recognizing that μ_i^{el} represents a departure from ideal behavior, the corresponding activity coefficient γ_k^{el} can be defined from equation (2.48) as

$$\mu_k^{el} = k_\mathrm{B}T\ln(\gamma_k^{el}). \tag{2.49}$$

Substituting equation (2.46) into equation (2.49) leads to;

$$\ln(\gamma_k^{el}) = -\frac{z_k^2 q^2}{8\pi k_\mathrm{B}T\varepsilon_s}\frac{\kappa_0}{1+\kappa_0 a}. \tag{2.50}$$

The single ion activity coefficients in equation (2.50) cannot be measured experimentally. It is therefore common to define a mean ionic activity coefficient, which for a binary salt $\mathrm{C}_{\nu_+}\mathrm{D}_{\nu_-}$ that dissociates according to the expression $\mathrm{C}_{\nu_+}\mathrm{D}_{\nu_-} \rightarrow \nu_+\mathrm{C}^{z_+} + \nu_-\mathrm{D}^{z_-}$ is defined as

$$\ln\left(\gamma_\pm^{el}\right) = \frac{\nu_+\ln(\gamma_+^{el}) + \nu_-\ln(\gamma_-^{el})}{\nu_+ + \nu_-}. \tag{2.51}$$

Substituting equation (2.50) into equation (2.51) leads to

$$\ln\left(\gamma_\pm^{el}\right) = -\frac{q^2}{8\pi k_\mathrm{B}T\varepsilon_s}\frac{\kappa_0}{1+\kappa_0 a}\left(\frac{\nu_+z_+^2 + \nu_-z_-^2}{\nu_+ + \nu_-}\right). \tag{2.52}$$

The electroneutrality condition from equation (2.22) fulfills

$$\nu_+ z_+ = -\nu_- z_-, \tag{2.53}$$

such that equation (2.52) can be rewritten as

$$\begin{aligned} \ln\left(\gamma_{\pm}^{el}\right) &= -\frac{q^2}{8\pi k_{\mathrm{B}} T \varepsilon_s} \frac{\kappa_0}{1+\kappa_0 a} \left(\frac{-\nu_- z_- z_+ - \nu_+ z_+ z_-}{\nu_+ + \nu_-} \right) \\ &= -\frac{q^2}{8\pi k_{\mathrm{B}} T \varepsilon_s} \frac{\kappa_0}{1+\kappa_0 a} \| z_+ z_- \|. \end{aligned} \tag{2.54}$$

Performing a Taylor expansion of $\ln\left(\gamma_{\pm}^{el}\right)$ in equation (2.54) about $\kappa_0 = 0$ leads to the mean ionic activity series expansion expression that is used in this work;

$$\ln(\gamma_{\pm}^{el}) = -\frac{q^2 \| z_+ z_- \|}{8\,\varepsilon_s\,\pi\,k_{\mathrm{B}} T} \kappa_0 + \frac{q^2 a \| z_+ z_- \|}{8\,\varepsilon_s\,\pi\,k_{\mathrm{B}} T} {\kappa_0}^2 - \frac{q^2 a^2 \| z_+ z_- \|}{8\,\varepsilon_s\,\pi\,k_{\mathrm{B}} T} {\kappa_0}^3 + O\left({\kappa_0}^4\right). \tag{2.55}$$

For sufficiently dilute electrolyte solutions equation (2.55) simplifies to

$$\ln(\gamma_{\pm}^{el}) = -\frac{q^2 \| z_+ z_- \|}{8\,\varepsilon_s\,\pi\,k_{\mathrm{B}} T} \kappa_0. \tag{2.56}$$

Equation (2.56) is known as the Debye–Hückel limiting law.

2.2 Non-Primitive Electrolyte Model

This section describes the simple non-primitive electrolyte model that this work investigates and compares to the primitive Debye–Hückel theory in subsequent sections.

One of the the simplest models for a solvent particle is that of the Stockmayer particle. A Stockmayer particle interacts according to the Lennard-Jones (LJ) potential with an embedded point-dipole at its center [20]. The Lennard-Jones potential is a potential that models both the repulsion and dispersion forces observed between neutral atoms [21]. The Lennard-Jones potential between particles i and j is

$$u_{ij}^{LJ} = 4\epsilon_{LJ} \left[\left(\frac{\sigma}{r_{ij}} \right)^{12} - \left(\frac{\sigma}{r_{ij}} \right)^{6} \right], \tag{2.57}$$

where σ is the collision diameter of the particles and $-\epsilon_{LJ}$ is the minimum value of the potential. Similar to the Stockmayer representation of a solvent particle, a simple model for an ion is that of the charged Lennard-Jones particle. A charged Lennard-Jones particle interacts according to the Lennard-potential with a point-charge at its center. The pair potential experienced between particles i and j in a system of charged Lennard-Jones particles and Stockmayer particles is

$$u_{ij} = u_{ij}^{LJ} + u_{ij}^{cc} + u_{ij}^{cd} + u_{ij}^{dc} + u_{ij}^{dd}, \tag{2.58}$$

where u_{ij}^{LJ}, u_{ij}^{cc}, u_{ij}^{cd}, u_{ij}^{dc} and u_{ij}^{dd} are the Lennard-Jones, charge-charge, charge-dipole, dipole-charge and dipole-dipole interaction terms, respectively. Some of the terms in equation (2.58) are zero depending on whether particles i and j correspond to Stockmayer or charged Lennard-Jones particles. For example, if particle i is a charged Lennard-Jones particle and particle j is a Stockmayer particle, then the pair potential is

$$u_{ij} = u_{ij}^{LJ} + u_{ij}^{cd}. \tag{2.59}$$

Pair potential expressions for the interactions between point-charges and point-dipoles can be found from classical electrostatics as

$$u_{ij}^{cc} = \frac{z_i z_j q^2}{4\pi\varepsilon_0} \frac{1}{r_{ij}}, \tag{2.60}$$

$$u_{ij}^{cd} = \frac{z_i q}{4\pi\varepsilon_0} \frac{\boldsymbol{\mu}_j \cdot \mathbf{r}_{ij}}{r_{ij}^3}, \tag{2.61}$$

$$u_{ij}^{dc} = -\frac{z_j q}{4\pi\varepsilon_0} \frac{\boldsymbol{\mu}_i \cdot \mathbf{r}_{ij}}{r_{ij}^3}, \tag{2.62}$$

and

$$u_{ij}^{dd} = \frac{1}{4\pi\varepsilon_0 r_{ij}^3} \left[\boldsymbol{\mu}_i \cdot \boldsymbol{\mu}_j - 3\frac{(\boldsymbol{\mu}_i \cdot \mathbf{r}_{ij})\,(\mathbf{r}_{ij} \cdot \boldsymbol{\mu}_j)}{r_{ij}^2} \right] \tag{2.63}$$

[22][23][24]. $\boldsymbol{\mu}_i$, $\mathbf{r}_i$, $\mathbf{r}_{ij}$, r_{ij}, and ε_0 are the dipole moment of a particle i, the position of a particle i, the position of a particle j subtracted from the position of a particle i ($\mathbf{r}_{ij} \equiv \mathbf{r}_i - \mathbf{r}_j$), the distance between the particles i and j ($r_{ij} \equiv \|\mathbf{r}_{ij}\|$), and the vacuum permittivity, respectively. A similar model to that presented in equation (2.58) is

$$u_{ij} = u_{ij}^{WCA} + u_{ij}^{cc} + u_{ij}^{cd} + u_{ij}^{dc} + u_{ij}^{dd}, \tag{2.64}$$

where the Lennard-Jones potential is replaced by the Weeks–Chandler–Andersen (WCA) potential

$$u_{ij}^{WCA} = \begin{cases} 4\epsilon_{LJ}\left[\left(\frac{\sigma}{r_{ij}}\right)^{12} - \left(\frac{\sigma}{r_{ij}}\right)^{6}\right] + \epsilon_{LJ} & r \leq 2^{1/6} \\ 0 & r > 2^{1/6} \end{cases}. \tag{2.65}$$

The WCA potential is essentially the repulsive part of the Lennard-Jones potential shifted upwards by ϵ_{LJ} [25]. Figure 2.2 illustrates both the Lennard-Jones and WCA potentials as a function of inter-particle separation.

Both the Lennard-Jones and WCA based electrolyte models presented in this section are used in the work. The Lennard-Jones model from equation (2.58) is used to compare results with literature values and verify the molecular dynamics and post-processing results. The WCA model from equation (2.64) is the primary model used to investigate the thermodynamic and dielectric properties of electrolyte solutions.

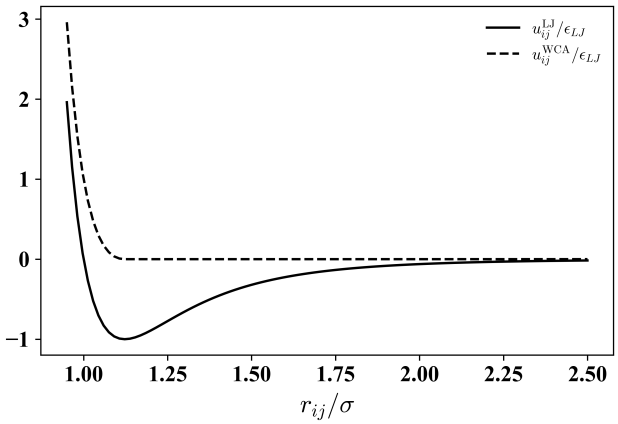

Figure 2.2: The Lennard-Jones (solid line) and Weeks-Chandler-Andersen (dashed line) potentials as a function of inter-particle separation.

There are several pairwise-potentials that could have been used instead of the WCA potential. The WCA potential is used in this thesis as it is a purely repulsive potential that is closely related to the Lennard-Jones potential. A purely repulsive potential is desirable as it ensures that all effects due to attractive terms can be attributed to attractive electrostatic interactions. Furthermore, the similarity between the WCA and Lennard-Jones potentials ensures an easy implementation of the model in third-party molecular dynamics software such as LAMMPS.

This work deals with molecular dynamics of strong electrolytes that consist of a solvent, an anion, and a cation species. Specifically, this works focuses on electrolyte solutions where the collision diameter and well depths are assumed to be the same for all interactions between cations, anions, and solvent particles. Furthermore, the charge of the anion and cation species is restricted to the case when they are equal in magnitude. This restriction, due to electroneutrality, leads to a model with the same number of anions and cations.

Some variables and parameters are not explicit in the pair potentials from equations (2.58) and (2.65), but necessary to model the electrolyte solution using molecular dynamics. These variables and parameters include:

- The mass of the anion, cation, and solvent particles. The mass of the particles are necessary to calculate the displacement of particles during molecular dynamics simulations. All of the particles are assumed to have the same mass m.

- The moment of inertia of the solvent particles I_s is necessary for calculating angular displacements.

- The ensemble temperature. During molecular dynamics simulations, the electrolyte solution's temperature is maintained using a thermostat and calculated using the equipartition theorem.

- The number density of the electrolyte solution ρ and the mole fraction of the ion and solvent particles in the solution. The number density of the electrolyte solution is defined as the total number of particles N_{tot}, divided by the volume of the electrolyte solution; $\rho = \frac{N_{tot}}{V}$. The number of particles can further be divided into the number of anions N_{an}, cations N_{cat}, ions $N_{ions} = N_{an} + N_{cat}$, and solvent particles N_{solv}. The mole fraction of ions and solvent particles are $x_{ions} = \frac{N_{cat}+N_{an}}{N_{tot}}$ and $x_{solv} = \frac{N_{solv}}{N_{tot}}$, respectively.

Section 3.1 gives a detailed explanation of how molecular dynamics is used to estimate thermodynamic properties for the simple non-primitive electrolyte model presented in this section.

Throughout this thesis, reduced Lennard-Jones units are used when modeling electrolyte solutions instead of real units. Lennard-Jones units use the particle mass m, collision diameter σ, the Lennard-Jones maximum well-depth ϵ_{LJ}, and the Coulomb constant $k_{\mathrm{C}} = \frac{1}{4\pi\varepsilon_0}$ [26] to scale physical quantities of interest. Table 2.1 summarizes the most important reduced quantities used in this work.

Table 2.1: A summary of the most important reduced properties used in this work.

Property	Property Symbol	Reduced Property Symbol	Reduced Property Definition
Temperature	T	T^*	$\frac{k_{\mathrm{B}}T}{\epsilon_{LJ}}$
Number density	ρ	ρ^*	$\rho\sigma^3$
Volume	V	V^*	$\frac{V}{\sigma^3}$
Time	t	t^*	$t\sqrt{\frac{\epsilon_{LJ}}{m\sigma^2}}$
Time-step	δt	δt^*	$\delta t\sqrt{\frac{\epsilon_{LJ}}{m\sigma^2}}$
Ion charge magnitude	$q_\pm$	$q^*_\pm$	$\frac{q_\pm}{[4\pi\varepsilon_0\sigma\epsilon_{LJ}]^{\frac{1}{2}}}$
Solvent particles' dipole moment magnitude	μ_s	μ^*_s	$\frac{\mu_s}{[4\pi\varepsilon_0\sigma^3\epsilon_{LJ}]^{\frac{1}{2}}}$
Solvent particles' moment of inertia	I_s	I^*_s	$\frac{I_s}{m\sigma^3}$
Dipole moment of a solution due to solvent particles	$\mathbf{M}_s$	$\mathbf{M}^*_s$	$\frac{\mathbf{M}_s}{[4\pi\varepsilon_0\sigma^3\epsilon_{LJ}]^{\frac{1}{2}}}$
Inverse Debye length	κ_0	κ^*_0	$\kappa_0\sigma$
Ionic-atmosphere radius	a	a^*	$\frac{a}{\sigma}$
Debye–Hückel electrostatic energy	U^{el}	U^{el*}	$\frac{U^{el*}}{\epsilon_{LJ}}$
Total electrostatic energy	U^{elec}	U^{elec*}	$\frac{U^{elec*}}{\epsilon_{LJ}}$

Chapter 3

Molecular Dynamics Simulations and Post-Processing Techniques

The subsequent sections describe the molecular dynamics and post-processing procedure this work uses to observe the non-primitive electrolyte model's dielectric and thermodynamic behavior. Whereas section 3.1 describes the molecular dynamics simulation procedure, section 3.2 explains the various post-processing techniques used to analyze the molecular dynamics data.

3.1 Molecular Dynamics Simulations

This section describes how the non-primitive model from section 2.2 was implemented and its thermodynamic properties evaluated using the open-source LAMMPS molecular dynamics software [27]. This section summarizes the choices made during the modeling process, rather than extensively describe LAMMPS' molecular dynamics implementation.

Figure 3.1 summarizes the different stages in this works' molecular dynamics procedure. These stages are:

1. **Initialization Stage** Specify the initial positions and velocities of the particles, the pair-potentials, particle properties, and boundary conditions used in the molecular dynamics simulation.

2. **Calibration Stage** Perform a predetermined number of molecular dynamics time-steps until the system has reached equilibrium at a desired temperature in the canonical ensemble. A molecular dynamics time-step consists of calculating the force experienced by the particles (from the pair-potentials) and updating the particle coordinates and velocities using a numerical integrator scheme. A molecular dynamics simulation in the canonical ensemble requires a thermostat for temperature control.

3. **Calculation Stage** Perform a large number of molecular dynamics time-steps in the canonical ensemble, where thermodynamic properties and particle coordinates are dumped at regular intervals.

4. **Post-Processing Stage** Estimate the thermodynamic ensemble averages from the data dumped during the calculation stage and perform additional analysis techniques.

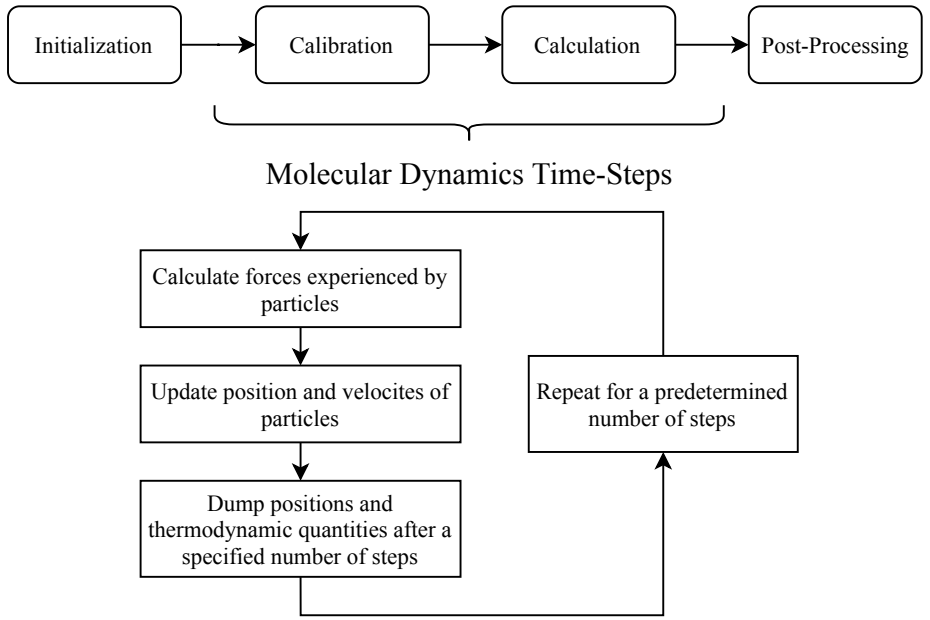

Figure 3.1: A flowchart of the different stages used when modeling the non-primitive electrolyte model from section 2.2 using the LAMMPS molecular dynamics software. The four primary steps are the initialization, calibration, calculation, and post-processing stages. The calibration and calculation stages consist of performing a large number of molecular dynamics time-steps. One molecular dynamics time-step consists of calculating the force experienced by each particle, updating the particle's coordinates and velocities, and occasionally dumping quantities of interest.

The remainder of this section describes how this work implements each of these stages using LAMMPS.

Initialization Stage

The purpose of the initialization stage is to specify all of the particle and simulation box parameters, as well as to initialize the particles' coordinates and velocities.

The first step in the initialization stage is to assign all of the parameters necessary to specify a particular non-primitive electrolyte from section 2.2. Electrolyte model parameters that need to be specified include the number of ions, the number of solvent particles, the number

density, the magnitude of the ions' charge, the magnitude of the solvent particles' dipole moment, the solvent particles' moment of inertia, the ensemble temperature at equilibrium, and the pair-potentials. Table 3.1 summarizes the parameters used to model non-primitive electrolyte solutions in this work. Appendix A show the LAMMPS scripts that were used to model system 1 from table 3.1 for 10 cations and 10 anions.

Table 3.1: A summary of the non-primitive electrolyte solutions this work studies using molecular dynamics. The second column indicates whether the system uses a WCA or a Lennard-Jones soft-core interaction between the particles. Sequence A indicates that the system was studied for 0, 1, 2, 3, 5, 7, 10, 15, 25, and 50 ion-pairs. Sequence B indicates that the system was studied for 0, 2, 4, 6, 10, 14, 20, 30, 50, and 100 ion-pairs. Sequence C indicates that the system was studied for a total of 8, 16, 32, 64, 128, 256, and 512 number of particles.

System	Potential	ρ^*	N_{tot}	N_{cat} and N_{an}	$q^*_{\pm}$	μ^*_s	I^*_s	T^*
1	LJ	0.8	256	Sequence A	8.0	1.8	0.025	1.35
2	WCA	0.8	256	Sequence A	8.0	1.8	0.025	1.35
3	WCA	0.6	256	Sequence A	8.0	1.8	0.025	1.35
4	WCA	0.8	256	Sequence A	8.0	1.5	0.025	1.35
5	WCA	0.8	512	Sequence B	8.0	1.8	0.025	1.35
6	WCA	0.8	256	128	8.0	–	0.025	1.35
7	WCA	0.8	256	Sequence A	1.0	1.8	0.025	1.35
8	WCA	0.8	256	Sequence A	0.2	1.8	0.025	1.35
9	WCA	0.8	256	Sequence A	8.0	1.8	0.025	13.5
10	WCA	0.8	256	Sequence A	8.0	1.8	0.025	135
11	WCA	0.8	Sequence C	0	–	1.8	0.025	1.35
12	WCA	0.8	256	Sequence A	0.2	0.05	0.025	1.35

This work uses cubic periodic boundary conditions where the inner box is replicated in the x, y, and z directions. The next subsection discusses how the pair-potentials from section 2.2 were specified in LAMMPS.

The positions of the particles are initialized to random coordinates in the simulation box, and then adjusted iteratively using the LAMMPS MINIMIZE energy minimization procedure [28]. This energy minimization procedure ensures that the particles do not overlap at the start of the molecular dynamics simulations. The velocities of the particles are initialized to a Maxwell-Boltzmann distribution that corresponds to a temperature. The dipole moments of the solvent particles are initialized to random directions.

Molecular Dynamics Simulation Time-Step

Both the calibration and calculation stages consist of iterating over a large number of time-steps. This subsection describes what constitutes a molecular dynamics time-step.

A molecular dynamics time-step consists of calculating the force acting on each particle from the pair potentials and particle configurations, before using an integration scheme to estimate the particle configurations and velocities after a time-step δt. This work uses LAMMPS' NVE/SPHERE integrator [29] with a reduced time-step of $\delta t^* = 0.0025$ for all systems in table 2.2, except for system 10 which uses a reduced time-step of $\delta t^* = 0.00025$ due to a higher temperature. This integrator updates both the translational and angular coordinates and velocities of the particles using a velocity Verlet based procedure.

LAMMPS' PAIR_STYLE LJ/CUT/DIPOLE/LONG [30] command is used to specify the pair-potential from equation (2.58) and (2.64). LAMMPS treates forces due to electrostatic interactions differently from those due to Lennard-Jones (and WCA) interactions.

The Lennard-Jones and WCA interactions are calculated by truncating the pair-potential at a distance r_{cut}. Unlike the WCA potential, where the pair-potential is by definition truncated at the Lennard-Jones potential minimum $r_{cut} = 2^{1/6}\sigma$, there is no best way of truncating the Lennard-Jones potential. This work truncates the Lennard-Jones potential at the arbitrary length $r_{cut} = 3.42\sigma$, which corresponds to half a simulation box length for a system of 256 particles at $\rho^* = 0.8$. At this separation, the Lennard-Jones particles experience less than 0.02% of the force the particles experience for a particle separation of $r = \sigma$. This work strictly uses simulations with a Lennard-Jones soft-core potential to verify the molecular dynamics and post-processing results. A cutoff of $r_{cut} = 3.42\sigma$ is adequate for this purpose.

The KSPACE_STYLE EWALD/DISP command [31] along with the aforementioned PAIR_STYLE LJ/CUT/DIPOLE/LONG command ensures that LAMMPS calculates all of the electrostatic forces and energies using a modified Ewald-summation procedure. This command requires the input of a largest tolerated error. This tolerated error is equal to 10^{-5} for all systems in table 3.1, with the exception of systems 8 and 12 where it is 10^{-7}. Section 3.2.2 gives a more detailed description of Ewald summation and how the largest tolerated error dictates several Ewald-summation parameters.

The ensemble temperature is calculated using the equipartition theorem, considering both translational and the solvent's rotational degrees of freedom. For molecular dynamics simulations in the canonical ensemble a temperature T^* is maintained using a thermostat. This work employs a Langevin thermostat through LAMMPS' FIX LANGUIVIN [32] command. The Langevin thermostat maintains a temperature by adding a friction and a random force to the individual particle forces. The magnitude of these frictional and random forces is dictated by a damping constant. This work follows LAMMPS' suggestion of using a damping constant of 100.

Calibration and Calculation Stages

The purpose of the calibration stage is to equilibrate the electrolyte from the initialization process to an electrolyte at a constant temperature T^*. Conversely, the calculation stage's objective is to sample the equilibrated electrolyte's thermodynamic properties for a large number of particle configurations over long time-periods. The sampled thermodynamic data can be used in the post-processing stage to estimate ensemble averages and other properties

of interest. Both the calibration and the calculation stages achieve their respective objectives by iterating over a large number of molecular dynamics time-steps.

The calibration stage consists in this report of two substages. The first substage consists of performing many molecular dynamics time-steps in the microcanonical (NVE) ensemble to equilibrate the system from the initialization process. The second substage consists of regulating the system's temperature to the desired simulation temperature by performing a molecular dynamics simulation in the canonical (NVT) ensemble. In this work, each of the calibration substages consists of 50 000 time-steps. This large number of time-steps ensures that the system has leveled off to where the system's energy is distributed equally between the various degrees of freedom after the calibration substages. In hindsight, instead of having two substages, the calibration process could consist of a single sufficiently long canonical ensemble simulation.

The calculation stage is responsible for sampling thermodynamic quantities of interest for a large number of possible particle configurations over long time-periods. In this work, the calculation stage consists of a canonical ensemble simulation of at least 250 000 time-steps. All simulations with less than 5 anions and 5 cations comprise of a calculation stage of at least 500 000 molecular dynamics time-steps. The particle coordinates and thermodynamic properties of interest are dumped every 100 time-steps.

Post-Processing Stage

The post-processing stage calculates ensemble averages and other properties of interest from the particle coordinates and thermodynamics data dumped during the calculation stage.

In molecular dynamics the thermodynamic ensemble average of a property P is estimated from its time average;

$$\langle P \rangle = \frac{1}{t_s} \sum_{i=1}^{t_s} P_i. \tag{3.1}$$

P_i is the value of property P at a particular time-step i. The average from equation 3.1 becomes increasingly accurate for averages performed over longer time-spans and a larger number of time-steps t_s.

A simulation can be split into N_{block} different blocks, where each block consists of 50 000 time-steps. In this work the particle coordinates and thermodynamic properties are dumped every 100 steps, such that each block contains $t_b = \frac{50000}{100} = 5000$ dumped time-steps. From equation (3.1) the ensemble average for a block b becomes

$$\langle P \rangle_b = \frac{1}{t_b} \sum_{i=1}^{t_b} P_i. \tag{3.2}$$

The ensemble average can be calculated from the block averages as

$$\langle P \rangle = \frac{1}{N_{\text{block}}} \sum_{b=1}^{N_{\text{block}}} \langle P \rangle_b. \tag{3.3}$$

Assuming that the different block ensemble averages are close to statistically independent, the uncertainty of $\langle P \rangle$ can be described by the standard deviation of the block averages;

$$\text{std}(\langle P \rangle) = \sqrt{\frac{1}{N_{block} - 1} \sum_{b=1}^{N_{block}} \left(\langle P \rangle_b - \langle P \rangle\right)^2}. \tag{3.4}$$

Sections 3.2.1 and 3.2.2 present additional post-processing techniques.

3.2 Post-Processing Techniques

This section describes the post-processing techniques this work uses to investigate the dielectric and thermodynamic behavior of the non-primitive model from section 2.2. Section 3.2.1 describes the procedure used to estimate the relative permittivity of the non-primitive model, and section 3.2.2 gives a short description of how to calculate the ion-ion electrostatic energy in a periodic system using Ewald summation. All of the post-processing methods were implemented in Python.

3.2.1 Relative Permittivity

Debye–Hückel theory characterizes the solvent in electrolyte solutions as a continuous dielectricum of constant permittivity. In reality, the solvent is not a continuous dielectricum but consists of a finite number of molecules. As such, the permittivity is strictly speaking a function of a solution's microscopic configurations. This section describes a post-processing method for estimating the relative permittivity of the non-primitive model from section 2.2 using the particle configurations dumped during the calculation stage of molecular dynamics simulations.

The relative permittivity ε_r is the ratio of a material's permittivity to that of a vacuum. An explicit and exact expression for the relative permittivity of a system with periodic boundary conditions, non-polarizable point-charge ions, and point-dipole solvent particles is

$$\varepsilon_r = 1 + \frac{\left\langle \mathbf{M}_s^2 \right\rangle - \langle \mathbf{M}_s \rangle^2}{3\varepsilon_0 V k_{\text{B}} T} \tag{3.5}$$

[33][34]. In equation (3.5) $\mathbf{M}_s$ is the sum of all the solvent particles' dipole-moments $\boldsymbol{\mu}_{s,i}$;

$$\mathbf{M}_s = \sum_{i=1}^{N_{solv}} \boldsymbol{\mu}_{s,i}. \tag{3.6}$$

This work refers to $\mathbf{M}_s$ as the solvent particles' contribution to the total dipole moment of an electrolyte solution. A thorough derivation of equation 3.5 is found in the works of

Levesque et al. [35].

Substituting the reduced temperature, volume and solvent particles' contribution to the total dipole moment of an electrolyte solution into equation (3.5), the Lennard-Jones unit equivalent of equation (3.5) is

$$\varepsilon_r = 1 + \frac{4\pi}{3V^*T^*}\left[\langle \mathbf{M}_s^{*2}\rangle - \langle \mathbf{M}_s^{*}\rangle^2\right]. \tag{3.7}$$

The remainder of this section describes the procedure this work uses to calculate the relative permittivity from equation (3.7) for a given molecular dynamics simulation. This procedure is inspired by that of the open-source PyLAT post-processing software [34]. The major steps used to calculate the relative permittivity are:

1. Perform a molecular dynamics simulation of the non-primitive model from section 2.2 using the method from section 3.1. During the calculation stage, dump the dipole moment of all solvent particles at regular intervals. The reduced dipole elements in the x, y and z directions for a particle i at a dumped time-step are denoted $\mu_{s,i}^{(x)*}$, $\mu_{s,i}^{(y)*}$, and $\mu_{s,i}^{(z)*}$, respectively.

2. Split the dumped dipole moment data from step 1 into blocks of 50 000 time-steps as described in section 3.1.

3. For each block, calculate the solvent's contribution to the total dipole moment of the electrolyte solution $\mathbf{M}_{s,j}^{*}$ at each dumped time-step j;

$$\mathbf{M}_{s,j}^{*} = \sum_{i=1}^{N_{solv}} \left[\mu_{s,i}^{(x)*}\mathbf{e}_x + \mu_{s,i}^{(y)*}\mathbf{e}_y + \mu_{s,i}^{(z)*}\mathbf{e}_z\right]. \tag{3.8}$$

   In equation (3.8) $\mathbf{e}_k$ is the unit vector for the coordinate $k \in (x, y, z)$. Introducing the solvent particles' contribution to the dipole moment of the system in a direction k as

$$M_{s,j}^{(k)*} = \sum_{i=1}^{N_{solv}} \mu_{s,i}^{(k)*}, \tag{3.9}$$

   the solvent particle's contribution to the total dipole moment of the electrolyte solution at a time-step j is equal to

$$\mathbf{M}_{s,j}^{*} = M_{s,j}^{(x)*}\mathbf{e}_x + M_{s,j}^{(y)*}\mathbf{e}_y + M_{s,j}^{(z)*}\mathbf{e}_z. \tag{3.10}$$

4. Calculate the block ensemble averages for the $\langle \mathbf{M}_s^{*2}\rangle$ and $\langle \mathbf{M}_s^{*}\rangle^2$ terms in equation (3.7). In section 2.2 the block ensemble average of a property P was introduced as the time-average

$$\langle P\rangle_b = \frac{1}{t_b}\sum_{j=1}^{t_b} P_j. \tag{3.11}$$

Substituting equation (3.10) into equation (3.11), and noting that the square of a vector is a dot product, the block averages $\langle \mathbf{M}_s^{*2} \rangle_b$ and $\langle \mathbf{M}_s^{*} \rangle_b^2$ are

$$\begin{aligned} \langle \mathbf{M}_s^{*2} \rangle_b &= \frac{1}{t_b} \sum_{j=1}^{t_b} \mathbf{M}_{s,j}^{*2} = \frac{1}{t_b} \sum_{j=1}^{t_b} \mathbf{M}_{s,j}^{*} \cdot \mathbf{M}_{s,j}^{*} \\ &= \frac{1}{t_b} \sum_{j=1}^{t_b} \left[\left(M_{s,j}^{(x)*} \right)^2 + \left(M_{s,j}^{(y)*} \right)^2 + \left(M_{s,j}^{(z)*} \right)^2 \right] \end{aligned} \tag{3.12}$$

and

$$\begin{aligned} \langle \mathbf{M}_s^{*} \rangle_b^2 &= \left[\frac{1}{t_b} \sum_{k=1}^{t_b} \mathbf{M}_{s,j}^{*} \right]^2 = \frac{1}{t_b^2} \left(\sum_{j=1}^{t_b} \mathbf{M}_{s,j}^{*} \right) \cdot \left(\sum_{i=j}^{t_b} \mathbf{M}_{s,j}^{*} \right) \\ &= \frac{1}{t_b^2} \left[\left(\sum_{j=1}^{t_b} M_{s,j}^{(x)*} \right)^2 + \left(\sum_{j=1}^{t_b} M_{s,j}^{(y)*} \right)^2 + \left(\sum_{j=1}^{t_b} M_{s,j}^{(z)*} \right)^2 \right], \end{aligned} \tag{3.13}$$

respectively. The relative permittivity block estimates $\varepsilon_{r,b}$ are calculated by substituting the ensemble averages from equations (3.12) and (3.13) into equation (3.7).

5. Estimate the relative permittivity by averaging over the block averages;

$$\varepsilon_r = \frac{1}{N_{block}} \sum_{b=1}^{N_{block}} \varepsilon_{r,b}. \tag{3.14}$$

The corresponding standard deviation the relative permittivity is

$$\text{std}(\varepsilon_r) = \sqrt{\frac{1}{N_{block} - 1} \sum_{b=1}^{N_{block}} \left(\varepsilon_{r,b} - \varepsilon_r \right)^2}. \tag{3.15}$$

Algorithm 1 shows this procedure in pseudo-code representaion.

Algorithm 1: Calculating the Relative Permittivity of the Non-Primitive Model

initialize MD system;
while *performing MD simulation* **do**
  dump $\mu_{s,i}^{(x)*}$, $\mu_{s,i}^{(y)*}$ and $\mu_{s,i}^{(z)*}$ for each solvent particle at specified time-step intervals;
end
split the dumped solvent dipole moment results into N_{block} blocks where each block spans 50000 time-steps;
for *all blocks* **do**
  for *all dumped time-steps* **do**
    calculate $M_{s,j}^{(k)*} = \sum_{i=1}^{N_{solv}} \mu_{s,i}^{(k)*}$ for $k \in (x, y, z)$;
  end
  Calculate $\langle \mathbf{M}_s^{*2} \rangle$ and $\langle \mathbf{M}_s^{*} \rangle^2$ for each block using equations (3.12) and (3.13). From the ensemble averages calculate the block estimates for the relative permittivity $\varepsilon_{r,b}$ using equation (3.7);
end
Use equations (3.14) and (3.15) to calculate the mean and standard deviations of the relative permittivity from the block estimates;

3.2.2 Ewald Summation

A significant problem with third-party software is that the developer's underlying implementation and assumptions are often complex and challenging to understand. An example of this is LAMMPS's parallelized and efficiency-oriented implementation of the Ewald-summation procedure that this work uses to calculate the electrostatic forces and energies in the molecular dynamics procedure from section 3.1. Accordingly, this section gives a short introduction to Ewald summation and describes a post-processing method for verifying that the LAMMPS molecular dynamic procedure is correctly implemented to calculate the same forces and energies as an ordinary Ewald summation procedure.

The total electrostatic energy U^{elec} of a system with cubic periodic boundary conditions is equal to the electrostatic energy experienced by the central system due to interactions with all periodic systems;

$$U^{elec} = \frac{1}{2} \sum_{\mathbf{m}}{}' \left[\sum_{i=1}^{N} \sum_{j=1}^{N} \phi \left(\mathbf{r}_{ij} + L\mathbf{m}, \mathbf{\Omega}_i, \mathbf{\Omega}_j \right) \right] \tag{3.16}$$

[36]. In equation (3.16) L is the length of the simulation box, ϕ is the electrostatic pair potential, and Ω_i is the angular coordinate of a particle i. The outer sum in equation (3.16) is over all periodic boxes with integer coordinates $\mathbf{m} = (m_x, m_y, m_z)$. The two inner sums in equation (3.16) calculate the electrostatic energy due to the interaction between the system in the central simulation box and the system in periodic box $\mathbf{m}$. The prime on the outer sum indicates that the $i = j$ interactions are not included when calculating the

electrostatic energy within the central simulation box for $\mathbf{m} = (0, 0, 0)$. For a system of point charges ϕ is equal to $\frac{q_i q_j}{4\pi\varepsilon_0 r}$, such that equation (3.16) becomes

$$U^{elec} = \frac{1}{2} \sum_{\mathbf{m}}{}' \left[\sum_{i=1}^{N} \sum_{j=1}^{N} \frac{q_i q_j}{4\pi\varepsilon_0 \|\mathbf{r}_{ij} + L\mathbf{m}\|} \right]. \tag{3.17}$$

The issue with the infinite sums from equations (3.16) and (3.17) is that they converge slowly and are only conditionally convergent [37]. Ewald summation solves this issue by expanding equations (3.16) and (3.17) into a short-ranged summation in real-space and a long-ranged summation in reciprocal space. The resulting Ewald summation expression for point-charges is

$$\begin{aligned} U^{elec} =& \frac{1}{2} \frac{1}{4\pi\varepsilon_0} \sum_{i=1}^{N} \sum_{j=1}^{N} \left[q_i q_j \left(\sum_{\mathbf{m}}{}' \frac{\operatorname{erfc}\left(\alpha \|\mathbf{r}_{ij} + \mathbf{m}\|\right)}{\|\mathbf{r}_{ij} + \mathbf{m}\|} \right.\right. \\ &+ \left.\left. \frac{1}{\pi L^3} \sum_{\mathbf{k} \neq 0} \frac{4\pi^2}{\|\mathbf{k}\|^2} \exp\left(-\frac{\pi^2 \|\mathbf{k}\|^2}{\alpha^2} \right) \cos\left(\mathbf{k} \cdot \mathbf{r}_{ij}\right) \right) \right] \\ &- \frac{\alpha}{\pi^{1/2}} \sum_{i=1}^{N} q_i^2 + \frac{2\pi}{\left(2\varepsilon_{sm} + 1\right) L^3} \left\| \sum_{i=1}^{N} q_i \mathbf{r}_i \right\|^2 \end{aligned} \tag{3.18}$$

[36]. In equation (3.18) α is a damping parameter with units of inverse-length, $\mathbf{k}$ are reciprocal vectors equal to $2\pi\mathbf{m}/L^2$, and ε_{sm} is the permittivity of the surrounding medium. The first two terms in equation (3.18) corresponds to the real-space and inverse-space sums, respectively. The third and fourth terms are a self-term and a dipolar term that accounts for interactions with a surrounding dielectric medium.

The electrostatic energy calculated from (3.18) depends on the damping parameter α, the upper limit of the real-space sums $\mathbf{m}_{cut}$, and the upper limit of the inverse-space sums $\mathbf{k}_{cut}$. Choosing the correct α, $\mathbf{m}_{cut}$ and $\mathbf{k}_{cut}$ parameters is essential for equation (3.18) to converge accurately and quickly [37]. Kolafa and Perram [38] have investigated the error due to truncating the sums from equation (3.18) at $\mathbf{m}_{cut}$ and $\mathbf{n}_{cut}$. Their investigation includes developing expressions that relate the upper limit sum values and the damping parameter to a largest tolerated error of the real and inverse-sum terms from equation (3.18). In LAMMPS $\mathbf{m}_{cut}$, $\mathbf{k}_{cut}$, and α are determined using similar largest-tolerated error expressions.

Allen and Tildesley [11] have implemented Fortran and Python scripts that calculate the electrostatic energy of a system of point-charges using equation (3.18). Their code treats the surrounding medium as a vacuum, such that $\varepsilon_{sm} = \varepsilon_0$. LAMMPS, on the other hand, treats the surrounding medium as a continuum of infinite permittivity such that the last term in equation (3.18) is zero.

This work modifies Allen and Tildesley's code to verify that a system of ions has been correctly implemented in LAMMPS (at least for the calculated electrostatic forces and

energies). Demonstrating that the implementation for a system of ions is correct suggests that the closely related implementation of the non-primitive electrolyte model from section 3.1 is also correct. The following changes have been made to Allen and Tildesley's code:

- The surrounding medium is changed to have an infinite permittivity by setting the last term in equation (3.18) equal to zero.
- LAMMPS' $\mathbf{m}_{cut}$, $\mathbf{k}_{cut}$ and α parameters are used.
- The code is modified to iterate over the particle coordinates dumped during the LAMMPS molecular dynamics simulations from section 3.1.

The average electrostatic energy calculated using LAMMPS and this post-processing procedure should equal for a correct LAMMPS implementation.

This post-processing procedure focuses on charge-charge interactions. A more rigorous test would be to extend this section's procedure to include charge-dipole and dipole-dipole interactions. This extension would allow for a direct comparison with the total electrostatic energies dumped during a LAMMPS simulation of an electrolyte, instead of the electrostatic energies for a closely related system of ions. Extending this section's procedure to charge-dipole and dipole-dipole interactions is left as future work.

Chapter 4

Analysis Techniques

The next sections describe the techniques this work uses to investigate the solvent's role in Debye–Hückel theory and the non-primitive electrolyte model from section 2.2 in the limit of infinite dilution. Section 4.1 derives a series expansion expression for the mean ionic activity coefficient using a Debye–Hückel inspired theory where the permittivity depends on the concentration of ions. Section 4.2 develops a method for recovering Debye–Hückel theory thermodynamics from the non-primitive model's molecular dynamics simulation results. The analysis techniques presented in sections 4.1 and 4.2 were conceived during this thesis.

4.1 Debye–Hückel Theory with a Concentration-Dependent Permittivity

In Debye–Hückel theory electrolyte solutions are modeled as ions in a continuous dielectric medium of constant permittivity. As will become apparent in the results and discussion section, both the permittivity of the non-primitive model and real electrolyte solutions tend to depreciate with increasing ion concentration. This observation raises the question of how Debye–Hückel theory would change if the permittivity is no longer constant but depends on the ion concentration. Erich Hückel first introduced the concept of extending the Debye–Hückel theory by characterizing the solvent using a permittivity that depends on the ion concentration in 1925 [18][39]. Many have followed-up on this concept, including Shilov and Lyashchenko [39] whose work inspired this section.

This section develops a method for investigating whether characterizing the solvent using an ion concentration-dependent permittivity changes the Debye–Hückel theory's thermodynamics in the limit of infinite dilution. Specifically, this section derives an expression for the mean ionic activity coefficient using the methodology from section 2.1, but without assuming that the permittivity is independent of the ion concentration. The resulting mean ionic activity coefficient series expansion expression is compared to the corresponding ion

concentration-independent case from section 2.1.3 in the results and discussion section. It is of particular interest to investigate whether the permittivity's ion concentration dependence results in a first-order contribution that should be included in the Debye–Hückel limiting law. Section 4.1.1 derives the previously discussed mean ionic activity coefficient expression. Section 4.1.2 develops a method for determining when Debye–Hückel theory predicts that the permittivity's ion concentration-dependence becomes non-negligible for a sodium chloride solution.

4.1.1 Mean Ionic Activity Coefficient Expression

This section derives an expression for the mean ionic activity coefficient for the Debye–Hückel model presented in section 2.1, but where the permittivity that characterizes the solvent depends on the ion concentration. This section restricts itself to an electrolyte solution of two ionic species with the same ionic-atmosphere radius a. This work follows the derivation of the mean ionic activity coefficient from section 2.1.3, but without assuming a constant permittivity. All of the derivatives and integrals from this section were performed or verified using the Maple mathematics software.

The electrolyte model used in this section differs from the original Debye–Hückel theory from section 2.1.2 in that the permittivity changes with the concentration of ions according to an arbitrary function

$$\varepsilon = f(\kappa_0), \tag{4.1}$$

that in the limit of infinite dilution converges to the permittivity of the pure solvent

$$\lim_{\kappa_0 \to 0} f(\kappa_0) = \varepsilon_s. \tag{4.2}$$

In the original Debye–Hückel theory the inverse Debye length κ_0 is defined by equation (2.23). Similarly, the inverse Debye-length for a system with an ion concentration-dependent permittivity κ is

$$\kappa^2 = \frac{q^2}{\varepsilon k_\mathrm{B} T V} \sum N_i z_i^2. \tag{4.3}$$

Clearly, from equations (2.23), (4.1), and (4.3), κ is related to κ_0 through the expression

$$\kappa(\kappa_0) = \kappa_0 \sqrt{\frac{\varepsilon_s}{f(\kappa_0)}}. \tag{4.4}$$

Following the partial charging process from section 2.1.3, the ion concentration-dependent equivalent of the Helmholtz energy expression from equation (2.35) is

$$A^{el} = \int_0^1 \left(-N_+ \frac{\lambda z_+^2 q^2}{4\pi f(\lambda\kappa_0)} \frac{\lambda\kappa}{1+\lambda\kappa a} - N_- \frac{\lambda z_-^2 q^2}{4\pi f(\lambda\kappa_0)} \frac{\lambda\kappa}{1+\lambda\kappa a} \right) d\lambda. \tag{4.5}$$

Using equation (4.3) to express $N_+ z_+^2 + N_- z_-^2$ in terms of κ and equation (4.4) to express κ in terms of κ_0, equation (4.5) becomes

$$A^{el} = \int_0^1 -\frac{k_B T V \lambda^2 {\kappa_0}^3 \varepsilon_s^{3/2}}{4 f(\kappa_0 \lambda)\, \pi \left(\lambda \kappa_0 \sqrt{\varepsilon_s} a + \sqrt{f(\kappa_0 \lambda)}\right)} d\lambda. \tag{4.6}$$

Unlike the derivation from section 2.1.3, a Taylor expansion about $\kappa_0 = 0$ is performed before the integration in order to simplify subsequent derivation steps. The Taylor expanded equivalent of equation (4.6) about $\kappa_0 = 0$ is

$$\begin{aligned} A^{el} = \int_0^1 & -\frac{k_B T V \lambda^2}{4\pi} \varepsilon_s^{\frac{3}{2}} f(0)^{-\frac{3}{2}} {\kappa_0}^3 \\ & + \left(\frac{k_B T V \lambda^3 a \varepsilon_s^2}{4\pi f(0)^2} + \frac{3 k_B T V \lambda^2 \left(\frac{\partial f(0)}{\partial \kappa_0}\right) \varepsilon_s^{\frac{3}{2}}}{8\pi} f(0)^{-\frac{5}{2}} \right) {\kappa_0}^4 \\ & + \left(-\frac{k_B T V \lambda^4 a^2}{4\pi} \varepsilon_s{}^{\frac{5}{2}} f(0)^{-\frac{5}{2}} - \frac{k_B T V \lambda^3 \left(\frac{\partial f(0)}{\partial \kappa_0}\right) \varepsilon_s^2 a}{2\pi f(0)^3} \right. \\ & + \frac{3 k_B T V \lambda^2 \left(\frac{\partial^2 f(0)}{\partial \kappa_0^2}\right) \varepsilon_s^{\frac{3}{2}}}{16\pi} f(0)^{-\frac{5}{2}} \\ & \left. - \frac{15 k_B T V \lambda^2 \left(\frac{\partial f(0)}{\partial \kappa_0}\right)^2 \varepsilon_s^{\frac{3}{2}}}{32\pi} f(0)^{-\frac{7}{2}} \right) {\kappa_0}^5 + O\left({\kappa_0}^6\right) d\lambda. \end{aligned} \tag{4.7}$$

In the limit where κ_0 goes to zero, equation (4.2) demonstrates that $f(\kappa_0)$ and $\left(\frac{\partial f(\kappa_0)}{\partial \kappa_0}\right)$ are independent of ion concentrations and λ values. Using the notation $\varepsilon_s = \lim_{\kappa_0 \to 0} f(\kappa_0)$, $\varepsilon_s' = \lim_{\kappa_0 \to 0} \left(\frac{\partial f(\kappa_0)}{\partial \kappa_0}\right)$, and $\varepsilon_s'' = \lim_{\kappa_0 \to 0} \left(\frac{\partial^2 f(\kappa_0)}{\partial \kappa_0^2}\right)$, equation (4.7) can be expressed as

$$\begin{aligned} A^{el} = \int_0^1 & -\frac{k_B T V \lambda^2}{4\ \pi} {\kappa_0}^3 + \left(\frac{k_B T V \lambda^3 a}{4\ \pi} + \frac{3\, k_B T V \lambda^2 \varepsilon_s'}{8 \varepsilon_s \pi} \right) {\kappa_0}^4 \\ & + \left(-\frac{k_B T V \lambda^4 a^2}{4\ \pi} - \frac{k_B T V \lambda^3 \varepsilon_s' a}{2 \varepsilon_s \pi} \right. \\ & \left. + \left(\frac{3\, k_B T V \lambda^2 \varepsilon_s''}{16 \varepsilon_s \pi} - \frac{15\, k_B T V \lambda^2 \varepsilon_s'^2}{32 \varepsilon_s^2 \pi} \right) {\kappa_0}^5 \right. \\ & + O\left({\kappa_0}^6\right) d\lambda. \end{aligned} \tag{4.8}$$

Integrating equation (4.8) yields the final expression for A^{el}

$$\begin{aligned} A^{el} = &- \frac{k_B T V}{12\,\pi}{\kappa_0}^3 + \left(\frac{k_B T V a}{16\,\pi} + \frac{k_B T V \varepsilon_s'}{8\varepsilon_s \pi}\right){\kappa_0}^4 \\ &+ \left(-\frac{k_B T V a^2}{20\,\pi} - \frac{k_B T V a}{8\varepsilon_s \pi} + \frac{k_B T V \varepsilon_s''}{16\varepsilon_s \pi}\right. \\ &\left. - \frac{5\,k_B T V {\varepsilon_s'}^2}{32\varepsilon_s \pi}\right){\kappa_0}^5 + O\left({\kappa_0}^6\right). \end{aligned} \tag{4.9}$$

The next step is to find the corresponding chemical potential contribution expression for a binary salt. The cation and anion species are denoted by $k = \{+, -\}$. Noting that equation (4.9) is only a function of κ_0, the chemical potential is

$$\mu_k^{el} = \left(\frac{\partial A^{el}}{\partial N_k}\right)_{T,V,N_{i\neq k}} = \left(\frac{\partial A^{el}}{\partial \kappa_0}\right)_{T,V} \left(\frac{\partial \kappa_0}{\partial N_k}\right)_{T,V,N_{i\neq k}}. \tag{4.10}$$

The first term on the right hand-side of equation (4.10) is found by taking the partial derivative of equation (4.9) with respect to κ_0;

$$\begin{aligned} \left(\frac{\partial A^{el}}{\partial \kappa_0}\right)_{T,V,N_{i\neq k}} = &- \frac{k_B T V}{4\,\pi}{\kappa_0}^2 + \left(\frac{k_B T V a}{4\,\pi} + \frac{k_B T V \varepsilon_s'}{2\varepsilon_s \pi}\right){\kappa_0}^3 \\ &+ \left(-\frac{k_B T V a^2}{4\,\pi} - \frac{5\,k_B T V \varepsilon_s' a}{8\varepsilon_s \pi}\right. \\ &\left. + \frac{5\,k_B T V \varepsilon_s''}{16\varepsilon_s \pi} - \frac{25\,k_B T V {\varepsilon_s'}^2}{32\varepsilon_s^2 \pi}\right){\kappa_0}^4 \\ &+ O\left({\kappa_0}^5\right). \end{aligned} \tag{4.11}$$

The partial derivative of κ_0 with respect to N_k is found by expressing the sum in equation (2.43) in terms of κ_0 as

$$\left(\frac{\partial \kappa_0}{\partial N_k}\right)_{T,V,N_{i\neq k}} = \frac{z_k^2 q^2}{2 k_B T V \varepsilon_s \kappa_0}. \tag{4.12}$$

Combining equations (4.10), (4.11), and (4.12), the resulting chemical potential expression is

$$\begin{aligned} \frac{\mu_k^{el}}{k_B T} = &- \frac{q^2 z_k^2}{8\,\varepsilon_s\,\pi\,k_B T}\kappa_0 + \frac{q^2 z_k^2\,(a\varepsilon_s + 2\varepsilon_s')}{8\,{\varepsilon_s}^2 \pi\,k_B T}{\kappa_0}^2 \\ &- \frac{q^2 z_k^2}{64\,{\varepsilon_s}^3 \pi\,k_B T}\left(8\varepsilon_s^2 a^2 + 20\varepsilon_s \varepsilon_s' a - 10\varepsilon_s \varepsilon_s'' + 25{\varepsilon_s'}^2\right){\kappa_0}^3 \\ &+ O\left({\kappa_0}^4\right). \end{aligned} \tag{4.13}$$

The corresponding mean ionic activity coefficient is, by introducing equation (4.13) to its definition from equation (2.51) and applying the electroneutrality condition from equation (2.53), equal to

$$\begin{aligned}\ln(\gamma_{\pm}^{el}) = &- \frac{q^2\|z_+z_-\|}{8\,\varepsilon_s\,\pi\,k_BT}\kappa_0 + \frac{q^2\|z_+z_-\|\,(a\varepsilon_s + 2\varepsilon_s')}{8\,{\varepsilon_s}^2\pi\,k_BT}{\kappa_0}^2 \\ &- \frac{q^2\|z_+z_-\|}{64\,{\varepsilon_s}^3\pi\,k_BT}\left(8\varepsilon_s^2a^2 + 20\varepsilon_s\varepsilon_s'a - 10\varepsilon_s\varepsilon_s'' + 25{\varepsilon_s'}^2\right){\kappa_0}^3 \\ &+ O\left({\kappa_0}^4\right).\end{aligned} \tag{4.14}$$

When the derivatives of ε_r are equal to zero, equation (4.14) corresponds to equation (2.55) which has been derived under the assumption of a constant permittivity.

4.1.2 Ratio Between First and Second Order Expansion Terms

This section develops a method for estimating when the Debye–Hückel theory predicts that the permittivity's ion concentration-dependence is no longer negligible. The first-order term of the mean ionic activity coefficient from equation (4.14) is the only expansion term that does not depend on whether the permittivity is ion concentration-dependent. Accordingly, the ratio between the second and first-order expansion terms is a rudimentary measure for whether the permittivity's ion concentration-dependence is negligible, at least for describing the mean ionic activity coefficient.

The first part of this section derives an expression for the ratio between the second and first-order terms for the mean ionic activity coefficient from section 4.1.1, as a function of the ionic-atmosphere radius, salt concentration, and the permittivity. The second part uses the resulting expression and experimental data to calculate the ratio between the second and first-order terms for a sodium chloride solution.

Ratio Expression

This section develops an expression for the ratio between the second and first-order mean ionic activity coefficient expansion terms from section 4.1.1.

The ratio between the first two expansion terms from equation (4.14) is

$$\frac{\text{Second-order term}}{\text{First-order term}} = (a + 2\frac{\varepsilon_s'}{\varepsilon_s})\kappa_0. \tag{4.15}$$

ε_s' can be written in terms of salt concentration c_s, by applying the chain rule to its definition, as

$$\varepsilon_s' = \lim_{\kappa_0\to 0}\left(\frac{\partial f(\kappa_0)}{\partial\kappa_0}\right) = \lim_{c_s\to 0}\left(\frac{\partial f\,(c_s)}{\partial c_s}\right)\left(\frac{\partial c_s}{\partial\kappa_0}\right). \tag{4.16}$$

The next step is to estimate $\left(\frac{\partial c_s}{\partial\kappa_0}\right)$. The inverse Debye-length from equation (2.23) can be rewritten as

$$\kappa_0^2 = \frac{F^2}{\varepsilon_s RT}\sum_{i=1}^{s} c_i z_i^2, \tag{4.17}$$

where $R = k_{\mathrm{B}} N_{\mathrm{A}}$ is the universal gas constant, N_{A} is Avogadro's number , $F = qN_{\mathrm{A}}$ is Faraday's constant, and $c_i = N_i/(VN_{\mathrm{A}})$ is the concentration of ionic species i. For a salt that dissociates according to the expression $\mathrm{C}_{\nu_1}\mathrm{D}_{\nu_2}\cdots\mathrm{S}_{\nu_s} \rightarrow \nu_1\mathrm{C}^{z_1} + \nu_2\mathrm{D}^{z_2} + \cdots + \nu_s\mathrm{S}^{z_s}$ the total salt concentration is related to the individual ion concentrations through the relationship

$$c_s = c_i/\nu_i, \tag{4.18}$$

such that equation (4.17) becomes

$$\kappa_0^2 = \frac{F^2 c_s}{\varepsilon_s RT} \sum_{i=1}^{s} \nu_i z_i^2, \tag{4.19}$$

or equivalently

$$c_s = \frac{\kappa_0^2 \varepsilon_s RT}{F^2 \sum_{i=1}^{s} \nu_i z_i^2}. \tag{4.20}$$

Taking the partial derivative of equation (4.20) with respect to κ_0;

$$\left(\frac{\partial c_s}{\partial \kappa_0}\right) = \frac{2\kappa_0 \varepsilon_s RT}{F^2 \sum_{i=1}^{s} \nu_i z_i^2} = \left(\frac{4 c_s \varepsilon_s RT}{F^2 \sum_{i=1}^{s} \nu_i z_i}\right)^{1/2}. \tag{4.21}$$

Substituting equation (4.21) into equation (4.16) and the resulting expression into equation (4.15) leads to the ratio expression

$$\begin{aligned} \frac{\text{Second-order term}}{\text{First-order term}} =& a\kappa_0 + \frac{4\kappa_0^2 RT}{F^2 \sum_{i=1}^{s} \nu_i z_i^2} \left(\frac{\partial f(c_s)}{\partial c_s}\right) \\ =& \sqrt{\frac{a^2 F^2 \sum_{i=1}^{s} \nu_i z_i^2}{\varepsilon_s RT}} c_s^{1/2} + \frac{4c_s}{\varepsilon_s} \lim_{c_s \rightarrow 0} \left(\frac{\partial f(c_s)}{\partial c_s}\right). \end{aligned} \tag{4.22}$$

For binary univalent salts that dissociate completely, $\sum_{i=1}^{s} \nu_i z_i^2 = 2$ such that equation (4.22) simplifies to

$$\frac{\text{Second-order term}}{\text{First-order term}} = \sqrt{\frac{2a^2 F^2}{\varepsilon_s RT}} c_s^{1/2} + \frac{4c_s}{\varepsilon_s} \lim_{c_s \rightarrow 0} \left(\frac{\partial f(c_s)}{\partial c_s}\right). \tag{4.23}$$

There are three unknowns that need to be estimated using experimental data to apply equation (4.23) to an electrolyte solution. These are the ionic-atmosphere radius, the permittivity of the pure solvent and the partial derivative of the permittivity with respect to concentration in the limit of infinite dilution.

Ratio Expression for a Sodium Chloride Solution

The final step in estimating the ratio between the first two expansion terms is introducing experimental estimates for the ionic-atmosphere radius, the permittivity of the pure solvent, and the partial derivative of the permittivity in limit of infinite dilution to equation (4.23).

This subsection uses a sodium chloride solution at $25^{\circ}\mathrm{C}$ as an example.

The first parameter to be estimated is the ionic-atmosphere radius for a sodium chloride solution a_{NaCl}. Ribeiro et al. [40] have compared different methods for estimating the ionic-atmosphere radius for a variety of sodium salts in aqueous solutions. The different methods include fitting a to activity and diffusion coefficient models, computer simulations, and experimental estimates. The estimated ionic-atmosphere radius varies greatly with the estimation method. For example, Ribeiro et al.'s a estimates for sodium chloride range between $2.4 \times 10^{-10}\,\mathrm{m}$ and $7.7 \times 10^{-10}\,\mathrm{m}$. Since there is no single right way of estimating the ionic-atmosphere radii, this report uses Kielland [41]'s method where a_{NaCl} is estimated as the average of the effective radii of the hydrated ionic species in the electrolyte. Ribeiro et al. state that Kielland's estimate for a_{NaCl} is a good option for thermodynamic calculations. Kielland's estimate for a_{NaCl} is

$$a_{\mathrm{NaCl}} = 3.6 \times 10^{-10}\,\mathrm{m}. \tag{4.24}$$

The next step is to estimate ε_s and $\lim\limits_{c_s \to 0}\left(\dfrac{\partial f(c_s)}{\partial c_s}\right)$ for an aqueous sodium chloride solution. Tikanen and Fawcett [42] have regressed the permittivity data of different aqueous solutions at $25^{\circ}\mathrm{C}$ to the function

$$f(c_s) = \varepsilon_s - \delta_s c_s + b_s c_s^{3/2} \tag{4.25}$$

Recognizing that in the low concentration limit

$$\lim_{c_s \to 0}\left(\frac{\partial f(c_s)}{\partial c_s}\right) = \lim_{c_s \to 0}\frac{f(c_s) - \varepsilon_s}{c_s - 0} = -\delta_s, \tag{4.26}$$

Tikanen and Fawcett's estimates for ε_s and $\lim\limits_{c_s \to 0}\left(\dfrac{\partial f(c_s)}{\partial c_s}\right)$ for sodium chloride are

$$\varepsilon_s = \lim_{c_s \to 0} f(c_s) = 78.4\,\varepsilon_0 \tag{4.27}$$

and

$$\lim_{c_s \to 0}\left(\frac{\partial f(c_s)}{\partial c_s}\right) = -\delta_s = \ -16.2 \times 10^3\,\varepsilon_0\,\mathrm{mol\,m^{-3}} \tag{4.28}$$

respectively.

Substituting equation (4.24), (4.27), and (4.28) into equation (4.23) leads to the final ratio expression;

$$\frac{\text{Second-order term}}{\text{First-order term}} = \left[\frac{0.03745}{\mathrm{mol}^{\frac{1}{2}}\ \mathrm{m}^{-\frac{3}{2}}}\right] c_s^{1/2} - \left[\frac{826.53}{\mathrm{mol\,m^{-3}}}\right] c_s \tag{4.29}$$

Using Ribeiro et al.'s lower and upper estimates for the ionic-atmosphere radius of sodium chloride, $2.4 \times 10^{-10}\mathrm{m}$ and $7.7 \times 10^{-10}\mathrm{m}$, leads to

$$\frac{\text{Second-order term}}{\text{First-order term}} = \left[\frac{0.02496}{\mathrm{mol}^{\frac{1}{2}}\ \mathrm{m}^{-\frac{3}{2}}}\right] c_s^{1/2} - \left[\frac{826.53}{\mathrm{mol\,m^{-3}}}\right] c_s \tag{4.30}$$

and

$$\frac{\text{Second-order term}}{\text{First-order term}} = \left[\frac{0.08009}{\text{mol}^{\frac{1}{2}}\ \text{m}^{-\frac{3}{2}}}\right] c_s^{1/2} - \left[\frac{826.53}{\text{mol m}^{-3}}\right] c_s \tag{4.31}$$

respectively. Equations (4.30) and (4.31) are rough lower and upper estimates for the ratios between between the second and first-order expansion terms.

4.2 Regression Method for Recovering the Debye–Hückel Theory from the Non-Primitive Model

This section develops the regression method this work uses to investigate if it is possible to recover the Debye–Hückel theory's thermodynamics in the limit of infinite dilution from the non-primitive model's molecular dynamics results. This section introduces the regression method over three subsections;

1. Subsection 4.2.1 interprets what the Debye–Hückel electrostatic energy corresponds to in the non-primitive electrolyte model from section 2.2.
2. Subsection 4.2.2 uses the Debye–Hückel electrostatic energy interpretation and the method of intercepts to set the framework for the regression method.
3. Subsection 4.2.3 describes the regression method.

4.2.1 Interpretation of the Debye-Hückel Electrostatic Energy

This subsection interprets what the Debye–Hückel electrostatic energy from equation (2.33) corresponds to in the non-primitive electrolyte model from section 2.2. Correctly interpreting the Debye–Hückel theory has been a lengthy process and is, at least in the author of this work's opinion, not a trivial task.

Although Debye–Hückel theory is derived from an ion-ion interaction perspective, the resulting Debye–Hückel electrostatic energy expression in equation (2.33) does not correspond to a sum of the ion-ion interaction terms in the non-primitive model from section 2.2;

$$U^{DH} \neq \frac{1}{2}\sum_{j=1}^{N_{ion}}\sum_{i\neq j}^{N_{ion}} u_{ij}^{cc}. \tag{4.32}$$

These two interactions do not correspond, as the Debye–Hückel theory also considers the ions' interaction with the solvent through a macroscopic permittivity. One might also wrongly assume that the Debye–Hückel electrostatic energy represents a sum of all ion-ion and ion-solvent or ion-ion, ion-solvent, and solvent-solvent electrostatic interactions. These interpretations are incorrect, as both the ion-solvent and solvent-solvent electrostatic interaction terms go towards non-zero values in the limit of infinite dilution. The Debye–Hückel interaction energy, on the other hand, converges towards zero in this limit. The

correct interpretation of the Debye–Hückel electrostatic energy from equation (2.33) is *the difference between the electrostatic energy of an electrolyte solution and the electrostatic energy of the electrolyte solution if the ions were to interact as they would in an infinitely dilute solution*.

4.2.2 Regression Method Framework

This section introduces the method of intercepts and uses the Debye–Hückel electrostatic energy interpretation from subsection 4.2.1 to set the framework for the regression method.

In the absence of non pressure-volume work an extensive property B is a function of its partial derivatives;

$$B = \sum_i N_i \left(\frac{\partial B}{\partial N_i} \right)_{T,p,N_{j\neq i}} \tag{4.33}$$

[43]. For a binary mixture equation (4.33) can be rewritten in terms of the mole fractions of component 1 and 2, x_1 and x_2 respectively, as

$$\frac{B}{N_1 + N_2} = x_1 \overline{B}_1 + x_2 \overline{B}_2. \tag{4.34}$$

$\overline{B}_i = \left(\frac{\partial B}{\partial N_i} \right)_{T,p,N_{j\neq i}}$ is the partial molar B of component i. The partial molar quantities of a binary mixture can be calculated using the method of intercepts illustrated in figure 4.1 [44]. In this method the average of B is plotted as a function of composition, along with the tangent line of the composition in question. The values where the tangent line crosses $x_1 = 1 - x_2 = 0$ and $x_1 = 1$ correspond to the partial molar B with respect to component 2 and 1 at the composition under consideration.

The total electrostatic energy of a solution U^{elec} is an extensive property that is readily calculated using the molecular dynamics procedure from section 3.1. Although the non-primitive electrolyte model from section 2.2 is a ternary solution consisting of anions, cations and solvent particles, it can also be considered a binary mixture consisting of ion-pairs and solvent particles. Each ion-pair consists of one anion and one cation. Defining the number of ion-pairs as $N_{ip} = \frac{N_{cat}+N_{an}}{2}$, the ion-pair mole fraction as $x_{ip} = \frac{(N_{cat}+N_{an})/2}{(N_{cat}+N_{an})/2+N_{solv}}$, and the binary solvent mole fraction as $x_{bs} = \frac{N_{solv}}{(N_{cat}+N_{an})/2+N_{solv}}$, the average electrostatic energy of the non-primitive electrolyte solution is

$$\frac{U^{elec}}{N_{ip} + N_{solv}} = x_{ip} \overline{U}_{ip} + x_{bs} \overline{U}_{solv}. \tag{4.35}$$

Remembering that the Debye–Hückel electrostatic energy represents a departure from the electrolyte behavior at infinite dilution, the average electrostatic energy is (according to Debye–Hückel theory) the sum of the average of the Debye–Hückel electrostatic energy from equation (2.33) and terms representing the infinite dilution thermodynamics behavior of electrolytes;

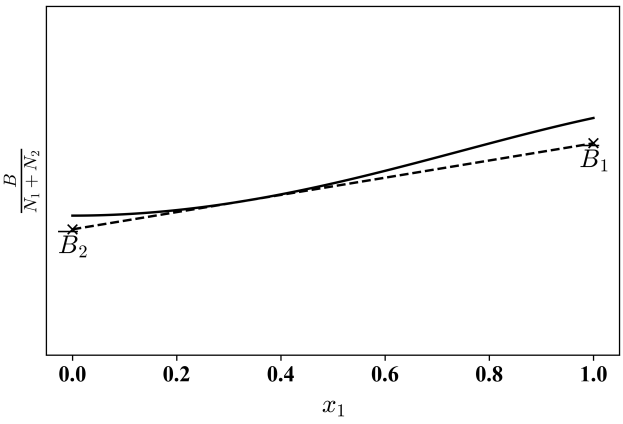

Figure 4.1: An illustration of the method of intercepts for an extensive property B. The solid line is the average B as a function of the mole fraction of component one. The dashed line indicates the tangent line of the average B for $x_1 = 0.33$. The values for the tangent line at $x_1 = 1$ and $x_1 = 1 - x_2 = 0$ are the corresponding partial molar values of component one and two respectively.

$$\frac{U^{elec}}{N_{ip} + N_{solv}} = x_{ip}\overline{U}_{ip} + x_{bs}\overline{U}_{solv} = \frac{U^{DH}}{N_{ip} + N_{solv}} + x_{ip}\overline{U}^{\infty}_{ip} + x_{bs}\overline{U}^{\infty}_{solv}. \quad (4.36)$$

The ∞ superscript indicates that the partial molar property corresponds to its infinite dilution limit value. In equation (4.36) $\overline{U}^{\infty}_{solv}$ is equal to the average electrostatic energy of an electrolyte solution without ions and can therefore readily be estimated from molecular dynamics simulation data. Equation (4.36) is true for a non-primitive electrolyte model that follows Debye–Hückel theory thermodynamics.

4.2.3 Regression Methods

This subsection introduces two methods for investigating whether it is possible to recover the Debye–Hückel theory's infinite dilution limiting behavior from the non-primitive electrolyte model. The first-method is largely unsuccessful but lays the framework for the improved second method used in this work.

There are three unknown terms in equation (4.36) that need to be estimated to get a Debye–Hückel electrostatic energy estimate for the non-primitive electrolyte model. These terms are the relative permittivity of the solution (implicit in the U^{DH} term), the ionic-atmosphere radius (implicit in the U^{DH} term), and the $\overline{U}^{\infty}_{ip}$ term. Appendix B demonstrates that in the limit of infinite dilution, the Debye–Hückel electrostatic energy behaves as if the ionic-atmosphere radius is zero. Consequently, since this regression method focuses on recovering the Debye–Hückel theory's infinite dilution limiting behavior from the non-primitive model, the ionic-atmosphere radius is set to zero. This work uses two different

methods for estimating the relative permittivity and the $\overline{U}_{ip}^{\infty}$ terms.

The first method consists of calculating the $\overline{U}_{ip}^{\infty}$ term using the previously described method of intercepts. The steps in the first method are:

1. Create a polynomial regression of the average electrostatic energy simulation data as a function of x_{ip}.

2. Create a tangent line for the average electrostatic energy at $x_{ip} = 0$ using the derivatives of the regression polynomial. The value at which the tangent line crosses $x_{ip} = 1$ corresponds to a method of intercepts estimate of $\overline{U}_{ip}^{\infty}$.

3. The permittivity of the solution can subsequently be estimated using the post-processing procedure from section 3.2.1 or an additional regression.

This method was flawed in that the resulting $\overline{U}_{ip}^{\infty}$ estimates were extremely sensitive to the simulation data and the choice of the polynomial regression model. Since it was difficult to obtain decisive conclusions using this method, it is not pursued any further in this report.

Although unsuccessful, the first-method did spur the development of an improved second method for extracting the Debye–Hückel electrostatic energy from the total electrostatic energy of the non-primitive model. Whereas the first method consists of a regression of the simulation data to find the unknown terms from equation (4.36), the second method uses the unknown relative permittivity and $\overline{U}_{ip}^{\infty}$ terms as regression coefficients to fit the right-hand and left-hand sides of equation (4.36). Rearranging (4.36) leads to a Debye–Hückel theory and a molecular dynamics estimate for the Debye–Hückel electrostatic energy of the electrolyte solution;

$$\underbrace{\frac{U^{elec}}{N_{ip}+N_{solv}} - x_{ip}\overline{U}_{ip}^{\infty} - x_{bs}\overline{U}_{solv}^{\infty}}_{\text{Molecular dynamics estimate}} = \underbrace{\frac{U^{DH}}{N_{ip}+N_{solv}}}_{\text{Debye–Hückel theory estimate}} . \tag{4.37}$$

If the non-primitive model follows Debye–Hückel theory's infinite dilution limiting behavior then the left and right hand sides of equation (4.37) should equal after the regression for an ionic-atmosphere radius of zero. Furthermore, the relative permittivity and $\overline{U}_{ip}^{\infty}$ regression parameters should converge to the their true electrolyte solution values.

The non-linear regression of equation (4.37) was performed using the Scipy Python library's constrained optimization optimize.minimize solver [45]. The optimize.minimize solver minimizes an objective function using various optimization algorithms for variables with a constrained domain. For an electrolyte system from table 3.1 that has been modeled for $1, 2, \cdots, \vartheta$ different ion-pairs using molecular dynamics, this work uses the 2-norm of the vector

$$\begin{bmatrix} \log(-\frac{U^{elec(1)}}{N_{ip}^{(1)}+N_{solv}^{(1)}} + x_{ip}^{(1)}\overline{U}_{ip}^{\infty} + x_{bs}^{(1)}\overline{U}_{solv}^{\infty}) - \log(-\frac{U^{DH(1)}}{N_{ip}^{(1)}+N_{solv}^{(1)}}) \\ \log(-\frac{U^{elec(1)}}{N_{ip}^{(2)}+N_{solv}^{(2)}} + x_{ip}^{(2)}\overline{U}_{ip}^{\infty} + x_{bs}^{(2)}\overline{U}_{solv}^{\infty}) - \log(-\frac{U^{DH(2)}}{N_{ip}^{(2)}+N_{solv}^{(2)}}) \\ \vdots \\ \log(-\frac{U^{elec(\vartheta)}}{N_{ip}^{(\vartheta)}+N_{solv}^{(\vartheta)}} + x_{ip}^{(\vartheta)}\overline{U}_{ip}^{\infty} + x_{bs}^{(\vartheta)}\overline{U}_{solv}^{\infty}) - \log(-\frac{U^{DH(\vartheta)}}{N_{ip}^{(\vartheta)}+N_{solv}^{(\vartheta)}}) \end{bmatrix} \tag{4.38}$$

as the objective function. The parenthesized integer superscripts on the x_{ip}, x_{bs}, N_{ip}, N_{solv} U^{elec}, and U^{DH} terms indicate which molecular dynamics simulation and number of ion-pairs the property corresponds to. The optimization occurs under the constraint that the relative permittivity is larger than one, as a relative permittivity under one is nonphysical. The objective function is logarithmic scaled since $-\frac{U^{DH}}{N_{ion}+N_{solv}}$ is close to linear in log-log units for an ionic-atmosphere radius equal to zero. The logarithmic scaling ensures no particular bias towards simulation-points with small or large x_{ip} values. This contrasts with other possible objective functions, such as an objective function that reduces the root mean square difference between the left and right-hand side of equation (4.37), which tend to have a bias towards simulation points with large x_{ip} values.

The regression presented in this section was implemented using Lennard-Jones units. In Lennard-Jones units equations (4.37) and (4.38) are

$$\underbrace{\frac{U^{elec*}}{N_{ip}+N_{solv}} - x_{ip}\overline{U}_{ip}^{\infty *} - x_{bs}\overline{U}_{solv}^{\infty *}}_{\text{Molecular dynamics estimate}} = \underbrace{\frac{U^{DH*}}{N_{ip}+N_{solv}}}_{\text{Debye–Hückel theory estimate}} \tag{4.39}$$

and

$$\begin{bmatrix} \log(-\frac{U^{elec*(1)}}{N_{ip}^{(1)}+N_{solv}^{(1)}} + x_{ip}^{(1)}\overline{U}_{ip}^{\infty *} + x_{bs}^{(1)}\overline{U}_{solv}^{\infty *}) - \log(-\frac{U^{DH*(1)}}{N_{ip}^{(1)}+N_{solv}^{(1)}}) \\ \log(-\frac{U^{elec*(1)}}{N_{ip}^{(2)}+N_{solv}^{(2)}} + x_{ip}^{(2)}\overline{U}_{ip}^{\infty *} + x_{bs}^{(2)}\overline{U}_{solv}^{\infty *}) - \log(-\frac{U^{DH*(2)}}{N_{ip}^{(2)}+N_{solv}^{(2)}}) \\ \vdots \\ \log(-\frac{U^{elec*(\vartheta)}}{N_{ip}^{(\vartheta)}+N_{solv}^{(\vartheta)}} + x_{ip}^{(\vartheta)}\overline{U}_{ip}^{\infty *} + x_{bs}^{(\vartheta)}\overline{U}_{solv}^{\infty *}) - \log(-\frac{U^{DH*(\vartheta)}}{N_{ip}^{(\vartheta)}+N_{solv}^{(\vartheta)}}) \end{bmatrix} \tag{4.40}$$

respectively. The $*$ superscript indicates that the quantity is in Lennard-Jones units. Appendix B derives the expanded $\frac{U^{DH*}}{N_{ip}+N_{solv}}$ expression that was used in the regression of equation (4.39).

Chapter 5

Results and Discussion

This thesis's objective is to investigate the asymptotic dielectric and thermodynamic behavior of dilute electrolyte solutions using a simplest-possible first-principle approach. Notably, this work examines how the Debye–Hückel theory's representation of the solvent as a dielectric continuum results in different thermodynamic and dielectric predictions than that of the non-primitive model from section 2.2. Each of the subsequent sections investigate a different aspect of the solvent's role in dilute electrolyte solutions;

- Section 5.1 investigates how the non-primitive electrolyte model's permittivity changes with increasing ion concentration.
- Section 5.2 investigates how the Debye–Hückel theory would change in the limit of infinite dilution if the permittivity is no-longer that of the pure solvent but depends on the ion concentration.
- Section 5.3 investigates if it is possible to extract the Debye–Hückel theory's thermodynamics in the limit of infinite dilution from the non-primitive model's molecular dynamics results.

5.1 Dielectric Properties of the Non-Primitive Electrolyte Model

This section investigates how the dielectric properties of the non-primitive model from section 5.3 change with increasing ion concentration. All of the dielectric and thermodynamic properties presented in this section are calculated using the molecular dynamics and post-processing procedures presented in section 3. Subsection 5.1.1 verifies the implementation of these molecular dynamics and post-processing procedures, whereas subsection 5.1.2 discusses the dielectric properties of the non-primitive model.

5.1.1 Verification

The purpose of this subsection is to verify the implementation of the molecular dynamics and post-processing procedure from section 3 this work uses to determine the dielectric properties of the non-primitive model from section 2.2. Concretely, this section:

- Verifies that the electrostatic forces and energies calculated using LAMMPS correspond to the independent Ewald summation post-processing procedure from section 3.2.2.
- Verifies the LAMMPS implementation by comparing calculated relative permittivity values to other authors' estimates.
- Examines the importance of finite-sized effects by plotting the relative permittivity as a function of the total number of particles in a molecular dynamics simulation.

Some general comments about the reliability of this work's results are presented at the end of this subsection.

The post-processing method from section 3.2.2 can be used to estimate the total electrostatic energy of a system of ions independently from LAMMPS. For example, the total electrostatic energy for system 6 from table 3.1 can be calculated using either LAMMPS or the independent Ewald summation code. The LAMMPS estimate for the total electrostatic energy in Lennard-Jones units U^{elec*} for system 6 is

$$\frac{U^{elec*}}{N_{tot}} = -50.9409268, \tag{5.1}$$

whereas the post-processing estimate is

$$\frac{U^{elec*}}{N_{tot}} = -50.9409376. \tag{5.2}$$

The two estimates differ by only 1.08×10^{-5}. The agreement between equations (5.1) and (5.2), as well as the similar molecular dynamics implementation of the non-primitive electrolyte model and system 6, suggests that this work's implementation of the Ewald summation method in LAMMPS is correct.

Section 3.2.1 presents a method for calculating the relative permittivity of the non-primitive model. The underlying expression for the relative permittivity (equation (3.7)) depends on both the temperature and the solvent particles' contribution to the solution's total dipole moment. The temperature and the solvent particles' dipole moment, in turn, depend on the LAMMPS implementation of the molecular dynamics procedure. Accordingly, correct relative permittivity calculations suggest that the implementation of the relative permittivity post-processing procedure from section 3.2.1 is correct, as well as the implementation of the non-primitive model in LAMMPS as a whole. Figure 5.1 shows the relative permittivity, calculated using the method from section 3.2.1, as a function the number of ion pairs for system 1 from table 3.1. Chandra and Patey's [1] relative permittivity estimates for 5 and

10 ion-pairs are included for comparison. The relative permittivity results are almost indistinguishable, and well within one standard deviation, from Chandra and Patey's estimates. This similarity suggests that the relative permittivity post-processing procedure and the implementation of the non-primitive model in LAMMPS are correct.

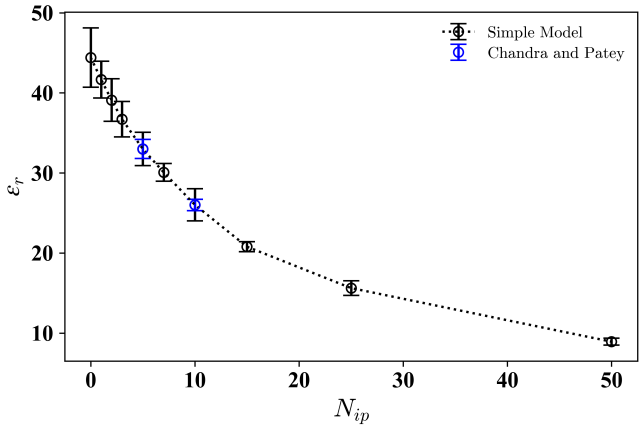

Figure 5.1: The relative permittivity as a function of the number of ion pairs for system 1 from table 3.1. The blue markers indicate the 5 and 10 ion-pair results by Chandra and Patey [1] for the same system.

In molecular dynamics, there are finite-size effects due to the boundary conditions and the finite number of particles in the simulation box. Gray et al. [46] have analyzed how the permittivity of a Stockmayer fluid simulation characterized by $\mu_s^* = 1.0$, $T^* = 1$, $\rho^* = 0.8$, and periodic boundary conditions change with the total number of particles in a simulation box. They concluded that the permittivity remains virtually unchanged for simulations with more than 108 particles. Figure 5.2 plots the relative permittivity of system 11 from table 3.1 as a function of the total number of particles in the simulation box. Figure 5.2 suggests that the relative permittivity results plateau before 256 particles. Gray et al.'s results, along with figure 5.2, suggests that finite-size effects are sufficiently small for 256 particles in molecular dynamics simulations to observe the qualitative permittivity trends of the non-primitive model from section 2.2.

The results presented in this section suggest that this work's LAMMPS implementation is correct and that the results are reliable. Nevertheless, this verification section does not *prove* that this work's implementation of the molecular dynamics simulation procedure from section 3.1 does not contain any errors. A more comprehensive verification process could compare more thermodynamic quantities to other authors' independent molecular dynamics estimates. Unfortunately, to the author of this work's knowledge, there is little published thermodynamics data for the non-primitive model from section 2.2.

A suggestion for future work within modeling simple non-primitive electrolytes using

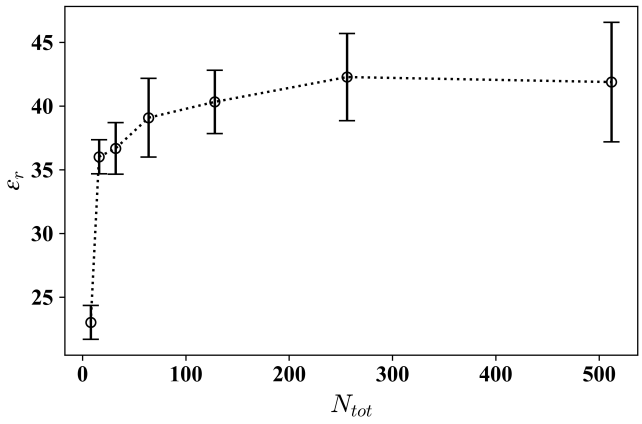

Figure 5.2: The relative permittivity of system 11 from table 3.1 as a function of the total number of particles in the simulation box.

computational chemistry techniques is to model the ions and solvent particles as hard-sphere, instead of Lennard-Jones or WCA, particles with a point-charge and point-dipole at their respective centers. There is a lot more published thermodynamic data for this hard-sphere model than the non-primitive electrolyte model from section 2.2 [47]. Another suggestion would be to write or use a molecular modeling code specific for the non-primitive electrolyte model, as this would ensure more control than when using third-party software such as LAMMPS.

5.1.2 Non-Primitive Electrolyte Model Results

This subsection presents and discusses the relative permittivity results for the non-primitive electrolyte model from section 2.2. This subsection begins by introducing a simple model of two ions and a solvent particle. The simple example is then used to explain some of the observed trends for the relative permittivity at increasing ion concentrations.

Simple Ions and Solvent Particle Example

This subsection evaluates the electrostatic energy of a simple system of two ions separated by a solvent particle. This simple system explains several of the observed trends for the permittivity of the non-primitive electrolyte model at increasing ion concentrations.

The energy required to bring a particle i of charge $z_i q$ from infinitely far away to a distance $r_{ij} = \|\mathbf{r}_{ij}\| = \|\mathbf{r}_i - \mathbf{r}_j\|$ of another particle j of charge $z_i q$ in a vacuum is equal to the charge-charge pair-potential term from section 2.2;

$$u_{ij}^{cc} = \frac{z_i z_j q^2}{4\pi\varepsilon_0} \frac{1}{r_{ij}}. \tag{5.3}$$

Similarly, the energy required to bring a point-charge or a point-dipole j to a distance r_{ij} of a point-dipole i is equal to

$$u_{ij}^{dc} = -\frac{z_j q}{4\pi\varepsilon_0}\frac{\boldsymbol{\mu}_i \cdot \mathbf{r}_{ij}}{r_{ij}^3} \tag{5.4}$$

and

$$u_{ij}^{dd} = \frac{1}{4\pi\varepsilon_0 r_{ij}^3}\left[\boldsymbol{\mu}_i \cdot \boldsymbol{\mu}_j - 3\frac{(\boldsymbol{\mu}_i \cdot \mathbf{r}_{ij})\,(\mathbf{r}_{ij} \cdot \boldsymbol{\mu}_j)}{r_{ij}^2}\right] \tag{5.5}$$

respectively [23] [24].

Figure 5.3 illustrates a simple system where a cation and an anion are at a distance $r_\pm$ apart, with a solvent particle in between them. The ions are represented as point-charges of the same magnitude $q_\pm \equiv z_+ q = -z_- q$, whereas the solvent particle is represented as a point-dipole with a dipole moment $\boldsymbol{\mu}$ of magnitude $\mu = \|\boldsymbol{\mu}\|$. The distances between the ions and the central solvent particle are $r_{\mu+} = r_{\mu-} = \frac{1}{2}r_\pm$. The subscripts $+$, $-$, and μ denote the cation, anion, and solvent particle, respectively.

(a) The dipole moment of the solvent particle points towards the cation.

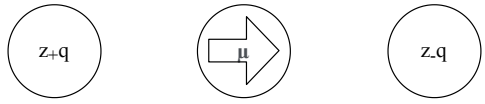

(b) The dipole moment of the solvent particle points towards the anion.

(c) The dipole moment of the solvent particle points in a perpendicular direction to the ions.

Figure 5.3: An illustration of a simple system where a cation with a point-charge $z_+ q$ and an anion with a point-charge $z_- q$ are a distance $r_\pm$ apart. The ions are separated by a solvent particle with a dipole moment $\boldsymbol{\mu}$. The arrows represents the direction of the solvent particle's dipole moment. The solvent particle is equidistant from both ions.

The energy required to bring the cation and anion to a distance of $r_\pm$ of each-other, as well as distances $r_{\mu+}$ and $r_{\mu-}$ of the point-dipole can be calculated from equations (5.3) and (5.4) as

$$U = \frac{z_+ z_- q^2}{4\pi\varepsilon_0}\frac{1}{r_\pm} - \frac{z_+ q}{4\pi\varepsilon_0}\frac{\boldsymbol{\mu} \cdot \mathbf{r}_{\mu+}}{r_{\mu+}^3} - \frac{z_- q}{4\pi\varepsilon_0}\frac{\boldsymbol{\mu} \cdot \mathbf{r}_{\mu-}}{r_{\mu-}^3}. \tag{5.6}$$

Equation (5.6) can be simplified, by introducing the identity $\mathbf{a} \cdot \mathbf{b} = \|\mathbf{a}\|\|\mathbf{b}\| \cos\theta_{\mathbf{ab}}$ and recognizing that $\mathbf{r}_{\mu+} = -\mathbf{r}_{+\mu} = -\mathbf{r}_{\mu-} = \mathbf{r}_{\mu-}$, as

$$U = -\frac{q_\pm^2}{4\pi\varepsilon_0}\frac{1}{r_\pm} + \frac{2q_\pm\mu}{\pi\varepsilon_0}\frac{1}{r_\pm^2}\cos\theta_{\boldsymbol{\mu}\mathbf{r}_{+\mu}}. \tag{5.7}$$

$\theta_{\boldsymbol{\mu}\mathbf{r}_{\mu+}}$ is the angle between the $\mathbf{r}_{\mu+}$ and $\boldsymbol{\mu}$ vectors. For the configurations in figures 5.3a, 5.3b, and 5.3c, equation (5.7) simplifies to

$$U = -\frac{q_\pm^2}{4\pi\varepsilon_0}\frac{1}{r_\pm} - \frac{q_\pm\mu}{\pi\varepsilon_0}\frac{2}{r_\pm^2}, \tag{5.8}$$

$$U = -\frac{q_\pm^2}{4\pi\varepsilon_0}\frac{1}{r_\pm} + \frac{q_\pm\mu}{\pi\varepsilon_0}\frac{2}{r_\pm^2}, \tag{5.9}$$

and

$$U = -\frac{q_\pm^2}{4\pi\varepsilon_0}\frac{1}{r_\pm} \tag{5.10}$$

respectively.

Equations (5.7) through (5.10) illustrate a lot of the physics necessary to understand the macroscopic permittivity of an electrolyte solution in terms of the solution's microscopic behavior.

The permittivity is a measure of a solution's ability to screen electric fields. For example, in Coulomb's law the permittivity describes the effective force f_{ij} felt between two particles i and j in a surrounding medium;

$$f_{ij} = \frac{z_i z_j q^2}{4\pi\varepsilon}\frac{1}{r_{ij}^2}. \tag{5.11}$$

This screening of ions due to the surroundings is also present in the simple system from figure 5.3. Equations (5.8), (5.9), and (5.10) demonstrate that the orientation of the solvent particles' dipole moment dictates whether the effective ion-ion interaction is larger, smaller, or unaffected by the presence of the solvent particle. For large ion separations or small dipole moments the solvent particle's effect on the effective ion-ion interactions disappears altogether.

These microscopic screening effects will be used to explain the permittivity behavior of the non-primitive electrolyte model from section 2.2.

The Relative Permittivity of the Non-Primitive Model

This subsection demonstrates how the relative permittivity of the non-primitive electrolyte model from section 2.2 changes with increasing ion concentration. All of the relative permittivities presented in this subsection are calculated using the post-processing method from section 3.2.1. Some general concluding remarks are given at the end of this subsection.

Figure 5.4 illustrates the relative permittivity of systems 2, 3, and 4 from table 3.1 as function of the number of ion-pairs in the solution. All of these systems experience a decrease in permittivity with increasing ion concentration. This phenomenon is known as dielectric decrement and is observed in both real electrolyte solutions and the non-primitive electrolyte model [48]. Ben-Yaakov et al. [2] attributes dielectric decrement to two primary mechanisms, namely ionic polarizability and solvation shells.

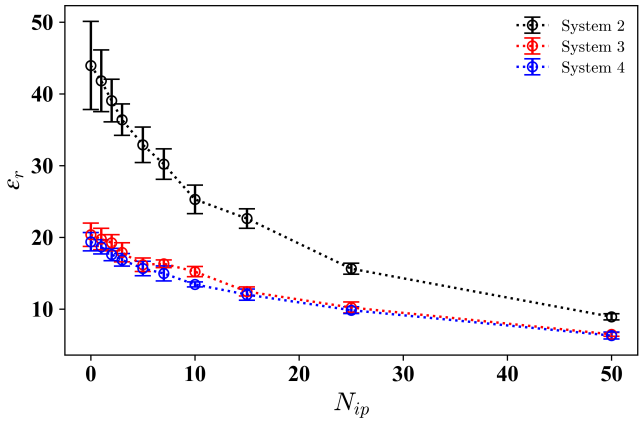

Figure 5.4: The relative permittivity as a function of the number of ion pairs for systems 2, 3, and 4 from table 3.1. System 3 differs from system 2 in that the reduced number density ρ^* is equal to 0.6 instead of 0.8. Systems 4 differs from system 2 in that the magnitude of the reduced dipole moment of the solvent particles μ_s^* is equal to 1.5 instead of 1.8. The similarity between system 3 and system 4 results is coincidental.

Ionic polarizability describes the process in which the addition of an ion creates a cavity in a solution and displaces the surrounding solvent particles. Since the ions have different electric properties, including other permanent dipole moments and polarizabilities, the solution's response to external fields change. This change in the solution's response to external fields results in a different permittivity. Ionic polarizability is responsible for some of the dielectric decrement observed in figure 5.4. The simulations in figure 5.4 are performed at a constant number of particles, but where ions replace some solvent particles for the simulations with a larger number of ion pairs. This replacement can be considered a displacement of solvent particles that affects the solution's permittivity and response to external fields.

Another contribution to dielectric decrement is the creation of solvation shells. Introducing an ion to a solution causes the surrounding solvent particles to align themselves with the ion's electric field in what is known as a solvation shell. The particles in solvation shells are less susceptible to aligning themselves with an external field, consequently reducing the solution's permittivity. Figure 5.5 show a simple illustration of ionic polarizability and the creation of solvation shells in an electrolyte solution.

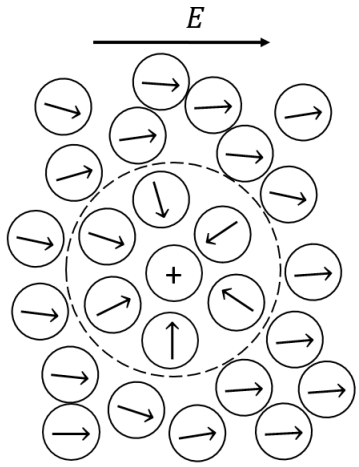

Figure 5.5: An illustration of solvent particles surrounding a cation in the presence of an external electric field $\mathbf{E}$. The direction of the external field is indicated by the long arrow. The plus sign, the short arrows, and the dashed line indicate the cation, the solvent particles' dipole orientation, and the solvation shell's extent. The solvent particles in the solvation shell are aligned according to the central cation's electric field lines, whereas solvent particles that are further away are more susceptible to orient themselves according to the external field. This reduction of solvent particles' ability to orient themselves with the external field results in a smaller screening effect and a lower permittivity. Furthermore, the cation has different electric properties than solvent particles, which results in further differences in the solution's response to external fields. The figure was inspired by Ben-Yaakov et al. [2].

Solvation shells reduce the average solvent particle's response to electric fields. In the post-processing method from section 3.2.1 the electrolyte's response to external fields is described by the $\langle \mathbf{M}_s^{*2} \rangle - \langle \mathbf{M}_s^* \rangle^2$ term from equation (3.7). Figures 5.6 and 5.7 plot $\langle \mathbf{M}_s^{*2} \rangle - \langle \mathbf{M}_s^* \rangle^2$ and $\frac{\langle \mathbf{M}_s^{*2} \rangle - \langle \mathbf{M}_s^* \rangle^2}{N_{solv}}$ for system 2. These figures demonstrate that both the solution's response and the solution's response per solvent particle to an external field decrease with increasing ion concentration. The reduction in the average per solvent particle response suggests that solvation shells are partly responsible for the non-primitive model's dielectric depreciation. A more in-depth comprehension of the observed dielectric depreciation would require a thorough investigation of how the non-primitive electrolyte's models' microscopic structure changes with increasing ion concentration. This investigation is left as future work.

Figure 5.4 demonstrates that the relative permittivity of the non-primitive model depends on the solution's number density and the dipole moment of the solvent particles. For instance, reducing the number density from that of system 2 to that of system 3 decreases the solution's relative permittivity. The previously introduced example of two ions separated by a solvent particle explains this phenomenon. Equation (5.7) predicts that the screening effects of solvent particles are small at large particle separations. Since particles are further apart for smaller number densities, the solvent particles' screening effect decreases along with the solution's relative permittivity. Another observation from figure 5.4 is that the permittivity

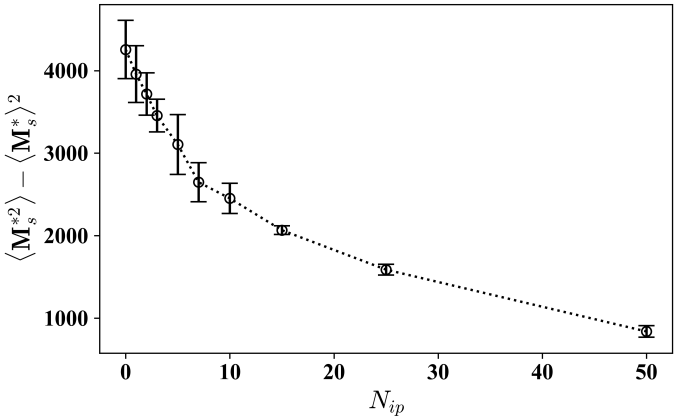

Figure 5.6: The $\langle \mathbf{M}_s^{*2} \rangle - \langle \mathbf{M}_s^* \rangle^2$ term from equation (3.7) as a function of the number of ion pairs for system 2 from table 3.1.

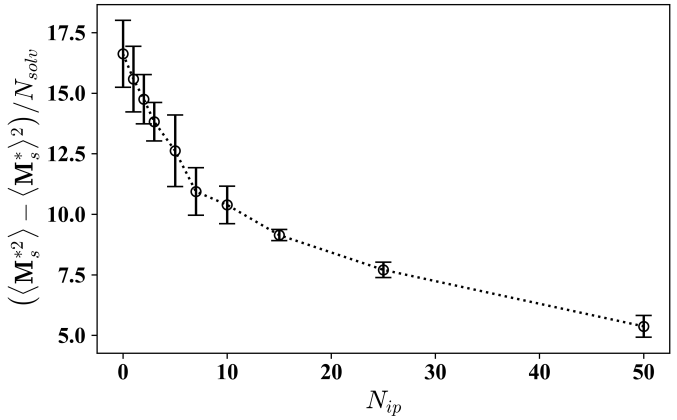

Figure 5.7: The $\frac{\langle \mathbf{M}_s^{*2} \rangle - \langle \mathbf{M}_s^* \rangle^2}{N_{solv}}$ term from equation (3.7) as a function of the number of ion pairs for system 2 from table 3.1.

decreases with a lowering of the solvent particle's dipole moment. This phenomenon can also be explained by a decrease in the solvent particles' screening ability, specifically due to the solvents' smaller dipole moment.

The relative permittivity results presented in this section demonstrate that the non-primitive model predicts a dielectric decrement also observed for real electrolyte solutions. This observation highlights a significant difference between non-primitive and primitive electrolyte models. Whereas a non-primitive solvent description naturally incorporates changes in the permittivity through changes in the electrolyte's microscopic structure, non-primitive models do not have this possibility. This disparity leads to several follow-up questions:

- When is the Debye–Hückel theory's assumption of a constant permittivity valid?
- Is it possible to relate the thermodynamics of the Debye–Hückel theory and the non-primitive model?

Sections 5.2 and 5.3 explore theses questions. .

5.2 The Solvent in Debye–Hückel Theory

Section 5.1 demonstrates that increasing the concentration of ions in an electrolyte solution leads to dielectric decrement. Dielectric decrement is not considered in Debye–Hückel theory, where the solvent is an incompressible dielectricum that does not change with temperature, the concentration of ions, or pressure. This simplistic representation raises the question of when Debye–Hückel theory's description of the solvent as a dielectricum of constant permittivity is valid. This section examines this question by investigating how the Debye–Hückel theory's expression for the mean ionic activity coefficient changes when using a permittivity that depends on the concentration of ions. I

A sodium chloride solution example is used to estimate the salt concentration when Debye–Hückel theory predicts that the permittivity's ion concentration-dependence becomes significant.

Intuitively, using the electrolyte solution's macroscopic permittivity when calculating the electrostatic interaction energy between two ions is expected to be reasonable if there are sufficiently many solvent molecules separating them. This use of a macroscopic permittivity does, as remarked by Fowler and Guggenheim [18], not make sense when two ions are in contact or close vicinity of one another. Debye–Hückel theory, where the macroscopic permittivity dictates the interaction between ions, is therefore expected to be reasonable for systems where the most significant contribution to the electrostatic energy is due to ions far away. As discussed in section 2.1, $1/\kappa_0$ represents a mean thickness of the ionic atmosphere surrounding an ion and is a measure of the distance at which the surrounding ions make significant contributions to the electrostatic energy. Consequently, Debye–Hückel theory's use of a macroscopic permittivity is expected to be appropriate when $1/\kappa_0$ is much larger than the dimensions of the ions ($1/\kappa_0 \gg a$).

Figure 5.8 compares the Debye–Hückel theory limiting law estimates for the mean ionic activity coefficients at different salt concentrations to the corresponding experimental values for a sodium chloride solution at $25°\mathrm{C}$. The Debye–Hückel limiting law results are calculated using equation (2.56), and the experimental values are from the RC Handbook of Chemistry and Physics [3]. Recognizing that the salt concentration is proportional to κ_0^2 for a monovalent salt that dissociates completely, figure 5.8 demonstrates that the Debye–Hückel limiting law expression is valid for small κ_0. The agreement between Debye–Hückel theory and experimental results at small ion concentrations supports the assertion that Debye–Hückel theory's use of a macroscopic permittivity is only valid when ions that contribute significantly to the electrostatic energy are on average far apart. The increased accuracy of Debye–Hückel theory at small concentrations is also due to other assumptions, such as the linearization of the Poisson-Boltzmann equation, being more

accurate for small ion concentrations.

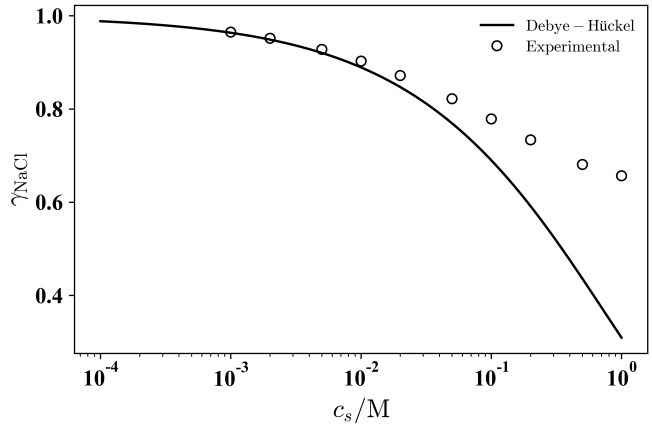

Figure 5.8: A comparison of the experimental and the Debye–Hückel limiting law estimated mean ionic activity coefficients for a sodium chloride solution as a function of concentration. The temperature of the solution is $25^\circ\mathrm{C}$ and the concentration is measured in molars. The experimental data is plotted as circles and the Debye–Hückel limiting law predictions as a solid black line. The experimental data was found in the RC Handbook of Chemistry and Physics [3].

In Debye–Hückel theory the permittivity is that of the pure solvent, regardless of ion concentration. However, as explained in section 5.1, introducing salt to a solution leads to a depreciation of the solution's permittivity. How to best account for this depreciation using Debye–Hückel theory differs between academics [9]. Michelsen and Mollerup [17] advocate for using a constant permittivity during the partial charging process (as in section 2.1), but letting the permittivity depend on concentration when calculating derivatives of the resulting Helmholtz energy expression. Kontogeorgis et al. [9] states that this methodology allows for analytical expressions that align-well with experimental results. Others assert that letting the permittivity change with ion concentration during the partial-charging process is more thermodynamically consistent [18] [39]. Section 4.1 uses the latter method. Specifically, section 4.1 derives a series expansion expression for the mean ionic activity coefficient using the same partial charging process from section 2.1.3, but where the permittivity now depends on the concentration of ions. Analytical expressions are obtained for the simple case when the electrolyte solution consists of a cation and an anion with the same ionic-atmosphere radius.

Comparing the mean ionic activity coefficient series expansion expression calculated using an ion concentration-dependent permittivity to its ion concentration-independent counterpart leads to an important conclusion about the solvent in the limit of infinite dilution. Equations (2.55) and (4.14) demonstrate that representing the solvent using an ion concentration-dependent permittivity does not change the Debye–Hückel limiting law or the Debye–Hückel theory's thermodynamics in the limit of infinite dilution. This conclusion is reasonable, considering that it is well-known that Debye–Hückel theory correctly describes

the thermodynamics of electrolyte solutions for very dilute solutions [49]. A more realistic electrolyte description, through an ion concentration-dependent permittivity, should lead to the same correct thermodynamics in the limit of infinite dilution. The permittivity's ion concentration-dependence does, however, lead to a second-order contribution.

To investigate when the permittivity's ion concentration-dependence becomes significant, section 4.1 derives an expression for the ratio between the second and first-order expansion terms for the ion concentration-dependent mean ionic activity coefficient of a sodium chloride solution. Figure 5.9 plots the resulting ratio as a function of ion concentration for a lower, middle, and upper estimates of the ionic-atmosphere radius. Figure 5.9 demonstrates that for a sodium chloride solution, the second-order term is smaller than one percent of the first-order term until a concentration of slightly above ten millimolar. Furthermore, figure 5.9 illustrates that the second-order expansion term is insensitive to the choice of ion-exclusion zone radius at this concentration. Accordingly, $10^{-2}\mathrm{M}$ can be considered a rough estimate for when Debye–Hückel theory predicts that its own assumption of constant permittivity is no longer valid for describing the mean ionic activity coefficient of a sodium chloride solution. In figure 5.8, the Debye–Hückel limiting law predictions differ significantly from the experimental mean ionic activity coefficient values already at $2 \times 10^{-3}\mathrm{M}$. This deviance suggests that other assumptions of the Debye–Hückel theory break down or that higher-order expansion terms are necessary for an accurate description of the thermodynamics at these concentrations.

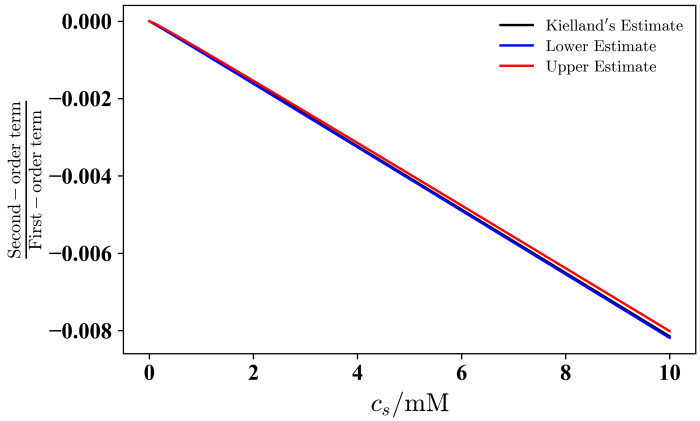

Figure 5.9: The ratio between the second and first-order mean ionic activity coefficient expansion terms for a sodium chloride solution at different salt concentrations. The mean ionic activity coefficient expansion terms are calculated, as described in section 4.1, from a Debye–Hückel theory with an ion concentration-dependent permittivity. The temperature of the solution is $25^{\circ}\mathrm{C}$ and the concentration is in millimolar. The black, blue, and red lines indicate the ratios for the Kielland, lower, and upper estimates of the ionic-atmosphere radius. The ratio expressions are given by equations (4.29), (4.30), and (4.31) in section 4.1.

5.3 Recovering the Debye–Hückel Theory's Thermodynamics in the Limit of Infinite Dilution from the Non-Primitive Electrolyte Model

Debye–Hückel theory correctly describes the thermodynamics of sufficiently dilute real electrolytes [10]. Accordingly, the thermodynamics of a correct non-primitive electrolyte model should converge to that of the Debye–Hückel theory in the limit of infinite dilution. Section 5.2 demonstrates that the Debye–Hückel theory predicts that dielectric decrement does not affect the thermodynamics of electrolytes in the limit of infinite dilution. Hence, it is reasonable to contemplate that the thermodynamics of the non-primitive model from section 2.2 converges to that of the Debye–Hückel theory in this limit.

Appendix B demonstrates that Debye–Hückel theory predicts that for anions and cations of the same size and with the same charge magnitude, the average Debye–Hückel electrostatic energy of an electrolyte is proportional to the mole fraction of ions to the power of $3/2$ in the limit of infinite dilution;

$$\frac{U^{DH}}{N_{tot}} \propto x_{ions}^{\frac{3}{2}}. \tag{5.12}$$

The Debye–Hückel theory characterizes the limit of infinite dilution by a sufficiently small inverse Debye length. Equations (2.23) and (B.8) demonstrate that the inverse Debye length increases with ion concentration and the ions' charge magnitude, but decrease with temperature or the solution's permittivity. This section uses the regression method from section 4.2 to investigate if it is possible to recover the proportionality from equation (5.12) from the non-primitive model's molecular dynamics results by sufficiently *increasing the temperature* or *decreasing the ions' charge magnitude*. As mentioned during the preface, this work does not attempt to recover the Debye–Hückel theory's thermodynamics in the limit of infinite dilution by decreasing the ion concentration due to limitations in this work's molecular dynamics procedure.

Figure 5.10 show the molecular dynamics and Debye–Hückel theory estimates for the Debye–Hückel electrostatic energy for system 2 from table 3.1 calculated using the regression method from section 4.2. Figure 5.11 plots the negative of the average Debye–Hückel electrostatic energy estimates from figure 5.10 on logarithmic axes. Although the molecular dynamics and Debye–Hückel estimates seem to converge for small ion mole fractions in figure 5.10, the logarithmic scaled figure 5.11 demonstrates that this is not the case. The disagreement between the molecular dynamics and Debye–Hückel theory estimates proves that system 2 does not follow the Debye–Hückel theory's thermodynamics in the limit of infinite dilution.

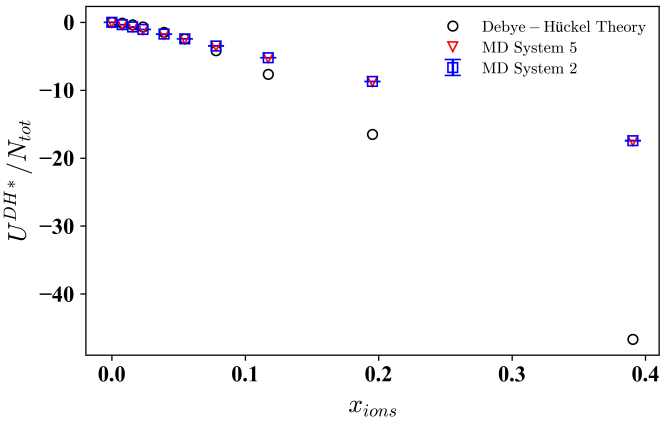

Figure 5.10: The molecular dynamics (blue squares) and Debye–Hückel theory estimates (black circles) for the average Debye–Hückel electrostatic energy for system 2 from table 3.1 as a function of the mole fraction of ions. The method from section 4.2 is used to calculate the regression coefficients that are used in the Debye–Hückel electrostatic energy estimates. The resulting regression coefficient values are $\varepsilon_r = 12.63$ and $\overline{U}_{ip}^{\infty *} = -96.70$. The system 5 estimates for the Debye–Hückel electrostatic energy are included for comparison. The system 5 estimates (red triangles) are calculated using the same regression coefficients as for system 2. The reduced ionic-atmosphere radius used in the Debye–Hückel theory estimate is equal to zero.

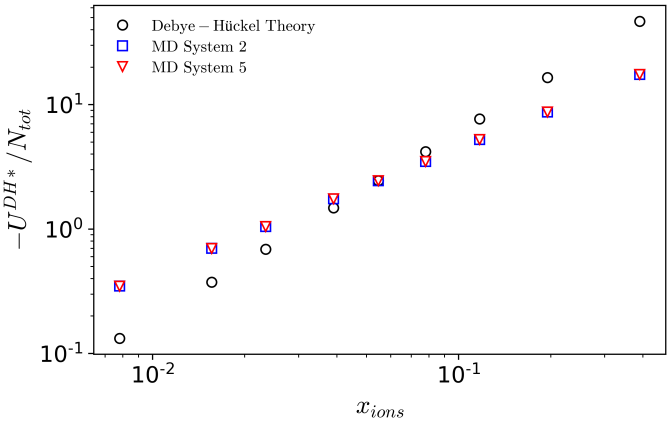

Figure 5.11: The negative of the electrostatic Debye–Hückel energy estimates from figure 5.10 for system 2 plotted using logarithmic x and y axes. The estimates for $x_{ions} = 0$ are not included as they are not easily represented in a log-log graph.

Figure 5.10 and 5.11 include the system 5 estimates for the Debye–Hückel electrostatic energy, calculated using system 2's ε_r and $\overline{U}_{ip}^{\infty *}$ regression coefficients, for comparison. System 5 has the same physical parameters as system 2 but uses twice the number of particles in its molecular dynamics simulation. Doubling the system size seems to have minimal effect on the resulting electrostatic energies. This observation suggests that non-physical finite-size effects in the molecular dynamics simulations of system 2 are negligible.

The slopes from figure 5.11 describe the Debye–Hückel theory and molecular dynamics estimates of the Debye–Hückel electrostatic energy's dependence on the ion concentration. A simple regression shows that the Debye–Hückel theory estimate has a slope of precisely $\frac{3}{2}$ and that the molecular dynamics estimate has a slope of almost exactly 1. A constant slope in a log-log plot indicates to which order the y-axis variable depends on the x-axis variable. Consequently, the observed slopes in figure 5.11 demonstrate that the Debye–Hückel theory and the molecular dynamics estimates for the average Debye–Hückel electrostatic energy are proportional to $x_{ions}^{\frac{3}{2}}$ and x_{ions}, respectively. As previously discussed, the Debye–Hückel theory estimate is expected to be proportional to $x_{ions}^{\frac{3}{2}}$ in the limit of infinite dilution. The next paragraphs investigate why the molecular dynamics estimate for the Debye–Hückel electrostatic energy for system 2 does not follow this trend but is proportional to the concentration of ions.

An electrostatic energy that is proportional to the concentration of ions indicates that the electrostatic energy felt by each ion does not change with the ion concentration. This phenomenon is observed in a variety of electrolyte models at sufficiently large inverse Debye lengths. A model closely related to the non-primitive electrolyte model from section 2.2 is the Mean Spherical Approximation (MSA) model. MSA electrolyte solutions are modeled as mixtures of dipolar hard spheres and charged hard spheres [50]. A private discussion with Johan Skule Høye, one of the pioneers behind MSA, revealed that the average electrostatic energy is proportional to the mole fraction of ions for MSA systems at sufficiently large ion concentrations [51]. Høye accredits this proportionality to short-range interactions. At large ion concentrations, the short-range repulsions prevent the particles from arranging themselves to allow for increased electrostatic interactions. The work of Xiao and Song [52] support Høye's assertion, as their expression for the restricted primitive MSA model's electrostatic energy is proportional to the concentration of ions at large inverse Debye lengths. However, MSA models are not the only electrolyte models that become linear at large ion concentrations and inverse-Debye lengths.

Debye–Hückel theory predicts that the Debye–Hückel electrostatic energy is proportional to the concentration of ions at sufficiently large inverse Debye lengths. Appendix B demonstrates this is the case, as long as the ionic-atmosphere radius is not zero. Figure 5.12 plots the molecular dynamics and Debye–Hückel theory estimates for the Debye–Hückel electrostatic energy for system 2 from table 3.1 in log-log units, but this time for a reduced ionic-atmosphere radius of 1. The slope of the Debye–Hückel estimate in figure 5.12 is closer to that of the molecular dynamics estimate than in figure 5.11. This observation, along with the previous MSA discussion, suggests that all of the data points in figure 5.12 are at inverse Debye lengths too large to recover the Debye-Hückel theory's thermodynam-

ics in the limit of infinite dilution from the non-primitive electrolyte model.

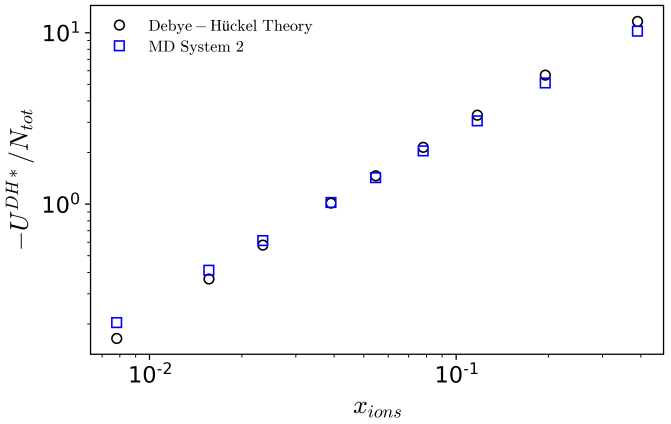

Figure 5.12: The molecular dynamics (blue squares) and Debye–Hückel theory estimates (black circles) for the average Debye–Hückel electrostatic energy for system 2 from table 3.1 as a function of the mole fraction of ions. The method from section 4.2 is used to calculate the regression coefficients that are used in the Debye–Hückel electrostatic energy estimates. The reduced ionic-atmosphere radius used in the Debye–Hückel theory estimate is equal to one. The resulting regression coefficient values are $\varepsilon_r = 1.0$ and $\overline{U}_{ip}^{\infty *} = -49.036$. The estimates for $x_{ions} = 0$ are not included as they are not easily represented in a log-log graph.

The previous paragraph introduced the notion that to observe the limiting behavior of the non-primitive model, one needs to reduce system 2's inverse Debye lengths. Equations (2.23) and (B.7) demonstrate that two methods for reducing the inverse Debye lengths is to reduce the ion's charge magnitude and increase the temperature. Systems 7 and 8 from table 3.1 differ from system 2 in that the charge magnitude has been decreased from $q_{\pm}^* = 8.0$ to $q_{\pm}^* = 1.0$ and $q_{\pm}^* = 0.2$, respectively. Systems 9 and 10 from table 3.1 differ from system 2 in that the temperature has been increased from $T^* = 1.35$ to $T^* = 13.5$ and $T^* = 135$, respectively. Figures 5.13 through 5.20 plot the molecular dynamics and the Debye–Hückel estimates for the Debye–Hückel electrostatic energy for systems 7, 8, 9 and 10 using both linear and log-log axes.

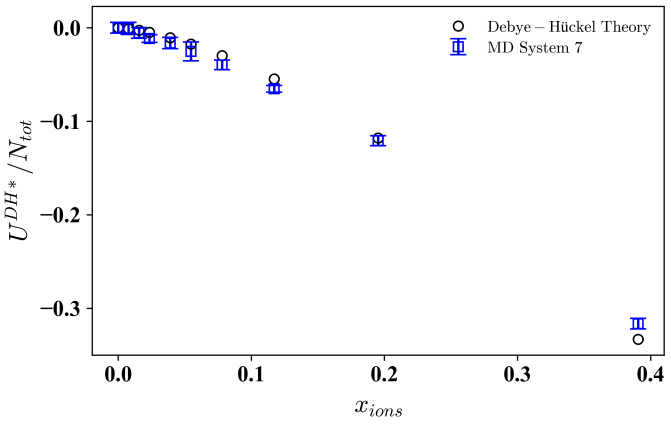

Figure 5.13: The molecular dynamics (blue squares) and Debye–Hückel theory estimates (black circles) for the average Debye–Hückel electrostatic energy for system 7 from table 3.1 as a function of the mole fraction of ions. The method from section 4.2 is used to calculate the regression coefficients that are used in the Debye–Hückel electrostatic energy estimates. The reduced ionic-atmosphere radius used in the Debye–Hückel theory estimate is equal to zero. The resulting regression coefficient values are $\varepsilon_r = 1.0$ and $\overline{U}_{ip}^{\infty *} = 2.348$.

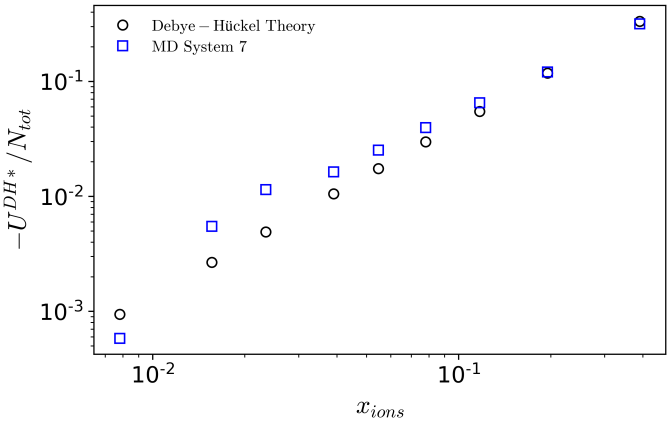

Figure 5.14: The negative of the electrostatic Debye–Hückel energy estimates from figure 5.13 for system 7 plotted using logarithmic x and y axes. The estimates for $x_{ions} = 0$ are not included as they are not easily represented in a log-log graph.

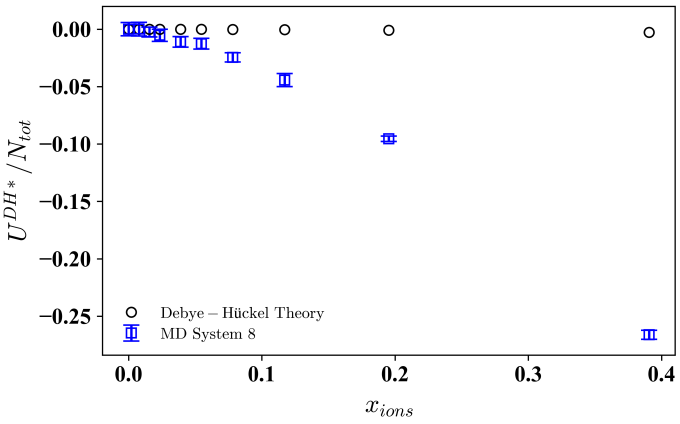

Figure 5.15: The molecular dynamics (blue squares) and Debye–Hückel theory estimates (black circles) for the average Debye–Hückel electrostatic energy for system 8 from table 3.1 as a function of the mole fraction of ions. The method from section 4.2 is used to calculate the regression coefficients that are used in the Debye–Hückel electrostatic energy estimates. The reduced ionic-atmosphere radius used in the Debye–Hückel theory estimate is equal to zero. The resulting regression coefficient values are $\varepsilon_r = 1.000$ and $\overline{U}_{ip}^{\infty *} = 3.480$.

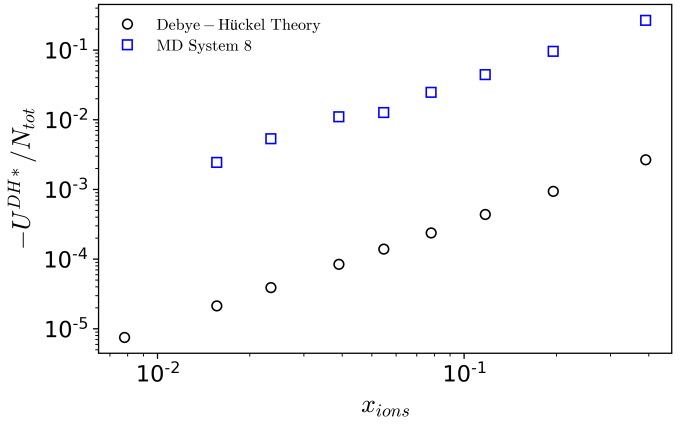

Figure 5.16: The negative of the electrostatic Debye–Hückel energy estimates from figure 5.15 for system 8 plotted using logarithmic x and y axes. The estimates for $x_{ions} = 0$ are not included as they are not easily represented in a log-log graph. The molecular dynamics estimate value for one ion-pair is not included due to the regression converging to a sign that is not easily represented in a log-log plot.

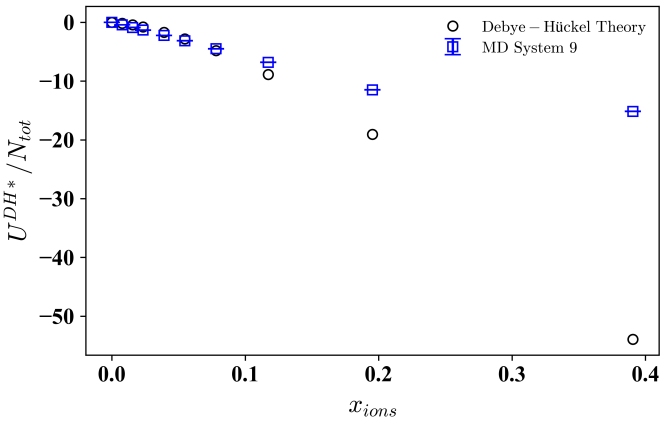

Figure 5.17: The molecular dynamics (blue squares) and Debye–Hückel theory estimates (black circles) for the average Debye–Hückel electrostatic energy for system 9 from table 3.1 as a function of the mole fraction of ions. The method from section 4.2 is used to calculate the regression coefficients that are used in the Debye–Hückel electrostatic energy estimates. The reduced ionic-atmosphere radius used in the Debye–Hückel theory estimate is equal to zero. The resulting regression coefficient values are $\varepsilon_r = 1.0$ and $\overline{U}_{ip}^{\infty *} = 34.483$.

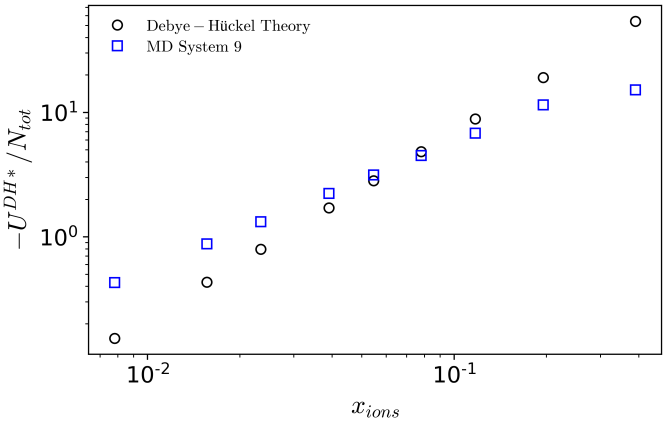

Figure 5.18: The negative of the electrostatic Debye–Hückel energy estimates from figure 5.17 for system 9 plotted using logarithmic x and y axes. The estimates for $x_{ions} = 0$ are not included as they are not easily represented in a log-log graph.

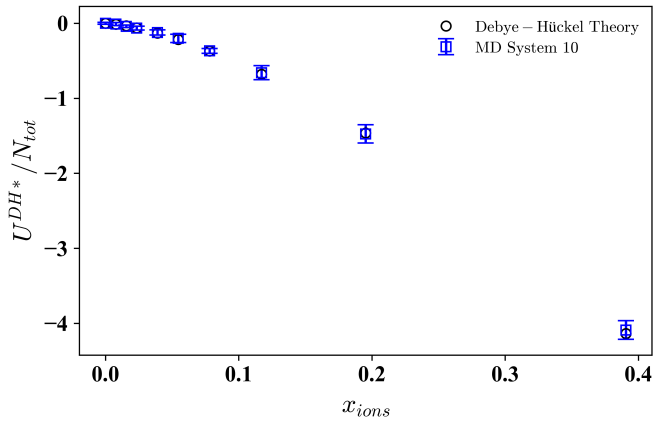

Figure 5.19: The molecular dynamics (blue squares) and Debye–Hückel theory estimates (black circles) for the average Debye–Hückel electrostatic energy for system 10 from table 3.1 as a function of the mole fraction of ions. The method from section 4.2 is used to calculate the regression coefficients that are used in the Debye–Hückel electrostatic energy estimates. The reduced ionic-atmosphere radius used in the Debye–Hückel theory estimate is equal to zero. The resulting regression coefficient values are $\varepsilon_r = 2.572$ and $\overline{U}_{ip}^{\infty *} = -32.400$.

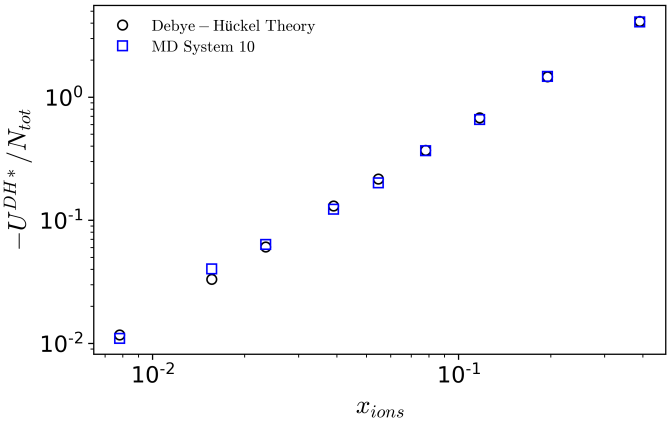

Figure 5.20: The negative of the electrostatic Debye–Hückel energy estimates from figure 5.19 for system 10 plotted using logarithmic x and y axes. The estimates for $x_{ions} = 0$ are not included as they are not easily represented in a log-log graph.

The disagreement between the molecular dynamics and the Debye–Hückel theory estimates in figures 5.13 through 5.18 demonstrate that systems 7, 8, and 9 do not follow the Debye–Hückel theory's thermodynamics in the limit of infinite dilution. Unlike for system 2, the slope of the molecular dynamics estimate in figures 5.14, 5.16, and 5.18 are not equal to one. This observation suggests that systems 7, 8, and 9 are no longer in the large inverse Debye length limit where the Debye–Hückel electrostatic energy is proportional to the concentration of ions.

Figures 5.19 and 5.20 demonstrate that there is almost no disagreement between system 10's molecular dynamics and the Debye–Hückel theory estimates for the Debye–Hückel electrostatic energy. The small difference between the molecular dynamics and the Debye–Hückel theory estimates observed for $x_{ions} = 0.0156$ in figure 5.20 is less than half a standard deviation and can, therefore, be attributed to uncertainty in the molecular dynamics simulation results. The similarity between the molecular dynamics and the Debye–Hückel theory estimates in figure 5.20 is conclusive evidence that it is possible to recover the infinite dilution asymptotic thermodynamic behavior of the Debye–Hückel theory from the non-primitive model in the large temperature limit.

The reduced inverse Debye lengths for systems 8 and 10 are in the ranges $\kappa_0^* \in (0, 0.0525)$ and $\kappa_0^* \in (0, 0.452)$, respectively. These reduced inverse Debye lengths were calculated using the pure solvent permittivity (calculated using the post-processing method from section 3.2.1) and an ionic-atmosphere radius of zero. Even though system 10 has a larger inverse Debye length than system 8, system 10 exhibits the Debye–Hückel theory's infinite dilution limiting behavior, whereas system 8 does not. This observation suggests that the non-primitive model does not recover the Debye–Hückel theory's infinite dilution limiting behavior in the limit of small ion charge magnitudes.

The previous paragraph's observation leads to the question: Does it make sense for a correct non-primitive electrolyte model to converge to the Debye–Hückel theory in the limit of small ion charge magnitudes? In contrast to the infinite dilution or high-temperature limit, ion charges are quantized such that no experiment can approach the limit of infinitely small ion charge magnitudes. There is thus no experimental evidence for the thermodynamics of real electrolytes converging to the Debye–Hückel theory in this limit.

A *hypothesis* for why the non-primitive model does not seem to recover the Debye-Hückel theory's asymptotic behavior in the limit of small ion charge magnitudes is that short-ranged soft-core interactions dominate in this limit. The non-electrostatic interactions being much larger than the ion's electrostatic interactions could cause the electrolyte to converge to a particle configuration that does not follow the Debye–Hückel theory. Figure 5.21 plots the radial distribution function between the cations and anions $g_{\pm}$ for systems 2, 8, 10 and 12 from table 3.1 for 10 ion-pairs. Figure 5.21 demonstrates that the radial distribution function is almost identical for systems 8 and 12, even though the permittivity (calculated using the post-processing method from section 3.2.1) is almost 40 times smaller in system 12 than in system 8. However, equations (2.16), (2.17), and (2.26) demonstrate that the Debye–Hückel theory predicts that changing the solution's permittivity should

affect the distribution of ions in the electrolyte. The disconnect between the observed radial distribution function behavior and Debye–Hückel theory is potential evidence that electrolytes converge to a particle configuration that does not follow the Debye–Hückel theory in the limit of small ion charge magnitudes. The future works section suggests a method for testing the hypothesis that non-electrostatic interactions cause the non-primitive model to have a different asymptotic behavior than the Debye-Hückel theory in the limit of small charge magnitudes.

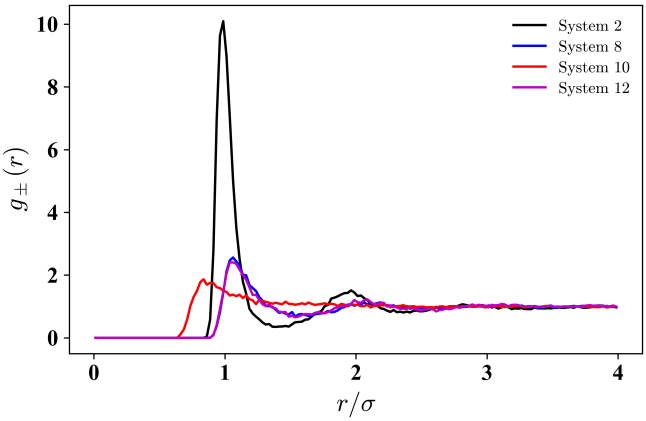

Figure 5.21: The radial distribution function between the cations and anions for systems 2, 8, 10 and 12 from table 3.1 for 10 ion-pairs. The radial distribution functions were calculated using the OVITO post-processing software [4].

Chapter 6

Conclusion

This thesis focuses on how representing the solvent using a primitive or non-primitive approach changes the dielectric and thermodynamic properties of electrolyte models in the limit of infinite dilution. Specifically, this work aims to understand the solvent's role in electrolytes by analyzing and comparing the dielectric and thermodynamic properties of the non-primitive electrolyte model from section 2.2 and the Debye–Hückel theory in three distinct stages.

The first stage examines how the permittivity of the non-primitive model changes with ion concentration. The non-primitive model's description of the solvent as dipolar particles is sufficiently complex to observe dielectric decrement at increasing ion concentrations. This dielectric decrement is probably due to ionic polarizability and the creation of solvation shells. Furthermore, the permittivity is observed to decrease when reducing the solvent particles' dipole moment or the electrolyte solution's number density. A simple system of two ions separated by a solvent particle suggests that this decrease is due to reduced screening by the solvent particles. This first stage highlights a significant difference between primitive and non-primitive electrolyte models. In contrast to primitive electrolyte models where the permittivity is an independent property, non-primitive models incorporate the permittivity through ensemble averages. Letting the permittivity be a function of the electrolyte's microscopic structure through ensemble averages leads to a natural description of dielectric decrement.

The second stage clarifies whether including a description of dielectric decrement, through an ion concentration-dependent permittivity, changes the Debye–Hückel theory's behavior in the limit of infinite dilution. Analyzing the terms of a series expanded mean ionic activity coefficient expression demonstrates that dielectric decrement does not affect the Debye–Hückel theory's thermodynamics in the limit of infinite dilution. The ratio between the first two series expansion terms is a rough estimate for when Debye–Hückel theory predicts that dielectric decrement is significant. This ratio demonstrates that characterizing the solvent using an ion concentration-dependent permittivity changes the Debye-Hückel

theory's mean ionic activity coefficient by 1 percent at approximately $10^{-2}\mathrm{M}$ for a sodium chloride solution at $25^{\circ}\mathrm{C}$. Since the Debye–Hückel theory does not predict that dielectric decrement affects the thermodynamics of electrolytes in the limit of infinite dilution, it is reasonable to contemplate that the non-primitive model's thermodynamics converges to that of the Debye–Hückel theory in this limit.

The final stage uses a regression method to investigate if it is possible to recover the Debye–Hückel theory's infinite dilution limiting behavior from the non-primitive model's molecular dynamics results. The molecular dynamics estimate for the Debye–Hückel electrostatic energy for system 2 from table 3.1 is proportional to the concentration of ions. This observation suggests that the inverse Debye lengths in system 2 are too large to observe the Debye–Hückel theory's infinite dilution limiting behavior. This thesis uses two methods for reducing the inverse Debye lengths, namely increasing the ensemble temperature and decreasing the ions' charge magnitude. The Debye–Hückel theory thermodynamics is recovered when increasing the temperature one hundredfold. This observation demonstrates that the non-primitive model correctly converges to the Debye–Hückel thermodynamics at large temperatures. Debye–Hückel theory thermodynamics are not recovered when decreasing the ions' charge magnitude by a factor of 40. This could be due to short-ranged non-electrostatic interactions causing electrolyte solutions to converge to particle configurations that do not follow Debye–Hückel theory in the limit of small ion charge magnitudes.

Chapter 7

Future Work

This thesis does not conclude if the non-primitive model from section 2.2 recovers the Debye–Hückel theory's infinite dilution asymptotic behavior for sufficiently small ion charge magnitudes. One approach for answering this question is to calculate radial distribution functions and use the regression method from section 4.2 for a broader range of temperatures, ion charge magnitudes, and ion concentrations than this work. Unfortunately, this approach would take too long using this thesis's molecular dynamics procedure.

Molecular dynamics is a tedious method for studying the asymptotic thermodynamic behavior of electrolyte models. Obtaining precise and reliable thermodynamics data from molecular dynamics simulations has been challenging and a hindrance to this work's progress. For example, this work does not focus on if it is possible to recover the Debye-Hückel theory's asymptotic behavior from the non-primitive model by reducing the ion concentration due to long simulation run-times. As mentioned during the preface, decreasing the ion concentration would require larger simulation boxes with more solvent particles. Considering that some of the relatively small simulations in this work took over a week to complete (using a conventional computer), increasing the number of solvent particles in the molecular dynamics simulations is difficult without significantly increasing computational power. Another complication with molecular dynamic simulations is ensuring that finite-size effects do not affect the calculated thermodynamic properties. Rather than reducing simulation run-times and finite-size effects by increasing computational power, future work should consist of non-primitive electrolyte models that do not require computer simulations.

An alternative to using molecular dynamic simulations is to use non-primitive electrolyte models with known analytical or numerical solutions. A promising non-primitive electrolyte model for future work is the MSA electrolyte model. The MSA electrolyte model for same-sized particles, which is essentially the non-primitive electrolyte from section 2.2 with a hard-sphere instead of a WCA or Lennard-Jones interaction, has been solved analytically by Blum [53] [54] and Adelman and Deutch [55]. Another promising electrolyte model is

the associative mean spherical approximation (AMSA) model from Holovko and Kapko [56]. The AMSA's simple procedure for calculating many thermodynamic properties of interest makes it an excellent candidate for further work.

Bibliography

[1] A. Chandra and G. N. Patey. Dielectric relaxation of electrolyte solutions: Molecular dynamics and theoretical results for ions in simple dipolar solvents. *The Journal of Chemical Physics*, 100(11):8385–8391, 1994. doi: 10.1063/1.466785. URL https://doi.org/10.1063/1.466785.

[2] Dan Ben-Yaakov, David Andelman, and Rudi Podgornik. Dielectric decrement as a source of ion-specific effects. *The Journal of Chemical Physics*, 134(7):074705, Feb 2011. ISSN 1089-7690. doi: 10.1063/1.3549915. URL http://dx.doi.org/10.1063/1.3549915.

[3] *CRC Handbook of Chemistry and Physics 2016-2017*. CRC Press, 97 edition, 2016.

[4] The OVITO Team. ovito.modifiers, . URL https://www.ovito.org/docs/current/python/modules/ovito_modifiers.php.

[5] Henry S. Frank and Peter T. Thompson. Fluctuations and the limit of validity of the debye-hückel theory. *The Journal of Chemical Physics*, 31(4):1086–1095, 1959. doi: 10.1063/1.1730508. URL https://doi.org/10.1063/1.1730508.

[6] Bob Eisenberg. Ionic interactions are everywhere. *Physiology*, 28(1):28–38, 2013. doi: 10.1152/physiol.00041.2012. URL https://doi.org/10.1152/physiol.00041.2012. PMID: 23280355.

[7] Eric Hendriks, Georgios M. Kontogeorgis, Ralf Dohrn, Jean-Charles de Hemptinne, Ioannis G. Economou, Ljudmila Fele Zilnik, and Velisa Vesovic. Industrial requirements for thermodynamics and transport properties. *Industrial & Engineering Chemistry Research*, 49(22):11131–11141, 2010. doi: 10.1021/ie101231b. URL https://doi.org/10.1021/ie101231b.

[8] J. M. Prausnitz, R. N. Lichtenthaler, and Edmundo Gomes de Azevedo. *Molecular Thermodynamics of Fluid-Phase Equilibria*. Prentice Hall, 3 edition, 1999.

[9] Georgios M. Kontogeorgis, Bjørn Maribo-Mogensen, and Kaj Thomsen. The debye-hückel theory and its importance in modeling electrolyte solutions. *Fluid Phase*

Equilibria, 462:130 – 152, 2018. ISSN 0378-3812. doi: https://doi.org/10.1016/j.fluid.2018.01.004. URL http://www.sciencedirect.com/science/article/pii/S0378381218300074.

[10] Joseph F. Masi, Eric F. Lype, and Roger Eichorn. *Progress in International Research on Thermodynamic and Transport Properties*. American Society of Mechanical Engineers, 1962.

[11] Michael P. Allen and Dominic J. Tildesley. *Computer Simulation of Liquids : Second Edition*. Oxford University Press USA - OSO, Oxford, 2017. ISBN 9780198803195.

[12] E.R Dobbs. *Basic Electromagnetism*. Physics and Its Applications. Springer Netherlands : Imprint: Springer, Dordrecht, first edition. edition, 1993. ISBN 94-011-2112-5.

[13] Peter Debye and Erich Hückel. Zur theorie der elektrolyte. i. gefrierpunktserniedrigung und verwandte erscheinungen. *Physikalische Zeitschrift*, 24(185):305, 1923. URL https://minds.wisconsin.edu/handle/1793/79225.

[14] J. Franklin. *Solved Problems in Classical Electromagnetism*. Dover Books on Physics. Dover Publications, 2018. ISBN 9780486813721.

[15] R. Serway, J. Faughn, and C. Vuille. *College Physics*. Number v. 10 in Available 2010 Titles Enhanced Web Assign Series. Cengage Learning, 2008. ISBN 9780495386933.

[16] K.L. Kaiser. *Electromagnetic Compatibility Handbook*. Electrical engineering handbook series. Taylor & Francis, 2004. ISBN 9780849320873.

[17] Michael L. Michelsen and Jørgen M. Mollerup. *Thermodynamic models: fundamentals & computational aspects*. Tie-Line Publications, 2 edition, 2018.

[18] Ralph H. Fowler and Edward A. Guggenheim. *Statistical thermodynamics: a version of statist. mechanics for students of physics and chemistry*. Univ. Press, 1952.

[19] N. Sato and Engineering Information Inc. *Chemical Energy and Exergy: An Introduction to Chemical Thermodynamics for Engineers*. Chemical, Petrochemical & Process. Elsevier Science, 2004. ISBN 9780444516459.

[20] D.J. Adams and E.M. Adams. Static dielectric properties of the stockmayer fluid from computer simulation. *Molecular Physics*, 42(4):907–926, 1981. doi: 10.1080/00268978100100701. URL https://doi.org/10.1080/00268978100100701.

[21] Jacob N. Israelachvili. *Intermolecular and Surface Forces*. Elsevier Academic Press, 3 edition, 2011.

[22] David J. Griffiths. *Introduction to electrodynamics*. Cambridge University Press, 3 edition, 2008.

[23] D. Levesque, J. J. Weis, and G. N. Patey. Charged hard spheres in dipolar hard sphere solvents. a model for electrolyte solutions. *The Journal of Chemical Physics*, 72(3):1887–1899, 1980. doi: 10.1063/1.439333. URL https://doi.org/10.1063/1.439333.

[24] Masahiro Yamamoto. Charge-charge, charge-dipole, dipole-charge, dipole-dipole interaction, Dec 2008. URL https://janheyda.files.wordpress.com/2015/08/electrostatics-multipoles.pdf.

[25] D. M. Heyes and H. Okumura. Some physical properties of the weeks-chandler-andersen fluid. *Molecular Simulation*, 32(1):45–50, 2006. doi: 10.1080/08927020500529442. URL https://doi.org/10.1080/08927020500529442.

[26] The LAMMPS Team. units command, . URL https://lammps.sandia.gov/doc/units.html.

[27] The LAMMPS Team, . URL https://lammps.sandia.gov/.

[28] The LAMMPS Team. minimize command, . URL https://lammps.sandia.gov/doc/minimize.html.

[29] The LAMMPS Team. fix nve/sphere command, . URL https://lammps.sandia.gov/doc/fix_nve_sphere.html.

[30] The LAMMPS Team. pair_style lj/cut/dipole/long command, . URL https://lammps.sandia.gov/doc/pair_dipole.html.

[31] The LAMMPS Team. kspace_style command, . URL https://lammps.sandia.gov/doc/kspace_style.html.

[32] The LAMMPS Team. fix nve/sphere command, . URL https://lammps.sandia.gov/doc/fix_langevin.html.

[33] J. M. Caillol, D. Levesque, and J. J. Weis. Electrical properties of polarizable ionic solutions. ii. computer simulation results. *The Journal of Chemical Physics*, 91(9):5555–5566, 1989. doi: 10.1063/1.457558. URL https://doi.org/10.1063/1.457558.

[34] Michael T. Humbert, Yong Zhang, and Edward J. Maginn. Pylat: Python lammps analysis tools. *Journal of Chemical Information and Modeling*, 59(4):1301–1305, 2019. doi: 10.1021/acs.jcim.9b00066. URL https://doi.org/10.1021/acs.jcim.9b00066. PMID: 30844269.

[35] D. Levesque, J. J. Weis, and G. N. Patey. Charged hard spheres in dipolar hard sphere solvents. a model for electrolyte solutions. *The Journal of Chemical Physics*, 72(3):1887–1899, 1980. doi: 10.1063/1.439333. URL https://doi.org/10.1063/1.439333.

[36] Christopher J. Fennell and J. Daniel Gezelter. Is the ewald summation still necessary? pairwise alternatives to the accepted standard for long-range electrostatics. *The Journal of Chemical Physics*, 124(23):234104, 2006. doi: 10.1063/1.2206581. URL https://doi.org/10.1063/1.2206581.

[37] Christian Holm and Kurt Kremer. *Advanced computer simulation approaches for soft matter sciences II*. Springer, 2005.

[38] Jiri Kolafa and John W. Perram. Cutoff errors in the ewald summation formulae for point charge systems. *Molecular Simulation*, 9(5):351–368, 1992. doi: 10.1080/08927029208049126. URL https://doi.org/10.1080/08927029208049126.

[39] Ignat Yu. Shilov and Andrey K. Lyashchenko. The role of concentration dependent static permittivity of electrolyte solutions in the debye-hückel theory. *The Journal of Physical Chemistry B*, 119(31):10087–10095, 2015. doi: 10.1021/acs.jpcb.5b04555. URL https://doi.org/10.1021/acs.jpcb.5b04555. PMID: 26132734.

[40] Ana C.F. Ribeiro, Miguel A. Esteso, Victor M.M. Lobo, Hugh D. Burrows, Ana M. Amado, Antonio M. Amorim da Costa, Abilio J.F.N. Sobral, Eduarda F.G. Azevedo, and Maria A.F. Ribeiro. Mean distance of closest approach of ions: Sodium salts in aqueous solutions. *Journal of Molecular Liquids*, 128(1):134 – 139, 2006. ISSN 0167-7322. doi: https://doi.org/10.1016/j.molliq.2005.12.004. URL http://www.sciencedirect.com/science/article/pii/S0167732206000213.

[41] Jacob Kielland. Individual activity coefficients of ions in aqueous solutions. *Journal of the American Chemical Society*, 59(9):1675–1678, 1937. doi: 10.1021/ja01288a032. URL https://doi.org/10.1021/ja01288a032.

[42] Alex C. Tikanen and W.Ronald Fawcett. Application of the mean spherical approximation and ion association to describe the activity coefficients of aqueous 1:1 electrolytes1dedicated to professor k.b. oldham on the occasion of his retirement from trent university.1. *Journal of Electroanalytical Chemistry*, 439(1): 107 – 113, 1997. ISSN 1572-6657. doi: https://doi.org/10.1016/S0022-0728(97)00376-8. URL http://www.sciencedirect.com/science/article/pii/S0022072897003768.

[43] Svein Stølen and Tor Grande. *Chemical thermodynamics of materials: macroscopic and microscopic aspects*. John Wiley & Sons, 2004.

[44] Morten Helbaek and Signe Kjelstrup. *Fysikalsk kjemi*. Fagbokforlaget, 2 edition, 2006.

[45] ScipyTeam. scipy.optimize.minimize, 2020. URL https://docs.scipy.org/doc/scipy/reference/generated/scipy.optimize.minimize.html.

[46] C. G. Gray, Y. S. Sainger, C. G. Joslin, P. T. Cummings, and S. Goldman. Computer simulation of dipolar fluids. dependence of the dielectric constant on system size: A comparative study of ewald sum and reaction field approaches. *The Journal of Chemical Physics*, 85(3):1502–1504, 1986. doi: 10.1063/1.451189. URL https://doi.org/10.1063/1.451189.

[47] Marc Theiss and Joachim Gross. Nonprimitive model electrolyte solutions: Comprehensive data from monte carlo simulations. *Journal of Chemical & Engineering Data*, 65(2):634–639, 2020. doi: 10.1021/acs.jced.9b00855. URL https://doi.org/10.1021/acs.jced.9b00855.

[48] J. B. Hasted, D. M. Ritson, and C. H. Collie. Dielectric properties of aqueous ionic solutions. parts i and ii. *The Journal of Chemical Physics*, 16(1):1–21, 1948. doi: 10.1063/1.1746645. URL https://doi.org/10.1063/1.1746645.

[49] Henry S. Frank and Peter T. Thompson. Fluctuations and the limit of validity of the debye and hückel theory. *The Journal of Chemical Physics*, 31(4):1086–1095, 1959. doi: 10.1063/1.1730508. URL https://doi.org/10.1063/1.1730508.

[50] Johan S. Høye and Enrique Lomba. Mean spherical approximation (msa) for a simple model of electrolytes. i. theoretical foundations and thermodynamics. *The Journal of Chemical Physics*, 88(9):5790–5797, 1988. doi: 10.1063/1.454753. URL https://doi.org/10.1063/1.454753.

[51] Lodin Ellingsen and Johan Skule Høye. Personal conversation, Jun 2020.

[52] Tiejun Xiao and Xueyu Song. A molecular debye-hückel theory and its applications to electrolyte solutions. *The Journal of Chemical Physics*, 135(10):104104, 2011. doi: 10.1063/1.3632052. URL https://doi.org/10.1063/1.3632052.

[53] L. Blum. Solution of a model for the solvent-electrolyte interactions in the mean spherical approximation. *The Journal of Chemical Physics*, 61(5):2129–2133, 1974. doi: 10.1063/1.1682224. URL https://doi.org/10.1063/1.1682224.

[54] L. Blum. Mean spherical model for a mixture of charged spheres and hard dipoles. *Chemical Physics Letters*, 26(2):200 – 202, 1974. ISSN 0009-2614. doi: https://doi.org/10.1016/0009-2614(74)85396-0. URL http://www.sciencedirect.com/science/article/pii/0009261474853960.

[55] S. A. Adelman and J. M. Deutch. Exact solution of the mean spherical model for strong electrolytes in polar solvents. *The Journal of Chemical Physics*, 60(10):3935–3949, 1974. doi: 10.1063/1.1680841. URL https://doi.org/10.1063/1.1680841.

[56] Myroslav Holovko and V. Kapko. Ion-dipole model for electrolyte solutions: Application of the associative mean spherical approximation. *Condensed Matter Physics*, 10, 09 2007. doi: 10.5488/CMP.10.3.397.

Appendix

A Input Scripts LAMMPS

This appendix illustrates the LAMMPS scripts used to perform the initialization, calibration, and calculation stages of the molecular dynamics procedure from section 3.1.

Initialization and Calibration Script

This subsection presents the LAMMPS script that is used to perform the initialization and calibration stages of the molecular dynamics procedure from section 3.1 for the non-primitive model from section 2.2. Specifically this is the calibration script for system 1 from table 3.1 with 10 anions and 10 cations.

```
################################################################################
# Initialization script
# Lodin Ellingen
# Description:
# ------------
#
# LAMMPS input script for creating equilibrated configuration to be used in
# calculation script.
################################################################################


# log file
log             "log.LJ.init_lattice"

# SIMULATION SETTINGS
# timestep
variable        dt      equal 0.0025

# number of melting time steps
variable        Nmelt   equal 50000

# number of equilibriation time steps
variable        Nprod   equal 50000

# thermo print
variable        therm_print equal 100

# seed
variable  seed equal 187202

# SYSTEM SETTINGS
units           lj
atom_style      hybrid sphere dipole

# thermodynamic properties
variable        init_temp   equal 3.0
variable        temperature equal 1.35
```

```
variable        rho         equal 0.8

# settings for LJ-potential
variable        rc_LJ   equal 3.42
variable        epsilon equal 1.0
variable        sigma   equal 1.0
variable        mass    equal 1.0

# settings dipole moment
variable Dlen equal 1.8

# settings for Coulomb potential
variable rc_C   equal 3.42

# box dimensions
variable Ntot  equal 256
variable Nion equal 10
variable Nsolv equal ${Ntot}-(2*${Nion})

variable        Lx      equal (${Ntot}/${rho})^(1/3)
variable        Ly      equal ${Lx}
variable        Lz      equal ${Lx}

# create configuration
lattice         fcc ${rho}
region          box block 0.0 ${Lx} 0.0 ${Ly} 0.0 ${Lz} units box
create_box      3 box
create_atoms  1 random ${Nsolv} 103 NULL units box
create_atoms  2 random ${Nion} 104 NULL units box
create_atoms  3 random ${Nion} 105 NULL units box

# set group type
group  solvent type 1
group  cation  type 2
group  anion   type 3

#Set diameter
set type 1 diameter 0.50
set type 2 diameter 0.50
set type 3 diameter 0.50

#Set charge
set type 1 charge 0.0
set type 2 charge 8.0
set type 3 charge -8.0


# set pair style and coefficients
pair_style      lj/cut/dipole/long ${rc_LJ} ${rc_C}
pair_coeff      * * ${epsilon} ${sigma}
mass            * ${mass}
kspace_style    ewald/disp 1.0e-5

#set dipole
set group solvent  dipole/random ${seed} ${Dlen}
set group cation dipole 0 0 0
set group anion  dipole 0 0 0

# set timestep
timestep        ${dt}

# neighbor list settings
neighbor        0.5 bin
neigh_modify    every 10 delay 0 check yes

# thermo
compute tempSphere all temp/sphere
thermo_style    custom step time etotal ke pe lx density temp c_tempSphere press
```

```
thermo          ${therm_print}


# RUNNING SIMULATION
# Minimize configuration
minimize 1.0e-4 1.0e-6 100000 1000000

# give intitial velocity
velocity        all create ${init_temp} 3068102

# production run
fix             ensNVE1 all nve/sphere update dipole
run  ${Nmelt}
unfix  ensNVE1

# integrator and ensemble
fix  ensNVE2 all nve/sphere update dipole
fix  ensNVE3 all langevin ${temperature} ${temperature} $(100.0*dt) 573456 omega yes
run  ${Nprod}

# write end configuration
write_data      "config.LJ.init_lattice"
```

Calculation Script

This subsection presents the LAMMPS script that is used to perform the calculation stage of the molecular dynamics procedure from section 3.1 for the non-primitive model from section 2.2. Specifically this is the calibration script for system 1 from table 3.1 with 10 anions and 10 cations.

```
################################################################################
#
# Lodin Ellingsen
#
# # Description:
# ------------
# Computation script for LAMMPS charge-dipole system.
# The script depends on having an equilibrated system as input.
#
################################################################################

# log file
log             "log.LJ.nvt"

# SIMULATION SETTINGS
# timestep
variable        dt      equal 0.0025

# total number of time steps
variable        Nprod equal 250000

# thermo print
variable        therm_print equal 100

# sampling settings for fix ave/time
variable        Nevery  equal 100
variable        Nrepeat equal 1
variable        Nfreq   equal ${Nevery}*${Nrepeat}


# SYSTEM SETTINGS
# units and atom style
units           lj
atom_style      hybrid sphere dipole
```

```
# thermodynamic properties
variable        temperature equal 1.35

# settings for LJ-potential
variable        rc_LJ   equal 3.42
variable rc_C equal 3.42
variable        epsilon equal 1.0
variable        sigma   equal 1.0
variable        mass    equal 1.0


# pair style
pair_style      lj/cut/dipole/long ${rc_LJ} ${rc_C}

# read start configuration
read_data       "config.LJ.eq_nvt"

# box dimensions
variable        Lx      equal xhi-xlo
variable        Ly      equal yhi-ylo
variable        Lz      equal zhi-zlo

# pair style coefficients
pair_coeff      * * ${epsilon} ${sigma}
kspace_style ewald/disp 1.0e-5
mass            * ${mass}

# set timestep
timestep        ${dt}

# neighbor list settings
neighbor        0.5 bin
neigh_modify    every 10 delay 0 check yes

# thermo
thermo_style    custom step time etotal ke pe lx density temp press
thermo          ${therm_print}


# RUNNING SIMULATION
# integrator and ensemble
fix  ensNVE2 all nve/sphere update dipole
fix  ensNVE3 all langevin ${temperature} ${temperature} $(100.0*dt) 573456 omega yes



# computing temperature, pressure and per atom pressure tensor
compute         temp all temp
compute         pres all pressure temp
compute         pe all pe
compute         ke all ke
compute         peatom all pe/atom

compute muCalc all property/atom mu mux muy muz
compute         cc1 all chunk/atom type
compute  tempSphere all temp/sphere

# dump positions and per particle energies
dump            d_posen all custom ${Nevery} "dump.LJ_nvt" id type x y z mu mux muy muz
dump_modify     d_posen sort id

# dump first and last configuration
dump            d_check all custom ${Nprod} "dump.LJ_check_nvt" id type x y z

# production run
run             ${Nprod}
```

```
# write end configuration
write_data      "config.LJ.end_nvt"
```

B Debye–Hückel Electrostatic Energy in Lennard-Jones Units

This section derives an expression for the average Debye–Hückel electrostatic energy in Lennard-Jones units for an electrolyte solution that consists of two ionic species with the same charge magnitude and ionic-atmosphere radius. The resulting expression demonstrates that the average Debye–Hückel electrostatic energy is proportional to the mole fraction of ions to the $\frac{3}{2}$ power in the limit of infinite dilution or when the ionic-atmosphere radius is zero.

Section 2.1.2 demonstrates that Debye-Hückel theory predicts a Debye–Hückel electrostatic energy U^{DH} that is equal to

$$U^{DH} = -\sum_{i=1}^{s} \frac{N_i}{2} \frac{z_i^2 q^2}{4\pi\varepsilon_s} \frac{\kappa_0}{1+\kappa_0 a_i}, \tag{B.1}$$

where the inverse Debye length κ_0 is defined as

$$\kappa_0 = \sqrt{\frac{q^2}{\varepsilon_s k_\mathrm{B} T V} \sum_{i=1}^{s} N_i z_i^2}. \tag{B.2}$$

q is the elementary charge, z_i is the integer charge number of ionic species i, ε_s is the permittivity of the pure solvent, k_B is the Boltzmann constant, s is the number of ionic species, N_i is the number of particles of ionic species i, a_i is the ionic-atmosphere radius of ionic species i, T is the temperature, and V is volume of the solution. For an electrolyte solution that consists of a single cation and anion species with the same charge magnitude $q_\pm$ and the same ionic-radius a, equations (B.1) and (B.2) simplify to

$$U^{DH} = -\frac{N_{ions}}{2} \frac{q_\pm^2}{4\pi\varepsilon_s} \frac{\kappa_0}{1+\kappa_0 a}, \tag{B.3}$$

and

$$\kappa_0 = \sqrt{\frac{q_\pm^2 N_{ions}}{\varepsilon_s k_\mathrm{B} T V}}. \tag{B.4}$$

N_{ions} is the number of ions and N_{solv} is the number of solvent particles. Dividing equation (B.3) by the total number of particles in the solution $N_{tot} = N_{solv} + N_{ions}$ and substituting the mole fraction of ions $x_{ions} = \frac{N_{ions}}{N_{tot}}$ into equations (B.3) and (B.4) leads to

$$\frac{U^{DH}}{N_{tot}} = -\frac{x_{ions}}{2} \frac{q_\pm^2}{4\pi\varepsilon_s} \frac{\kappa_0}{1+\kappa_0 a}, \tag{B.5}$$

and

$$\kappa_0 = \sqrt{\frac{q_{\pm}^2 x_{ions} N_{tot}}{\varepsilon_s k_{\mathrm{B}} T V}}. \tag{B.6}$$

The final step is to express the different quantities in equations (B.5) and (B.6) in terms of Lennard-Jones units. Introducing the reduced temperature T^*, inverse Debye length κ_0^*, density ρ^*, ionic-atmosphere radius a^*, and the charge magnitude $q_{\pm}^*$ as defined in table 2.1 from section 2.2, equations (B.5) and (B.6) become

$$\frac{U^{DH*}}{N_{tot}} = -\frac{x_{ions} q_{\pm}^{*2}}{2\varepsilon_r} \frac{\kappa_0^*}{1 + \kappa_0^* a^*} \tag{B.7}$$

and

$$\kappa_0^* = \sqrt{\frac{4\pi q_{\pm}^{*2} x_{ions} \rho^*}{\varepsilon_r T^*}}. \tag{B.8}$$

ε_r is the relative permittivity of the solvent. When the ionic-atmosphere is equal to zero or x_{ions} is sufficiently small, the $\kappa_0^* a^*$ term is equal or close zero such that $\frac{U^{DH*}}{N_{tot}} \propto x_{ions}^{\frac{3}{2}}$. Oppositely, when κ_0^* is sufficiently large $\frac{\kappa_0^*}{1+\kappa_0^* a^*} \approx \frac{1}{a^*}$ such that $\frac{U^{DH*}}{N_{tot}} \propto x_{ions}$.

The regression method from section 4.2 uses a $\frac{U^{DH*}}{N_{ip}+N_{solv}}$ expression which is closely related to equation (B.7), except the number of ion-pairs N_{ip} is used instead of the number of ions. An expression for $\frac{U^{DH*}}{N_{ip}+N_{solv}}$ is readily found from equation (B.7) by multiplying both sides of the equation by $\frac{N_{tot}}{N_{ip}+N_{solv}}$.

Lodin Ellingsen

NTNU
Norwegian University of
Science and Technology